A **CRCPress** FreeBook

Oil & Gas Industry Efforts FreeBook

CRC Press
Taylor & Francis Group

TABLE OF CONTENTS

Introduction

This freebook embraces all aspects of petroleum science and engineering, with a special focus on emerging trends and technologies in drilling, production, and reservoir engineering. Having a broad scope that includes but is not limited to analytical, experimental, and numerical studies, methods, and field cases, the series covers fundamentals as well as advancements of great impact on today's petroleum industry, from resovoirs, the shale revolution, fluid engineering, unconventional resources, and natural gas.

This freebook comprises chapters from the following Taylor & Francis titles:

- *Asphaltene Deposition: Fundamentals, Prediction, Prevention, and Remediation*

  This book offers concise yet thorough coverage of the complex problem of asphaltene precipitation and deposition in oil production. It covers fundamentals of chemistry, stabilization theories and mechanistic approaches of asphaltene behavior at high temperature and pressure.

- *Unconventional Oil and Gas Resources Exploitation and Development*

  As the shale revolution continues in North America, unconventional resource markets are emerging on every continent. This book provides a comprehensive understanding of the latest advances in the exploitation and development of unconventional resources.

- *Data-Driven Analytics for the Geological Storage of CO2*

  Data-driven analytics is enjoying unprecedented popularity among oil and gas professionals. Drawing from actual case studies, this book demonstrates how smart proxy models can be developed for complex numerical reservoir simulation models. Smart proxy incorporates pattern recognition capabilities of artificial intelligence and machine learning to build smart models that learn the intricacies of physical, mechanical and chemical interactions using precise numerical simulations.

- *Hydraulic Fracturing*

  Hydraulic Fracturing effectively busts the myths associated with hydraulic fracturing. It explains how to properly engineer and optimize a hydraulically fractured well by selecting the right materials, evaluating the economic benefits of the project, and ensuring the safety and success of the people, environment, and equipment.

CHAPTER

1

CRUDE OIL AND ASPHALTENE CHARACTERIZATION

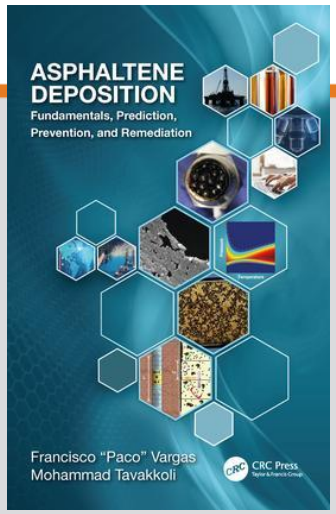

This chapter is excerpted from

Asphaltene Deposition: Fundamentals, Prediction, Prevention, and Remediation

by Francisco M. Vargas, Mohammad Tavakkoli

Learn more

CRUDE OIL AND ASPHALTENE CHARACTERIZATION

Excerpted from *Asphaltene Deposition*

Crude oil is one the most important substances used by modern society, and probably, the least understood. However, what it is known is that its behavior can be related to its chemical composition and physical properties. The first part of this chapter focuses on the description of the chemical and physical properties of crude oil and offers a review of the experimental methods involved in their determination. The properties discussed include density and API gravity, viscosity, molecular weight, water content, refractive index, and solubility parameter. The correlation between these properties is also highlighted. This part also gives an overview of the main methods to classify crude oils according to their boiling point, chemical structure, and the different polarities of its components, including the advantages and disadvantages of the methods used for each classification.

Because asphaltenes, the heaviest part of the crude oil, are responsible for the million-dollar losses caused by their deposition on wells and pipes, the second part of the chapter is dedicated to exploring more closely their properties, structure, and composition. Other properties, such as aromaticity, molecular weight, polydispersity, and wettability that help to understand, predict, and prevent their deposition are described as well.

2.1 CRUDE OIL

The word *petroleum* comes from the Latin words *petra*: *rock* and *oleum*: *oil*. Unrefined petroleum is better known as crude oil. This is a liquid mixture composed mainly of carbon and hydrogen but also containing some other elements such as oxygen, nitrogen, sulfur, and some trace heavy metals such as nickel, vanadium, copper, cadmium, and lead (Speight 2014). In fact, it is believed that these heavy metals acted as catalysts in the formation of petroleum (Riazi 2005). Because the diversity of its origin, its color, odor, and flow properties vary widely (Ceric 2012; Speight 2014). Nowadays, the most accepted theory about the origin of crude oil is that of an organic origin. According to this theory, dead organic material, including algae, zooplankton, and small aquatic animals, accumulated on the bottom of oceans, riverbeds, and swamps, mixing with clay, silt, and sand. Over time, more sediment piled up on top, increasing the heat and the pressure. In the absence of oxygen, anaerobic bacteria transformed the organic layer into a dark and waxy sub- stance known as kerogen. Left alone, the kerogen molecules cracked and broke up into shorter and lighter molecules composed almost solely of carbon and hydrogen atoms. It has been reported that the geologic time needed to produce petroleum is 1 million years, under a maximum pressure of 17 MPa and a maximum temperature of 373 K–393 K (Riazi 2005; Buryakovsky et al. 2005).

Crude oil did not originate in the place it is found today, but much deeper. Through time, it migrated near the surface of Earth and stopped in the sediments layer in which water was present and above which was a dense leak proof cover formed by marl, clay, and oil shell. This accumulation of crude oil is called a *reservoir*. Reservoirs can be found beneath land or the ocean floor, and they are *not* equally distributed around the globe.

The latest research in 2016 show that the largest proved reserves, or the quantities

CRUDE OIL AND ASPHALTENE CHARACTERIZATION

of petroleum determined by analysis of geological and engineering data, are found in

Venezuela (300 billion of bbl), Saudi Arabia (266 billion of bbl), Canada (170 billion of bbl), Iran (158 billion of bbl), and Iraq (143 billion of bbl). The United States is positioned in 11th place with 36.5 billion of bbl ("International Energy Statistics" 2017; "The World Factbook—Central Intelligence Agency" 2017).

Crude oil has been used since the times of the Sumerians (6000 years b.c.) in construction, in ornamental works, and as a fossil fuel. Other civilizations used it as sealer for ships, for plaster and coating production, moisture protection, road construction, mummification, lightening, and even as disinfection agent in medicine. After the Greek and Roman Empires went into decadence, its use and importance were greatly reduced; however, in the middle of the nineteenth century, its importance as an energy source gained force, and, now, it is still the most used one around the globe (Ceric 2012). According to the U.S. Energy Information Administration (2017), the total consumption of energy in the United States was of 97.7 quadrillions

BTU in 2015. Out of this amount, 81% was produced by the three major fossil fuels (crude oil: 36%, natural gas: 29%, and coal: 16%).

2.1.1 ProPerties

Crude oil is a mixture of widely varying constituents and proportions. Consequently, its physical properties also can vary widely. In appearance, for example, its color can go from yellow to black, passing for greenish, reddish, and dark brown (Donaldson et al. 1985). The color depends on the way the incident light interacts with the mol- ecules and molecular bonds in the fluid, and it is transmitted or reflected, giving it different hues. In a similar way, other properties can vary according to the composi- tion of crude oil. A summary of the most important properties is presented next.

2.1.1.1 Density and API Gravity

Density (ρ) is defined as the mass per unit of volume (e.g., kg/m3). It is a state function that depends on both temperature and pressure. The density of crude oil, as for other liquids, decreases as the temperature increases and the effect of pressure is usually negligible at moderated pressures—less than few bars (Riazi 2005). At higher pressures, the density of crude oil will increase because an increase in pres- sure will lead to a decrease in volume.

At the standard conditions for the petroleum industry (60°F or 288.65 K, 1 atm) the density of crude oil can vary from 800 kg/m3 to more than 1000 kg/m3 (Speight

2014). Density can also be reported as specific gravity (*SG*), which is the ratio of the density of a liquid at temperature, *T*, to the density of water at the same temperature (at standard conditions, the density of water is 999 kg/m3).

CRUDE OIL AND ASPHALTENE CHARACTERIZATION

In 1921, a more practical measurement to express the density of crude oil was created by the American Petroleum Institute (Huc 2010; Groysman 2014). The API gravity (°API) is a measurement of how heavy a crude oil is in relation to water and it is defined as:

$$\text{API gravity} = \frac{141.5}{SG\ (\text{at } 60°\text{F})} - 131.5 \qquad (2.1)$$

In this scale, water has an API gravity of 10°; crude oils with an API gravity larger than 10 are lighter and will float on water, whereas if it is less than 10, the crude oil is heavier and sinks.

The broad difference in density is used to divide the crude oil into four grades: light ($\rho < 870$ kg/m3; API > 31.1°), medium (870 < ρ < 920 kg/m3; 22.3° < API < 31.1°),

heavy (920 < ρ < 1000 kg/m3; 10° < API < 22.3°), and extra heavy (ρ > 1000 kg/m3; API < 10°) (Huc 2010; Ancheyta and Speight 2007; Jafarinejad 2016).

Density can be determined by the ASTM D287 2012, ASTM D1217 2015, and

ASTM D1298 2012. The first two methods make use of a hydrometer, which is a floating cylinder graduated by API gravity units. Also, both are based on the principle that the gravity of a liquid varies directly with the depth of immersion of a body floating it. The API gravity can be read from the hydrometer scale when this is left freely floating inside a cylinder full of crude oil at a determined temperature.

In the third method, density is measured with a Bingham pycnometer. The pycnometer is equilibrated to the desired temperature and filled with the sample. Then, it is weighted, and the weight of the sample is obtained by subtracting the weight of the empty pycnometer from the total weight. The density can be calculated by dividing this weight by the volume. If the specific gravity is needed, the same procedure can be done with pure water at the same temperature.

For measurements at higher pressures and temperatures, different and more sophisticated equipment is used. As an example, Wang et al. (2016) have reported the use of an Anton Paar DMA HPM high-pressure and high-temperature (HPHT) densitometer for density measurements of up to 137.4 MPa and 684.3 K. Table 2.1 shows the properties of some of the oils mentioned in this book.

2.1.1.1 Viscosity

Viscosity of a fluid is a measure of its resistance to gradual deformation by shear stress or tensile stress; in other words, it is the measure of a fluid's internal resistance dfss

CRUDE OIL AND ASPHALTENE CHARACTERIZATION

TABLE 2.1
Properties of Some of the Oils Mentioned in This Book

Crude Oil	Density (g/cm³; Tamb)	Viscosity (cP; Tamb)	Water Content (wt%)	Molecular Weight (g/mol)
A	0.884	56.0	0.07	273.0
C	0.885	22.0	0.03	245.0
P1	0.878	21.3	0.04	243.1
P60	0.911	338.9	0.06	339.9
P7	0.876	15.3	0.03	251.3
SB	0.867	60.5	0.03	176.1
SE	0.893	33.8	0.18	220.4
CN	0.899	55.0	0.08	278.9
S4	0.826	5.4	0.03	NA

Source: Courtesy of Vargas Research Laboratory, Rice University, Houston, TX.

to flow. It gives a notion of the thickness of the fluid. Knowing this parameter is useful for from designing the appropriate extraction process and transport of crude oil, to the planning and execution of measures for the remediation of spills in case of an accident.

Newton's viscosity law states that the shear stress between adjacent layers of a fluid is proportional to the gradients of velocity between the two layers (Riazi 2005). Figure 2.1 shows a representation of a fluid moving along a solid boundary at a laminar flow.

$$\tau \propto \frac{dv_x}{d_y} \text{ or } \tau = -\mu \frac{dv_x}{d_y} = -\nu_f \frac{d(\rho v_x)}{dy} \quad (2.$$

where:

$\nu_f = \frac{\mu}{\rho}$

τ is the shear stress (in N/m²)
v_x is the velocity (m/s)
dv_x/d_y is the velocity gradient or share rate (s^{-1})
ρ is the density of the fluid (kg/m³)
μ is the dynamic viscosity (Pa s)
ν_f is the kinematic viscosity (m²/s) (Bird et al. 2002)

CRUDE OIL AND ASPHALTENE CHARACTERIZATION

Dynamic viscosity (also known as *absolute viscosity*) is a measurement of a fluid's resistance to flow when an external force is applied, while the kinematic viscosity is a measurement of the resistive flow of a fluid under only the action of gravity. In other words, dynamic viscosity provides information on the force needed to make the fluid flow at a certain rate, whereas kinematic viscosity tells how fast the fluid is moving when a determined force is applied.

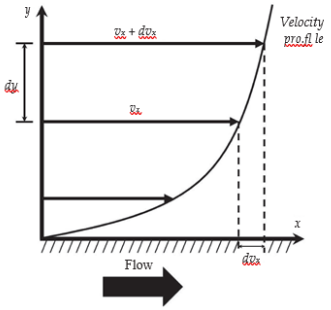

FIGURE 2.1 Laminar flow of a fluid along a solid boundary. (Adapted from Bird, R. B. et al., *Transport Phenomena,* 2nd ed., John Wiley & Sons, New York, 2002.)

Kinematic viscosity is determined experimentally by the ASTM D445 (2017). According to this method, the viscosity is determined at different temperatures, usually 298.15 K (77°F) and 373.15 K (212°F), by measuring the time that takes for a fixed volume of oil to flow under gravity through a calibrated viscometer. Other examples of viscometers can be found in the ASTM D445 (2017). The kinematic

viscosity is then calculated by multiplying the time by the calibration constant of the viscometer. Dynamic viscosity can also be calculated from this result by multiplying the kinematic viscosity by the density of crude oil at the same temperature.

It is important to remember at this point that crude oil is a non-Newtonian fluid; that is, its viscosity varies according to the applied stress. There is more sophisticated equipment to determine the dynamic viscosity as a function of the stress such as rotational viscometers (i.e., cone and plate, Stabinger viscosity). Several of these methods are specified in the ASTM D4287 (2014); ASTM D5481 (2013); ASTM D7042 (2016); ASTM D7395 (2007). In addition to these standards, ASTM D7152 (2011) provides a methodology to calculate the viscosity of blends of petroleum products.

Oil viscosity is a strong function of many thermodynamic and physical proper- ties such as oil composition, gas-to-oil ratio (GOR), temperature, and pressure and saturation pressure. As expected, viscosity increases with decreases in crude oil API gravity and decreases with temperature. Also, the gas dissolved decreases the viscosity. Above saturation pressure, viscosity increases almost linearly with pressure. Viscosity is usually determined by experimental methods at the temperature of the reservoir; however, many correlations have been developed to predict the viscosity of crude oil at the reservoir conditions of temperature and pressure (Alomair et al. 2016; Riazi and Al-Otaibi 2001; Al-Rawahi et al. 2012).

CRUDE OIL AND ASPHALTENE CHARACTERIZATION

2.1.1.1 Molecular Weight

Molecular weight is a fundamental physical property that can be used with other physical properties to characterize pure hydrocarbons and mixtures of them. The information about molecular weight is necessary for the application of many correlation-based methods that are used for determining the composition of the heavier fractions of petroleum. There are several experimental techniques available in the literature for molecular weight determination of crude oil samples. The most frequently used techniques are: (1) Freezing Point Depression; and (2) Thermoelectric Measurement of Vapor Pressure.

2.1.1.1.1 Freezing Point Depression

The molecular weight is measured by the freezing point depression or cryoscopic method, from the lowering of the freezing point, which a solution shows with respect to the pure solvent. This is made possible by the three fundamental concepts, found experimentally, and have historically led to the freezing point depression method (Biltz 1899):

1. A solution freezes at a lower temperature than the solvent.
2. The depression of the freezing point is proportional to the concentration of the solution.
3. Equimolecular solutions in the same solvent show an equal depression of the freezing point.

The solvent that is normally used for measuring the molecular weight of a crude oil sample using the freezing point depression method is benzene.

2.1.1.1.2 Thermoelectric Measurement of Vapor Pressure

This method has been published as the standard method ASTM D2503 (1992) for measurement of hydrocarbons molecular weight. It can be applied to petroleum fractions with molecular weights up to 3000 g/mol; however, the precision of the method has not been established for the molecular weight values above 800 g/mol. The method should not be applied to oils with boiling points lower than 493.15 K (ASTM D2503 1992).

In this method, a weighed portion of the sample is dissolved in a known quantity of appropriate solvent. A drop of this mixture and a drop of the solvent are suspended, side by side, on separate thermistors in a closed chamber, which is

CRUDE OIL AND ASPHALTENE CHARACTERIZATION

saturated with solvent vapor. Because the vapor pressure of the solution is lower than that of the solvent, solvent condenses on the sample drop and causes a temperature difference between the two drops. This change in temperature is measured and used to determine the molecular weight of the sample using a previously prepared calibration curve (ASTM D2503 1992).

Other techniques for determination of molecular weight are the boiling point method and the method based on the principle of lowering of solubility. The boiling point technique is similar to the freezing point depression and is based on these fundamental statements: A solution boils at higher temperature than the solvent; the rise in the boiling point is proportional to the concentration; and finally, the equimolecular solutions in the same solvent show the same rise in boiling point. The experimental technique on the principle of lowering of solubility works based on the relative lowering of the capacity to dissolve a second liquid, which a solvent experiences on adding a foreign substance (Biltz 1899).

2.1.1.2 Water Content

The determination of the amount of water in crude oil and petroleum products has always been important. Rather than paying the cost of crude oil for a mixture of oil and water, contracts have been based on net dry oil. This is calculated by removing the amount of water and sediment, which is determined by analyzing a sample of the oil from the total gross standard volume. Knowledge of the water content of petroleum products is important in refining, purchase and sale, and transfer of products and is use- ful in predicting the quality and performance characteristics of the products (Nadkarni 2000). There are three different methods for determining the water content of crude oil and petroleum products: centrifugation, distillation, and Karl Fischer titration.

2.1.1.2.1 Centrifugation

The oldest and most widely used method to determine the water content of a crude oil sample is the centrifuge test. In this method, known volumes of crude oil and solvent are placed in a graduated centrifuge tube and heated up to 333 K. After centrifugation, the volume of the higher density water and sediment at the bottom of the tube is read. For some waxy crude oils, temperatures of 343 K or higher may be required to completely melt the wax crystals. In this case, waxes will not be measured as

sediment (ASTM D4007 2002; ASTM D2709 1996). This test is detailed in several standard methods, including ASTM D4007 (2002) and ASTM D2709 (1996). Even if all details of this method are followed carefully, the total water content will be underestimated for most types of crude oil samples.

CRUDE OIL AND ASPHALTENE CHARACTERIZATION

2.1.1.2.2 Distillation

During the past few years, the determination of the water content by distillation test (also called the *Dean and Stark test*), has been used more frequently because it is more accurate compared to the centrifuge test. Also, it is the accepted referee method when parties cannot agree on centrifuge results. In the test, which is described in detail in ASTM D4006 (2005), the sample is heated under reflux conditions with a water immiscible solvent, which co-distills with the water in the sample. Condensed solvent and water are continuously separated in a trap; the water settles in the graduated section of the trap, and the solvent returns to the distillation flask (ASTM D4006 2005).

2.1.1.2.3 Karl Fischer Titration

The third method for water content determination is based on the titration of the sample with Karl Fischer reagent, described in ASTM D4928 (2000) and ASTM D6304 (2007). This method has been used for many years to determine the water content of liquid petroleum products, but it has not been used for crude oil samples until the past few years. In this technique, a small amount of sample is injected into the titration vessel of a Karl Fischer apparatus in which iodine for the Karl Fisher reaction is coulometrically generated at the anode. When all the water has been titrated, excess iodine is detected by an electrometric end-point detector, and the titration is termi- nated. Based on the stoichiometry of the reaction, 1 mol of iodine reacts with 1 mol of water; and therefore, according to Faraday's Law, the quantity of water is proportional to the total integrated current (ASTM D4928 2000; ASTM D6304 2007).

The Karl Fischer method has several advantages over the other water determination methods, the most important of which is increased accuracy. Also, samples can be analyzed in less than 5 minutes, compared to at least 30 minutes for the centrifuge test and several hours for the distillation test. The Karl Fischer text can be used in the back of a pickup truck for field use, on an offshore platform for production use, and in a laboratory for quality control and other applications.

2.1.1.3 Refractive Index

One of the fundamental physical properties that can be used with other physical properties to characterize pure hydrocarbons and their mixtures is the Refractive Index (Nadkarni 2000). Refractive index is the ratio of the velocity of light in air at a specific wavelength to its velocity in the substance under study (ASTM D1747 2004). The relative index of refraction is defined as the sine of the angle of incidence divided by the sine of the angle of refraction, as light passes from air into the substance. If absolute refractive index (referred to vacuum) is needed, this value should be multiplied by the factor 1.00027; 1.00027 is the absolute refractive index of air. The refractive index of liquids varies inversely with both wavelength and temperature (ASTM D1218 2002).

The refractive index is an important optical parameter of crude oils that is used in various calculations related to their compositions. It is also used in a number of

CRUDE OIL AND ASPHALTENE CHARACTERIZATION

industrial applications such as determination of the asphaltene precipitation onset and the solubility parameter measurement (Speight 2014; Otremba 2000; Buckley 1999; Buckley et al. 1998).

The most widely used technique to measure the refractive index of crude oils is based on the ASTM D1218 (2002). There are commercially available refractometers, which are used to measure the refractive index of transparent, light-colored, or strongly colored hydrocarbons in the range of 1.33–1.50 (or above) based on the ASTM D1218. In this method, the refractive index is measured by the critical angle method using monochromatic light from a sodium lamp. The instrument is previously calibrated using certified liquid standards (ASTM D1218 2002). In the standard D1218, the test temperature varies from 293 K to 303 K. There is another method, ASTM D1747 (2004), which covers the measurement of refractive index of transparent and light-colored viscous hydrocarbon liquids and melted solids that have refractive indices in the range between 1.33 and 1.60, and at temperatures from 353 K to 373 K. Temperatures lower than 353 K can be used if the melting point of the sample is at least 10 K below the test temperature (ASTM D1747 2004).

There are also other techniques in the literature, which are not commercially available, for measuring the refractive index of a crude oil system such as the use of a capillary tube interferometer (El Ghandoor et al. 2003). In this technique, the oil-filled capillary tubes are illuminated by a thick helium-neon (HeNe) laser sheet and the obtained transverse interference patterns are projected on a screen, which its plane is perpendicular to the plane of the laser sheet. The patterns show bell-shaped fringes. The characteristic bell shape is mathematically demonstrated by calculating the optical path difference between a reference ray and a ray that passes through the oil sample. The refractive indices of the crude oil samples are then determined by measuring the detection angles of the fringes (El Ghandoor et al. 2003).

2.1.1.1 Solubility Parameter

The solubility parameter (δ) is a numerical value that indicates the relative solvency behavior of a specific solvent. To understand the solubility parameter, it is necessary to explore the relationship among solubility, van der Waals forces, and the cohesive

energy density.

Van der Waals forces are the attractive forces (or intermolecular forces) that hold molecules together. The three most common types are London forces, dipole-dipole forces, and hydrogen bonding. London forces are the weakest of the intermolecular forces; they are the product of the temporary charges spontaneously developed in all compounds. Dipole-dipole are forces of medium intensity found in molecules with permanent or even partial charges (dipoles). Hydrogen bonding is the strongest of the three intermolecular forces, and it is a case of the dipole-dipole forces between atoms of hydrogen and fluorine, oxygen or nitrogen.

CRUDE OIL AND ASPHALTENE CHARACTERIZATION

For a solute to be dissolved in a solvent, all intermolecular attractions should be broken, including the solvent-solvent and solute-solute forces. Once these forces do not exist, a new intermolecular attraction should be formed between solvent and solute molecules (solvation). This is accomplished best when the attractions between molecules of both components are similar.

A similar situation happens when a liquid is evaporated. When a liquid is heated to the boiling point, the applied heat will increase first the temperature of the liquid, but at the boiling point, the temperature will remain constant and all heat will be used to increase the kinetic energy of the molecules to a point in which the attraction forces will be broken. This energy is the heat of vaporization, and because it is a direct indication of the energy necessary to separate the molecules of a liquid, it is also an indication of the van der Waals forces associated with that liquid.

This energy is also known as cohesive energy (E), and when it is expressed as the quotient between the heat of vaporization and the molar volume, it receives the name of cohesive energy density (CED) (Burke 1984; Hansen 2007; Krevelen and Nijenhuis 2009).

Hildebrand defined the solubility parameter as the square root of the cohesive energy density (Barton 1991). In the following equation, E is the heat of vaporization, the product RT is the energy of the same material as an ideal gas at the same temperature, and $V\mu$ the molar volume (Kitak et al. 2015). This approximation is more detailed explained in Section 4.2.2.1.

$$\delta = \sqrt{\text{CED}} = \sqrt{\frac{E - RT}{\bar{V}}} \qquad (2.3)$$

The Hildebrand solubility parameter was developed for simple liquid mixtures and does not account for the molecular association caused by polar interactions, including hydrogen bonding.

Many other researchers have added some other considerations to the development of this equation or have proposed other methodologies to include a vaster number of sub- stances. For example, Hansen (1967) introduced a model that included the three forces when calculating the cohesion energy (Burke 1984). Other proposed methods use the group contribution of the molecular structure, (Fedors 1974; Krevelen and Nijenhuis 2009; Stefanis and Panayiotou 2008), some others use the refractive index (Karger et al. 1978; Wang and Buckley 2001), and others have used parameters such as density and viscosity (Correra et al. 2005). Also, some methodologies have been developed to calculate the solubility parameter at high temperature and pressure (Wang et al. 2016).

2.1.1.1 Correlation between Properties

CRUDE OIL AND ASPHALTENE CHARACTERIZATION

Measuring each of the crude oil properties is time consuming, but the use of correla- tions between these properties helps to reduce the experimental time. On the other hand, the result of these correlations can be used both as a baseline and to verify the experimental data. Some of these correlations are described next.

2.1.1.1.1 Solubility Parameter

The solubility parameter is often needed for the modeling of complex systems such as asphaltenic crude oils, however, its experimental determination can be quite challenging. To simplify its determination, Wang and Buckley (2001) proposed a correlation between the solubility parameter and the refractive index of a non-polar hydrocarbon.

$$\delta = 52.042 F_{RI} + 2.904 \qquad (2.4)$$

where:

d is the solubility parameter in MPa0.5

FRI is a function of the refractive index (*n*) and is calculated by:

$$F_{RI} = \frac{n^2 - 1}{n^2 + 2} \qquad (2.5)$$

Vargas and Chapman (2010) proposed a one-third rule for a wide range of hydrocarbons according to the Lorentz–Lorenz model (A relationship between molar refractivity, *Rm*, and molecular weight, *Mw*).

$$R_m = \left(\frac{n^2 - 1}{n^2 + 2}\right)\frac{M_w}{\rho} = F_{RI}\frac{M_w}{\rho} \qquad (2.6)$$

Based on "One-Third" rule, the *FRI* divided by the mass density, ρ, is a constant approximately equal to one-third. There is a deviation from one-third value for light and heavy hydrocarbons. The ratio of *FRI*/ρ is approximately constant in a temperature range of 283 K–343 K. Also, it is possible to apply one-third rule in the Wang- Buckley correlation to find the relation between the solubility parameter and the mass density. For the light components, it is better to use the Lorentz–Lorenz expansion in Equation 2.7 to correlate the solubility parameter (in MPa0.5) to the mass density (in g/cm3).

CRUDE OIL AND ASPHALTENE CHARACTERIZATION

$$\delta = 2.904 + 26.302\rho - 20.5618\rho^2 + 12.0425\rho^3 \quad (2.8)$$

$$\frac{F_{RI}}{\rho} = \frac{1}{\rho^\circ} = 0.5054 - 0.3951\rho + 0.2314\rho^2 \quad (2.9)$$

2.1.1.1.1 Viscosity

As mentioned previously, oil viscosity plays an important role in oil production, transportation, and oil recovery processes. Different correlations have been proposed to predict oil viscosity.

Beggs and Robinson (1975) proposed a correlation for the viscosity as a function of API gravity and temperature:

$$\log(\mu_{od} + 1) = a_1 + a_2\gamma_0 + a_3 \log T \quad (2.10)$$

where:

γ_0 is the oil gravity (°API)
T is the temperature (°F)
a_1, a_2, and a_3 are constants
μ_{od} is the viscosity of the dead oil (cP)

Later, (Egbogah and Ng 1990) found a significant difference between the experimental and calculated viscosity by the Beggs and Robinson correlation. For this reason, they added a new parameter—the pour point temperature—to the correlation which decreased the absolute error and modified the viscosity correlation.

$$\log(\mu_{od} + 1) = a_1 + a_2 T_p + a_3 SG + (a_4 + a_5 T_p + a_6 SG)\log(T - T_p) \quad (2.11)$$

CRUDE OIL AND ASPHALTENE CHARACTERIZATION

where:

m*od* is the viscosity of dead oil (cP)

SG is the specific gravity (°API)

T is the temperature of interest (K)

Tp is the pour point temperature (K)

Despite Equation 2.10 provides better results than Equation 2.11, the results are still not accurate enough, probably because oil behaves like a non-Newtonian liquid at high temperatures.

The most accurate viscosity model was proposed in by Alomair et al. (2016) as a function of the temperature and the density:

$$\ln \mu_{od} = \hat{a} + \frac{\hat{b}}{T^2} + \hat{c}\left(\rho_{od}^2\right) \ln \rho_{od} \qquad (2.12)$$

where:

m*od* (in cP) and r*od* (in kg/m3) are the viscosity and density of the dead oil

$\hat{a}, \hat{b}, \hat{c}$ ¡are constants that are defined based on two different temperature ranges: normal temperature 293 K–373 K and high temperature 373 K–433 K

The average absolute error for this model is 8%.

In this model, the density is calculated according to the Standing method as shown in Equation 2.12. Dr*p* and Dr*T* are the changes in density resulting from changes in pressure and thermal expansion (Alomair et al. 2016).

$$\rho = \rho_{sc} + \Delta\rho_p + \Delta\rho_T \qquad (2.13)$$

$$\Delta\rho_p = \left[0.167 + (16.181)10^{0.0425\rho_{sc}}\right]\left(\frac{P}{1000}\right) \qquad (2.14)$$

$$\Delta\rho_T = \left[0.013 + 152.4\left(\rho_{sc} + \Delta\rho_p\right)^{-2.45}\right](T - 520) - \left[8.1\left(10^{-6}\right) - (90.06)10^{-0.764\left(\rho_{sc} + \Delta\rho_p\right)}\right] \qquad (2.15)$$

CRUDE OIL AND ASPHALTENE CHARACTERIZATION

where:

P is the pressure (in bar)

T is the temperature (in °R)

r*sc* is the measured density at standard conditions (in kg/m3)

A more common way to find the density is the cubic equation of state (EOS) as explained in Section 4.2.3.1. It is also possible to calculate the viscosity of oil by applying the Vazquez and Beggs (1980) correlation.

$$\mu_o = \mu_{ob}\left(\frac{P}{BP}\right)^{\left[2.6P^{1.187}10^{(-3.9\times10^{-5}P-5)}\right]} \qquad (2.16)$$

The bubble point oil viscosity (m*ob*) can be calculated with the Chew and Connally (1959) correlations.

$$\mu_{ob} = A\mu_{od}^{B} \qquad (2.17)$$

$$A = 0.2 + \frac{0.8}{10^{(0.00081R_s)}} \qquad (2.18)$$

$$B = 0.43 + \frac{0.57}{10^{(0.00072R_s)}} \qquad (2.19)$$

Dead oil viscosity (m*od*) can be calculated by the Glaso (1980) correlation:

$$\mu_{od} = \left(\frac{3.141\times10^{10}}{T^{3.444}}\right)\log\gamma_o^{[10.313\log T-36.447]} \qquad (2.20)$$

where:

μ_o is the oil viscosity in cP
BP is the bubble point pressure in Psia
T is the temperature in °F
γ_o is the oil gravity in °API
R_s is the solution GOR in scf/STB

CRUDE OIL AND ASPHALTENE CHARACTERIZATION

2.1.1.1.1 Molecular Weight

Some other correlations between properties are reported in the literature, such as the one between the molecular weight and the viscosity (ASTM D2502 2014). In this method, the molecular weight of crude oil is calculated from kinematic viscosity measurements at 311 K (100°F) and 372 K (210°F). As limitations, this method can be only used for samples with mean relative molecular masses in the range from 250

to 700 g/mol and cannot be applied to crude oils that represent extremes of composition or with extremely narrow molecular weight.

2.1.2 Crude oil FraCtionation

Crude oil contains different hydrocarbon molecules ranging from very light components to very heavy ones, such as highly asphaltenic crudes (Powers 2014). The study of the crude oil components, species by species, is not feasible because of the

large amount of hydrocarbon types. Instead, a hydrocarbon group type analysis is commonly employed (Powers 2014).

Crude oil fractionation is important because there is a wide variation in the properties of the lightest crude oil to the heaviest one. For example, heavy oil has higher viscosity, asphaltene content, and metals in comparison to conventional oil.

There are three main methods of crude oil fractionation: based on the boiling point, based on chemical structure, and based on polarity.

2.1.2.1 Based on Boiling Point

The most common and oldest way to separate the crude oil into its fractions is based on the different boiling temperature of its components. This process is better known as *fractional distillation*.

In a distillation tower (Figure 2.2), the crude oil is heated up until the evaporation of the most volatile components. At the top of the column, the lighter products such as butane, other liquid petroleum gasses (LPG), gasoline blending components, and naphtha are recovered. The components with a midrange boiling point stay in the middle of the distillation tower such as jet fuel, kerosene, and distillates. At the bot-

tom of the column, at a temperature of 811 K (1000°F), the heaviest products such as residual fuel oil are recovered (Speight 2014).

The true boiling point (TBP) curve can be obtained based on the (ASTM D2892 2016). In this method, each component is separated at the same time. There is a

CRUDE OIL AND ASPHALTENE CHARACTERIZATION

large distillation column with 15 to 18 trays and a large reflux ratio of 5:1. The reboiler temperature and the distilled volume are recorded to plot the TBP curve. This method is time consuming and expensive in practice.

Another distillation method is the ASTM D86 (2016). This method is faster than the ASTM D2892 because there is no reflux. The sample is heated, and the vapors are collected and condensed while they are produced. The vapor temperature and the cumulative volume of liquid collected are recorded.

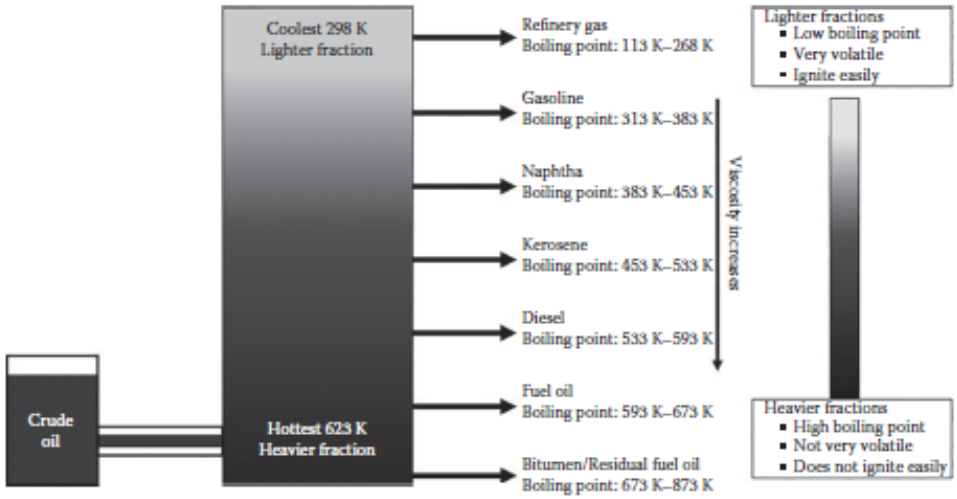

FIGURE 2.2 Crude oil distillation products. (Adapted from Aitani, A. M., *Encyclopedia of Energy*, 715–729, 2004.)

Because hydrocarbons start to crack when the temperature is higher than 613 K, another distillation method, the ASTM D1160 (2015), is used for heavy fractions. In this method, vacuum is applied (1–50 mmHg) instead of increasing the temperature to higher than 613 K.

The separation based on the boiling points fails when there are chemical reactions or extractive separations based on polarity (Hay et al. 2013).

2.1.1.1 Based on the Chemical Structure

The hydrocarbons present in crude oil are categorized into:

- Paraffins, that is, saturated hydrocarbons with straight or branched chains, but without any ring structure.
- Cycloparaffins (naphthenes), that is, saturated hydrocarbons containing one or more rings, each of which may have one or more paraffin side-chains (more

CRUDE OIL AND ASPHALTENE CHARACTERIZATION

correctly known as alicyclic hydrocarbons).

Paraffins and naphthenes together are called the saturates.

- Aromatics, that is, hydrocarbons containing one or more aromatic nuclei such as benzene, naphthalene, and phenanthrene ring systems that may be linked up with (substituted) naphthalene rings or paraffin side-chains.
- High-molecular weight and highly branched aromatic hydrocarbons are known as asphaltene molecules, which are normally between 4 and 20 wt% of crude oil.

The characterization based on the type of hydrocarbons is better known as *n*-paraffinisoparaffin, olefin, naphthene, and aromatic (PIONA) analysis (Lundanes and Greibrokk 1994). Because olefins are not usually present in crude oil; this analysis for crude oil is known as PNA analysis. This technique was developed to study the hydrocarbon mixture thermodynamic properties, and it is based on two approaches. The first approach uses a micropacked multi-column gas chromatography (GC) system. The aromatic fractions are separated by a polar-based column; the saturates with boiling point lower than 473 K are divided into paraffins and cycloalkanes (naphthenes) by using a molecular-sieve (13Å) column, and the branched alkanes are separated from *n*-alkanes by using a molecular-sieve (5Å) column. This method is time consuming (the analysis time for each test is 1–5 hours), but it is possible to separate the paraffins/naphthenes/aromatics (PNA) and paraffins/isoparaffins/naphthenes/aromatics (PIPNA) (Lundanes and Greibrokk 1994).

The second approach is based on the use of a single high-resolution GC capillary column. In this method, the different fractions are identified and quantified by the use of detectors such as flame ionization detection (FID), electron ionization (EI), and mass spectrometry (MS) (Lundanes and Greibrokk 1994). The fluorescent indicator adsorption detector (FIA) is also used for the determination of aromatic (A), olefinic (O), and saturate (S). PIONA analysis is performed by capillary GC, which uses a non-polar bonded capillary column. The hydrocarbons are separated into as many peaks as possible. Each peak can be identified based on the number of carbons

CRUDE OIL AND ASPHALTENE CHARACTERIZATION

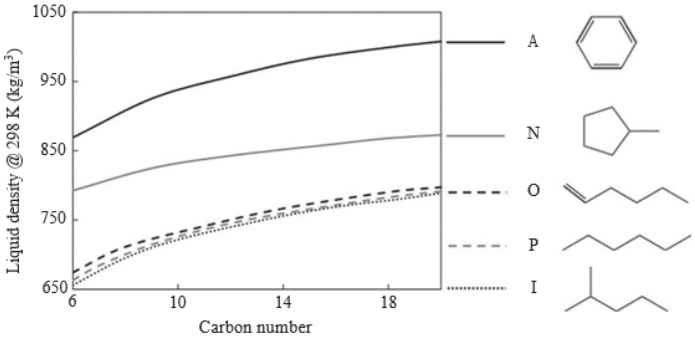

FIGURE 2.3 Crude oil fractionation based on PIONA analysis. (From Hay, G. et al., *Energy Fuels*, 27, 3578–3584, 2013.)

and hydrocarbon type. The disadvantages of this method are its long time of analysis and vulnerability to human error (Shimadzu excellence in science 2017).

Hay et al. (2013) developed a new PIONA characterization technique, based on the molecular structure of component groups. In this method, it is assumed that a group with the same carbon number has an average value of physical properties with different thermodynamic properties. This assumption introduces some error, as in the case of 1-butene, 2-butene, and iso-butene. Even if these three compounds have the same four carbons, their physical properties vary significantly (Hay et al. 2013). As an example (Aitani 2004), Figure 2.3 shows how the density changes in the PIONA molecular structure versus different carbon numbers at 298 K. Also, it shows the different groups of PIONA molecular structure with six carbon atoms.

2.1.1.1 Based on Polarity

Saturates, **a**romatics, **r**esins and **a**sphaltenes (SARA) analysis of crude oil is a physical fractionation method based on the solubility and polarity of the hydrocarbon components in various solvents and adsorbent materials. It is the most com- monly used method for crude oil characterization (Powers 2014). It separates the crude oil components based on their solubility and polarity into four parts. Each of these subfractions group compounds that share similar characteristics (YingShi et al. 2012). Saturates are *n*-paraffins, iso-paraffins, and cyclo-paraffins. Aromatic hydrocarbons are derivatives of benzene. Resins and asphaltenes are made of rela- tively high-molecular-weight, more polar, polycyclic and aromatic ring compounds with some aliphatic side chains. Jewell et al. (1972) started working on SARA analysis in 1972.

There are three main approaches to separate crude oil into SARA fractions. The first is the thin-layer chromatography with flame ionization detection (TLC-FID) or Iatroscan. The TLC-FID method uses silica-coated rods to carry out the chromato- graphic separation of the components, which are later identified by a flame ionization detector (Pearson and Gharfeh 1986). There are several advantages related to

CRUDE OIL AND ASPHALTENE CHARACTERIZATION

TLC-FID: Asphaltenes do not have to be removed from the sample and, in fact, they are also quantified; it uses a very small amount of sample (about 10 μL of sample per test); and the results are highly reproducible. However, a significant volume of volatile material, that contains saturates and aromatics, can be lost during the analysis meaning that this test is not viable for analyzing medium or light crude oils (Aske 2002; Jiang et al. 2008; Fan et al. 2002). Two more disadvantages are that loading the sample into a small spot can cause overloading and channeling at the origin of the silica-coated rods, and because resins have polar substituents like asphaltene, some of them might exist along with the asphaltene precipitated part. This causes some challenges to analyze the signals and to differentiate between the resins and asphaltenes signals (Pearson and Gharfeh 1986). Because of the possibility of having resins inside the asphaltenes fraction, the reported asphaltenes content may be different from the other methods.

The second method is a clay-gel adsorption-based chromatographic method described in the ASTM D2007 (2007). This system uses two columns filled with clay and silica gel. After asphaltene extraction, the remaining part called *maltene* (saturates, aromatics, and resins) is added to the columns. Resins are adsorbed ontattapulgus clay, whereas the aromatics are adsorbed onto the silica gel. The remaining saturates elute directly and are collected in a flask. The polar solvents toluene and toluene/acetone are used to dissolve and separate the aromatics and resins. This method requires large quantities of solvent and crude oil sample is time consuming and difficult to automate (Aske 2002). Fan and Buckley (2002) showed that there were some losses in the ASTM method that belonged to saturates fraction.

The third method is based on a high-pressure liquid chromatography (HPLC) analysis, which uses two columns of NH2-bonded silica to separate the de-asphalted crude oil (also known as *maltene fraction*) based on the polarity and solubility of the different components.

Asphaltenes are removed from the oil according to the IP-143 method (ASTM D6560 2005) and the remaining components are separated by HPLC. Saturates pass through the column without adsorption and are detected by a refractive index detector. Next, the aromatics fraction is detected by an UV detector. The resins stay adsorbed in the column and have to be eluted with a more polar solvent. A detector recognizes the different maltene fractions, and the various peaks are then related to the corresponding saturate, aromatics, and resins fractions by a calibration curve. Although HPLC techniques are faster and more reproducible, the operational costs are higher compared to a simple chromatography method (Fan and Buckley 2002). Also, a specific method is needed for each type of sample because there is no universal HPLC method for all kinds of hydrocarbons (Woods et al. 2008).

Nowadays, there are different methods proposed for SARA analysis based on the three main methods described. Sieben et al. (2017) proposed a new method for SARA analysis named microfluidic SARA analysis (Maze). The asphaltene separation is based on the ASTM D7996 (2015). Then, the maltene separation is done by a miniaturized chromatographic column. Figure 2.4 shows the schematically process of SARA analysis by Maze.

CRUDE OIL AND ASPHALTENE CHARACTERIZATION

The maltene passes through the mini-column and the mobile phase, which the solvent washes the column continually. Saturates content is calculated by measuring

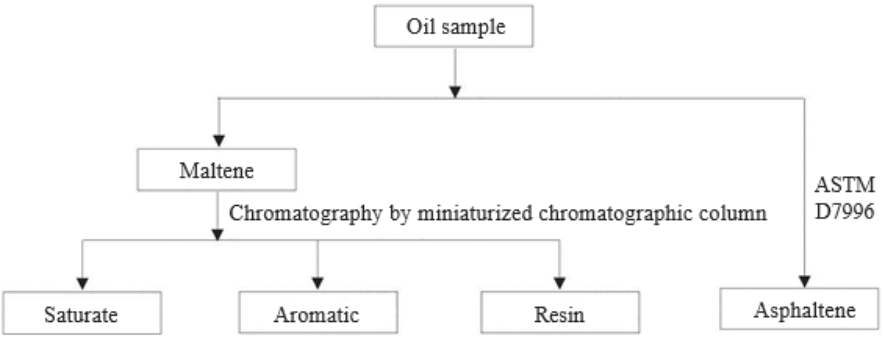

FIGURE 2.4 Maze method for SARA analysis. Part 1. Asphaltene content measurement by the microfluidic chip. Part 2. Maltene measurement by miniaturized chromatographic column. (Sieben, V. J. et al., *Energy & Fuels*, 31(4), 3684–3697, 2017.)

the refractive index of the sample. For resins and aromatics, the optical absorbance is measured by a spectrometer to find the content of each fraction. The advantages of this new method are that it is automated and the results are repeatable and reproduc- ible (Sieben et al. 2017).

Another chromatographic-based method is known as automated chromatographic columns system for maltenes analysis. In this method, the asphaltene separation is done based on the IP-143 method (ASTM D6560 2005). Maltene analysis is performed in an automated chromatography column. This system consists of two chromatographic columns: one of them containing silica gel and the other one containing Attapulgus clay as shown in Figure 2.5.

The process is carried out in two steps: during the first step, saturates, aromat- ics, and resins are separated by selective adsorption into the clay and the silica gel columns, and during the second step, these components are desorbed and recovered. Both steps are described here.

During the adsorption step, all the valves on the solid brown line are open (Figure 2.5a), and the rest of them remained closed during the whole adsorption process. During this step, a solution with known concentration of a mix of satu- rates, aromatics, and resins in *n*-heptane is prepared and placed in the solution container (the maltene amount is calculated by subtracting oil weight from the asphaltene content). The HPLC pump is then turned on, and the solution is fed into the clay column in which only resins is adsorbed. Then, the solution passes through the silica column where the aromatic compounds are adsorbed. The solution continues its path and is collected in the effluent container. After the whole solution passes through the columns, the effluent, which contains the saturates fraction, is collected. Heptane evaporates from the solution, at approximately 371.15 K, to quantify the amount of saturates (Rezaee et al. 2017a).

CRUDE OIL AND ASPHALTENE CHARACTERIZATION

After completing the first step, the columns are washed with the appropriate solvent(s) to recover resins and aromatics fractions separately. For the clay column

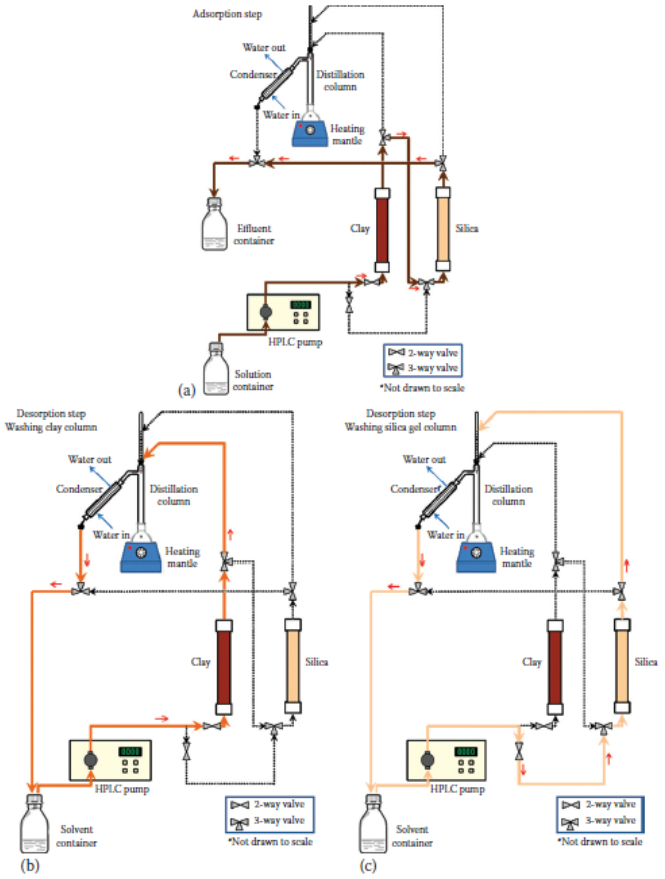

FIGURE 2.5 Automated chromatographic column: (a) Adsorption process, (b) resin desorption step, and (c) aromatic desorption step. (From Rezaee, S. et al., Crude oil characterization, fractionation and SARA analysis, In Preparation, 2017a.)

CRUDE OIL AND ASPHALTENE CHARACTERIZATION

wash, the valves on the solid line in Figure 2.5b are open, and the rest of them remain closed. For the silica gel column wash, the valves on the solid line in Figure 2.5c are open, and the rest of the valves are closed.

The solvent container is filled with dichloromethane (DCM) (50 vol%) and acetone (50 vol%) for the clay wash and with DCM (62 vol%) and hexane (38 vol%) for the silica wash. The solvent is then pumped through the columns. When passing through

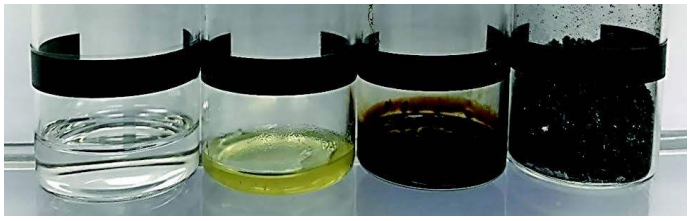

FIGURE 2.6 SARA separation by automated chromatographic columns. (From Rezaee, S. et al., Crude oil characterization, fractionation and SARA analysis, In Preparation, 2017a.)

the columns, the solvent dissolves the resins and aromatics from the clay and the silica gel media, respectively. The solution continues its way to the distillation system.

The solution of solvent and resins leaving the clay column is fed into the distillation column from the top side and is collected in a round-bottomed flask. The heating mantle maintains a temperature of around 321 K (118°F). At this temperature, the solvent evaporates and leaves the column as a vapor without burning the resins. At the top of the distillation column, there is a thermometer, which should always

indicate a temperature very close to the boiling point of the solvent to ensure that the vapor is pure solvent. Solvent as a vapor continues its path across the condenser. Cold water is used to condense the vapor into a pure liquid solvent, which is collected in the solution container. The same distillation process is followed for the aromatics leaving the silica gel column. Once the columns are completely cleaned with no resi- dues of resins or aromatics, the distillation is stopped, and both resins and aromatics are dried in an oven and are then weighed. Figure 2.6 shows the crude oil and the SARA fractions separated from the crude oil by the automated chromatographic columns system (Rezaee et al. 2017a).

2.1 ASPHALTENES

2.1.1 ComPosition and ChemiCal struCture

CRUDE OIL AND ASPHALTENE CHARACTERIZATION

As described in Chapter 1, asphaltenes consist primarily of carbon, hydrogen, nitrogen, oxygen, and sulphur, as well as trace amounts of vanadium, nickel, and other metals. It is practically undisputed that a molecule of asphaltene consists of a number of polyaromatic clusters with side aliphatic chains and other functional groups as previously shown in Figure 1.2. 13C NMR studies suggest that the clusters are formed by pericondensed aromatic groups instead of catacondensed groups (Mullins 2008).

It has been found by X-Ray absorption near-edge structures (XANES) that nitrogen is mainly present in the aromatic structure as pyrrolic nitrogen followed by pyri- dinic nitrogen (Mitra-Kirtley et al. 1993). Oxygen has been chemically identified as aliphatic hydroxyl groups but also in the form of aliphatic ketones, quinones, ethers, esters, carboxylic acids, and in combination with sulfur (Moschopedis and Speight 1976). By combustion and XANES tests, it has been determined that sulfur is most commonly found as part of thiophenes, sulfides, and sulfoxides (Mitra-Kirtley et al.

1999; Pomerantz et al. 2013). Nickel and vanadium are the most abundant metals in crude oil with concentrations reaching up to 340 ppm of nickel and 1580 ppm of vanadium. They can be found as porphyrins (organometallic complexes) or as high molecular weight complexes associated with asphaltenes (Barwise 1990).

In a larger scale, asphaltenes are defined according to their solubility in selected solvents, that is, *n*-alkanes and aromatic solvents such as toluene; in this way, *n*-C5+ (or simply C5+) asphaltenes are those that were precipitated with *n*-pentane, and *n*-C7+ are those precipitated with *n*-heptane, etc.

Even if asphaltenes have a similar solubility, their chemical characteristics can be very different (Luo et al. 2010). It is believed that asphaltenes contain up to 105 differ- ent types of molecules without repeating a molecular unit (Wiehe and Liang 1996).

A great variety of analytical techniques has been used to investigate the structure of asphaltenes. In this section, we will describe some of the most practical methods to obtain the elemental and chemical composition and the thermal decomposition pattern.

2.1.1.1 Determination of the Elemental Composition

To have a better understating of the chemical structure of crude oil and its fractions, elemental analysis experiments are performed. Asphaltenes mainly consist of hydro- carbons along with small amounts of heteroatoms such as oxygen, nitrogen, sul- fur, and traces of metals including, nickel, vanadium, and iron. However, crude oils from different origins have different asphaltene content and elemental compositions. Ancheyta et al. (2002) carried out the elemental compositions along with asphal- tene content of three different crude oils including Maya, Isthmus, and Olmeca. The results are tabulated in Table 2.2

As demonstrated, the content of heteroatoms in asphaltene fractions is higher than the crude oil itself, which suggests that the heteroatoms are likely to concen- trate in asphaltene fraction of crude oil. Moreover, the C7+ fractions have lower hydrogen-to-carbon (H/C) ratio and higher heteroatoms and metals content than

CRUDE OIL AND ASPHALTENE CHARACTERIZATION

the C5+ fraction. This observation is in agreement with asphaltenes' solubility behavior, which indicates that heptane insoluble asphaltenes (C7+ fraction) are less paraffinic, heavier and more polar than C5+ asphaltenes.

In a similar study, Gaweł et al. (2014) reported the compositional analysis of nine different crude oils alongside with their subsequent SARA fractions includ- ing, saturates, aromatics, resins, and asphaltenes. As expected, saturates have the highest H/C ratio followed by aromatic, resins, and asphaltenes. As it will be discussed later in this chapter, the H/C ratio can be used as an indication of the extent of ring condensation and a correlation between this ratio and the aromaticity factor can be derived. In general, the overall heteroatoms content of asphaltenes is higher than other fractions of crude oil. The results show that the distribution of sulfur is approximately even among the aromatic, resin, and asphaltene fractions. There is no sign of sulfur in saturates, meaning most of the sulfur exists within the poly- cyclic aromatic compounds or in alkyl sulfoxide groups attached to a polycyclic aromatic core (Sharma et al. 2002). Moreover, the oxygen and nitrogen contents of asphaltenes and resins are significantly higher than other fractions, which explain

CRUDE OIL AND ASPHALTENE CHARACTERIZATION

TABLE 2.2
Elemental Analysis of Three Crude Oils and Their Asphaltene Fractions

Origin	Maya			Isthmus			Olmeca		
Elemental Analysis (wt%)	Crude Oil	C_{5+} Asphaltene	C_{7+} Asphaltene	Crude Oil	C_{5+} Asphaltene	C_{7+} Asphaltene	Crude Oil	C_{5+} Asphaltene	C_{7+} Asphaltene
Carbon	83.96	81.23	81.62	85.4	83.9	83.99	85.91	86.94	87.16
Hydrogen	11.8	8.11	7.26	12.68	8	7.3	12.8	7.91	7.38
Oxygen	0.35	0.97	1.02	0.33	0.71	0.79	0.23	0.62	0.64
Nitrogen	0.32	1.32	1.46	0.14	1.33	1.35	0.07	1.33	1.34
Sulfur	3.57	8.25	8.46	1.45	6.06	6.48	0.99	3.2	3.48
H/C Atomic Ratio	1.687	1.198	1.067	1.782	1.144	1.043	1.788	1.092	1.016
Metals (wppm)									
Nickel	53.4	269	320	10.2	155	180	1.6	82	158
Vanadium	298.1	1217	1509	52.7	710	747	8	501	704

Source: Ancheyta, J. et al., *Energy Fuels*, 16, 1121–1127, 2002.

CRUDE OIL AND ASPHALTENE CHARACTERIZATION

the higher polarity of asphaltenes and resins. Additionally, the metal content of asphaltenes is much greater than other fractions. Metals in asphaltenes are present in mainly two forms. First, metals can exist in the form of metalloporphyrins, which are defined as heterocyclic macrocycle organic compounds in which metals can bind to interior ligands to form complexes. Second, metals can also be present directly in the aromatic core of asphaltenes through defects (Mullins and Sheu 1999).

The metal content of asphaltenes is usually measured by atomic absorption or mass spectroscopy. To do so, the sample needs to be free of organic components. The organic part of the sample is removed by a heat treatment (calcination) method followed by acidic digestion using concentrated (70 wt%) nitric acid. The sample is diluted with DI

water to reach a stock solution of approximately 2 wt% nitric acid. A blank sample is

also prepared to account for all the impurities and trace amount of metal ions present

or entered into the solution during the digestion and dilution processes. Inductively coupled plasma mass spectroscopy (ICP-MS) is commonly used for detection and quantification of metals in solutions with a detection limit of as low as one part in 1015. During the analysis, the solutions are pumped to the nebulizer one by one. A spray of the sample enters the plasma torch section of the instrument. The highly energetic plasma, made of argon ions, is responsible for the ionization of the elements present in the sample. The generated ions are separated based on their mass-to-charge ratio by electric and magnetic fields. Finally, the separated ions are detected and con- verted into electrical signals, which are processed by the software (Thomas 2016).

X-ray photoelectron spectroscopy (XPS) is a powerful surface characterization tool, mainly used in this study for identification and quantification of elemental composition and chemical state of the elements present at the surface of samples. It is relatively easy to use and requires minimal sample preparation. XPS is able to detect and quantify the composition of elements from the 10 nm outer layer with an atomic number of greater than three. In XPS, the sample is subjected to irradiation by a focused beam of X-rays under high vacuum. The interaction between the X-rays with the molecules of the sample results in the ejection of electrons from the first layers (10 nm). The escaped electrons are further detected by the detector and their kinetic energy is measured using an electron energy analyzer. Because the energy of the electrons that are bound to an atom is discrete and unique depending on the electron configuration of the atom, the binding energy of the ejected electron is a character- istic of the electron and its respective element. The number of ejected electrons and their binding energy values can be used for identification and quantification of the elements, respectively.

Enayat et al. (2017a) performed XPS analysis on C5+ asphaltenes from crude oil A, which results are shown in Figure 2.7. This figure includes a survey spectrum along

CRUDE OIL AND ASPHALTENE CHARACTERIZATION

with high-resolution spectra of the detected elements in the sample. The chemical state of each atom present in the sample is investigated by deconvolution of peaks into subpeaks using curve fitting. All the curve fittings are performed by the PHI Multipack software using a Gaussian-Lorentzian function. The atomic concentrations accompanied by relative binding energies of each peak and chemical assignments are provided in Table 2.3.

In Figure 2.7b, the carbon 1s spectrum is composed of three subpeaks assigned to aliphatic or aromatic carbon bonds (C–C/C–H), carbons single bonded to oxygen

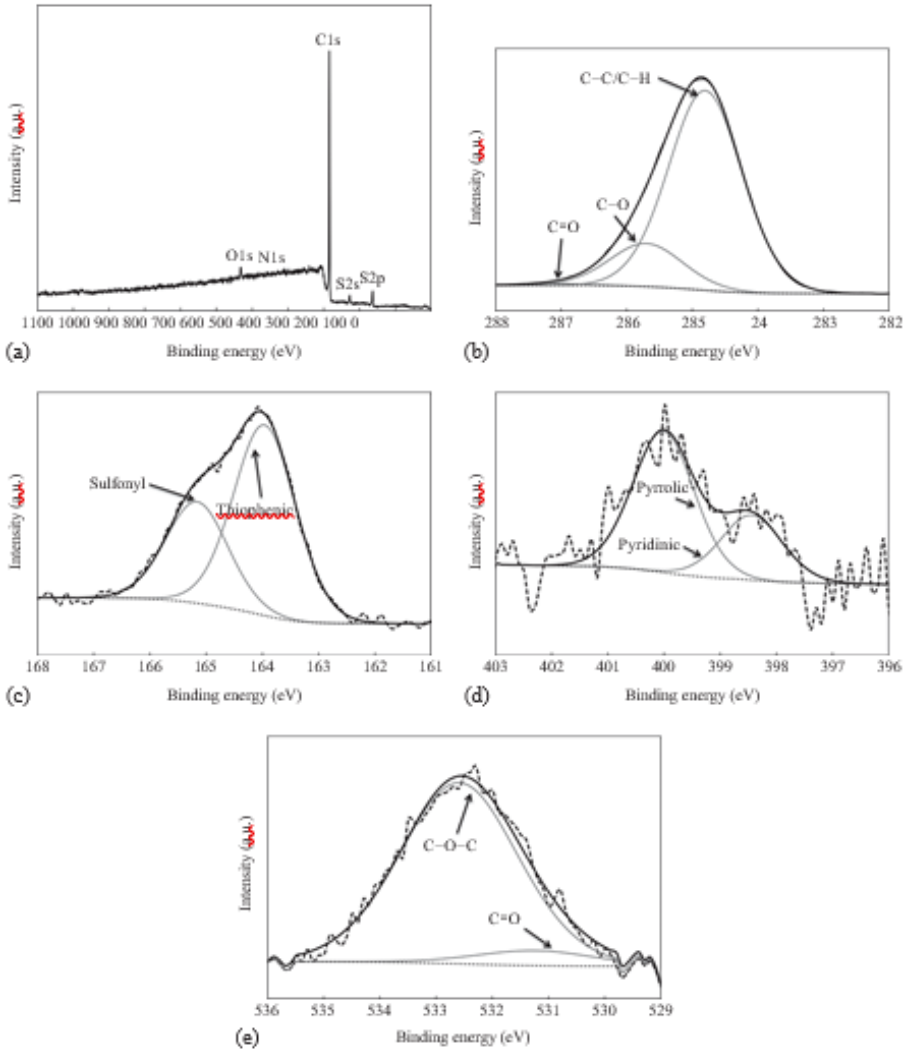

FIGURE 2.7 XPS analysis of C_{5+} Asphaltene from crude oil A: (a) survey spectrum High resolution spectra with fitting of (b) C 1s, (c) S 2p, (d) N 1s, and (e) O 1s. (Enayat, S. et al., Development of asphaltene coated melamine sponges for water-oil separation, In Preparation, 2017a.)

CRUDE OIL AND ASPHALTENE CHARACTERIZATION

(C–O), and carbons in carbonyl functional groups (C=O) with the binding energies of 284.76, 285.68, and 286.93 (eV), respectively. The deconvolution of the sulfur 2p spectrum, Figure 2.7c, reveals two peaks positioned at 163.95 and 165.21 (eV), which

are attributed to thiophenic and sulfonyl groups, respectively. Similarly, two peaks are chosen to fit the nitrogen 1s spectrum; the first peak at 398.44 eV is assigned to pyri- dinic moieties, whereas the second one (400.01 eV) corresponds to pyrrolic groups. Finally, the oxygen 1s peak is divided into two subpeaks, corresponding to ether/ hydroxyl (532.56 eV) and carbonyl functional groups (531.18 eV) (Enayat et al. 2017a).

TABLE 2.3

Summary of Atomic Concentration and Spectral Features of Elements in C_{5+} Asphaltene from Crude Oil A

Element	Atomic Concentration (%)	Binding Energy (eV)	FWHM (eV)	Area	Area Percentage	Functional Group
Carbon	93.18	284.76	1.34	15314	81.45	C—C/C—H
		285.68	1.34	3273	17.41	C—O
		286.93	1.34	215	1.15	C=O
Oxygen	2.98	531.18	2.49	117	8.14	C=O
		532.56	2.49	1316	91.86	C—O
Nitrogen	0.97	398.44	1.29	68	32.42	Pyridinic
		400.01	1.29	142	67.58	Pyrrolic
Sulfur	2.86	163.95	1.34	882	64.43	Thiophenic
		165.21	1.34	487	35.57	Sulfonyl

Source: Enayat, S. et al., Development of asphaltene coated melamine sponges for water-oil separation, In Preparation, 2017a.

2.1.1.1 Determination of the Chemical Structure

2.1.1.1.1 Fourier Transform Infrared and Raman Spectroscopy

Fourier transform infrared (FTIR) spectroscopy is an analytical technique used to identify organic and some inorganic materials. It is based on the absorption of mid-infrared radiation, located between the wavelengths of 2.5 μm (4000 cm−1) and 25 μm (400 cm−1) of the light spectrum. When exposed to infrared radiation, the different bonds in the molecule selectively absorb radiation of specific wavelengths, which changes their dipole moment and, therefore, the excited vibrational state. The wavelength of light absorbed by a specific bond is a function of the energy difference between the basal and excited vibrational states, therefore, the wavelengths absorbed by the sample are a characteristic of its molecular structure. The result, the FTIR spectrum, is a plot of absorbance (or transmittance) of radiation versus wavenumber in cm−1, where wavenumber is the

CRUDE OIL AND ASPHALTENE CHARACTERIZATION

reciprocal of the wavelength (Silverstein et al. 2014). Table 2.4 shows the main adsorption peaks for the components of crude oil.

Figure 2.8a shows an example of the FTIR spectrum of C5+ asphaltenes from a light oil. The spectrum was recorded in a Nicolete FTIR Infrared Microscope with 64 scans and a 4 cm−1 resolution at Rice University. Not all absorption bands are visible because of the small proportion of some functional groups in the asphaltene molecule.

The fact that the functional groups can be determined and their absorbance of radiation can be recorded has been used to determine some characteristics of the crude oil and asphaltenes, that is, the amount of asphaltenes in an oil (Wilt et al. 1998), the paraffinicity and aromaticity of asphaltenes (Castro 2006; Riley et al. 2016), the existence and relative proportion of heteroatomical functional groups versus aliphatic compounds, and the degree of condensation in the polyaromatic compounds (Asemani and Rabbani 2016; Permanyer et al. 2007). These parameters have been used to characterize the geochemical evolution and the correlation of oils

CRUDE OIL AND ASPHALTENE CHARACTERIZATION

TABLE 2.4
Absorption Bands (FTIR) for the Different Components of Crude Oil

Functional Group	Chemical Structure	Absorption Bands, FTIR (cm^{-1})
Alkanes and cycloalkanes	CH_{3-}, $-CH_{2-}$	2950–2850 1470–1350 725–720
Aromatics		3080–3030 1625–1575 1525–1450
Pyrrolic Nitrogen	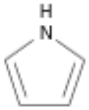	3500–3400 1590–1560 1540–1500
Pyridinic Nitrogen	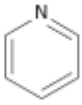	3450–3200 1610–1360
Alcohols	R-OH	3550–3200 1250–970
Ketones	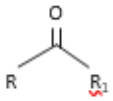	1750–1680
Quinones	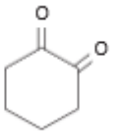	1650–1630
Ethers	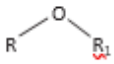	1150–1085
Esters	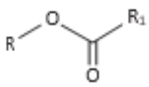	1750–1735
Carboxylic acids	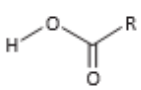	3550–2500 1780–1710
Sulfoxides		1225–980

(Continued)

CRUDE OIL AND ASPHALTENE CHARACTERIZATION

TABLE 2.4 (*Continued*)
Absorption Bands (FTIR) for the Different Components of Crude Oil

Functional Group	Chemical Structure	Absorption Bands, FTIR (cm^{-1})
Thiophenes		710–570
Sulfides		710–570

Source: Data from Silverstein, R. M. et al., *Spectrometric Identification of Organic Compounds*, John Wiley & Sons, Hoboken, NJ, 2014.

from different locations as well as to model the behavior of asphaltenes in crude oil (Asemani and Rabbani 2016; Permanyer et al. 2005, 2007).

Infrared active molecules are not Raman active. Hence, Raman spectroscopy is a good complement to FTIR in providing additional information to clarify the molecular structure. Raman spectroscopy is not an absorption-based technique but a technique based on light scattering. A monochromatic light, usually from a laser in the visible, near infrared or near ultraviolet range, is irradiated onto a sample. Part of this light is absorbed, and the other part interacts with the polarizability of the sample by inducing a dipole moment. The radiation is emitted by the induced dipole moment at a different frequency and it is called *Raman scattering* (Lewis and Edwards 2001; Person and Zerbi 1982; Simanzhenkov and Idem 2003). The Raman spectrum is a plot of the intensity of Raman scattered radiation as a function of the frequency difference from the incident radiation (in units of cm−1). This difference is called the *Raman shift*. Figure 2.8b shows an example of the Raman Spectrum of asphaltenes.

Raman spectrometry is widely used in the study of commercial graphite-like or diamond-like polycyclic aromatic hydrocarbon (PAH) compounds, and therefore is suitable to be applied to the study of the solid structure of asphaltenes (Bouhadda et al. 2007). As seen in Figure 2.8b, the two frequencies of the Raman bands for asphaltenes are located at around 1600 and 1350 cm−1. The first band (band G) is as a result of the stretching vibration of sp2 carbons in an ordered polycondensed aromatic structure. The band at 1350 cm−1, or band D1, represents the disorder in the aromatic structure induced by the in-plane defects and the heteroatoms located at the periphery of the microcrystalline structure of the asphaltene

CRUDE OIL AND ASPHALTENE CHARACTERIZATION

molecules (Riedeman et al. 2016). Based on these two bands, several researchers have devel- oped correlations to calculate the size of the fused-ring system and the number of rings contained on it.

Abdallah and Yang (2012) determined the average aromatic sheet size of asphaltenes to be between 1.52 and 1.88 nm of size and to contain seven to eight

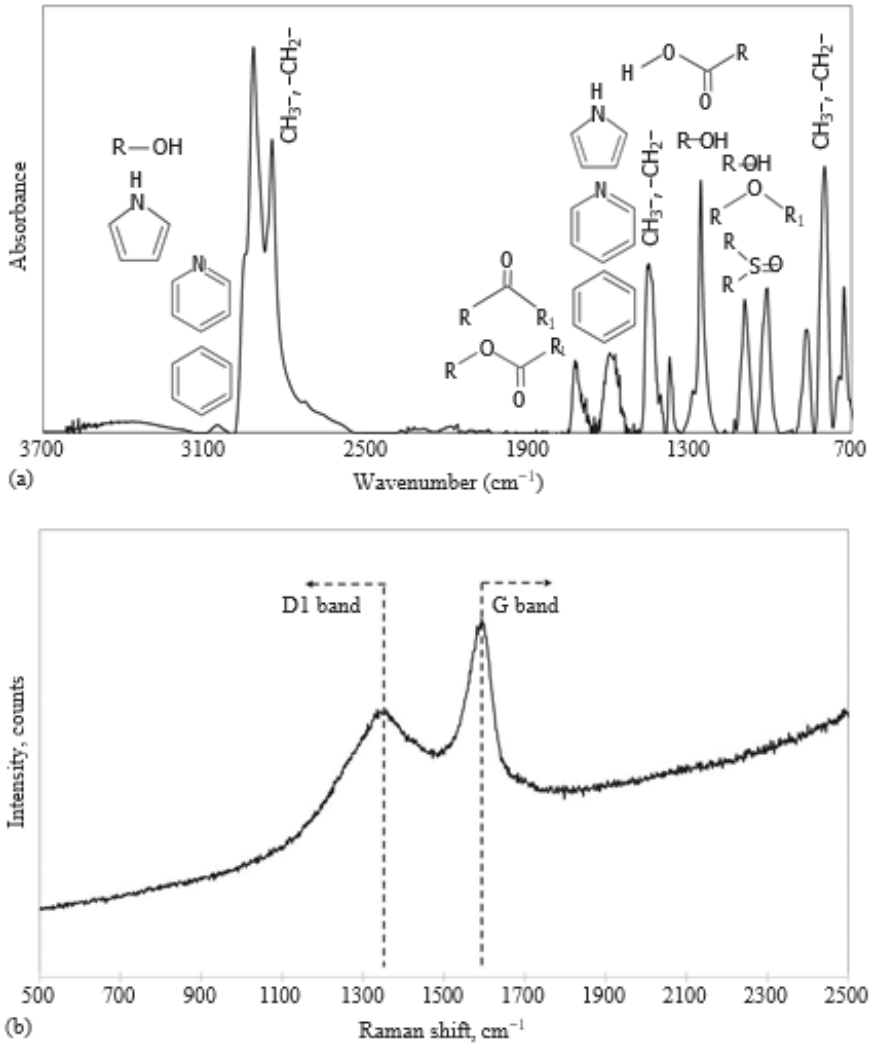

FIGURE 2.8 Typical (a) FTIR and (b) Raman spectra of asphaltene molecules. (Courtesy of Rezaee and Doherty, Rice University.)

CRUDE OIL AND ASPHALTENE CHARACTERIZATION

aromatic rings. Riedeman et al. (2016) determined that the average aromatic size sheet is 21Å by following the Raman bands at 1350, 1580, and 1600 cm−1, respectively; Bouhadda et al. (2007), determined the aromatic sheet diameter to be 11–17Å by using a combination of Raman spectroscopy and X-Ray diffraction. Wu and Kessler (2015) calculated that approximately six to seven aromatic rings are fused together during the formation of the polyaromatic core of the asphaltene molecules.

2.1.1.1.1 Nuclear Magnetic Resonance Spectroscopy

Nuclear magnetic resonance (NMR) is a property of the nucleus of an atom, related to what is known as nuclear spin (the nucleus acting like a miniature bar magnet). When the atomic nucleus spins, it generates a magnetic field, and if an external

magnetic field is present, the nucleus aligns either with or against the field of the external magnet. The difference between the energy of the aligned and the misaligned nuclei depends on the applied magnetic field; the greater the strength of the magnetic field, the larger the energy difference. If radio waves are applied, the nuclei in the lower energy state absorb the energy and jump to the higher energy state and then, they undergo relaxation and return to the original energy state. When relaxing, electromagnetic signals are emitted at determined frequencies that depend on the difference in energy. These signals are recorded on a graph of intensity versus signal frequency (or chemical shift, in ppm). The most common nuclei analyzed by NMR are 1H, 13C, 15N, and 31P; however, only 1H and 13C are used in asphaltene char-

acterization. Figure 2.9 shows the NMR spectra of C5+ asphaltenes of crude oil S6. NMR is mainly used in the crude oil industry to calculate the aromatic and ali-

phatic carbon fractions, the alkyl-substituted, and the unsubstituted aromatic carbons of asphaltenes (Silva et al. 2004; Östlund et al. 2004; Castro 2006). A better discus- sion on the methodology to perform these calculations can be found in Section 2.2.2.1.

2.1.1.2 Determination of Thermal Decomposition Patterns

The shortage of light and easy accessible crude oil has led to an increase in the refining and conversion of bitumen or heavy crude oil, which is done by different processes such as coking, hydroconversion, and catalytic cracking. Asphaltene, as one of the main components of bitumen or heavy crude oil, has a high tendency to coke formation at high temperatures. If the coking process takes place without the presence of oxygen it is called *pyrolysis*. The asphaltene sample goes into several changes during the coke formation. The results after carbonization indicate that H/C ratio as well as the ratio of aliphatic to aromatic carbons decreases (Enayat et al. 2017b; Barneto et al. 2016; Savage et al. 1988). Based on the results, several reac- tions have been proposed for asphaltene pyrolysis. According to Savage et al. (1988), the high temperature causes some weaker bonds between aliphatic chains to break down. This leads to the formation of some relatively light hydrocarbons, along with H2S, leaving the reactor in the form of gas. Moreover, the generated

CRUDE OIL AND ASPHALTENE CHARACTERIZATION

radicals can attach to each other and create aromatic functional groups. Ultimately the naph- thenic cycles lose their hydrogen and along with other aromatic rings form bigger aromatic cores in the molecular structure of asphaltenes (Zhao et al. 2010).

Studying the thermal behavior of different asphaltene fractions in the presence of both oxygen and an inert gas such as argon or nitrogen is necessary to have a better understanding of the thermal stability of asphaltenes (Enayat et al. 2017b). In a general thermogravimetric analysis (TGA), a known amount (2–5 mg) of a solid sample is placed in an alumina or a platinum pan, depending on the maximum temperature of the analysis. Then, the pan is placed in a small cylinder that acts as a furnace. The weight of the sample is constantly measured as it gets heated with an average rate of 10 K–20 K/min. Different carrier gasses can be used in the experiment. In the case of an inert gas like nitrogen or argon, the material undergoes thermal degradation or pyrolysis. However, in the presence of oxygen, oxidation cracking is the dominant phenomenon (Enayat et al. 2017b).

As shown in Figure 2.10 pyrolysis of asphaltene mainly consists of two periods: before 673 K, in which, only light and volatile components of asphaltene start to

CRUDE OIL AND ASPHALTENE CHARACTERIZATION

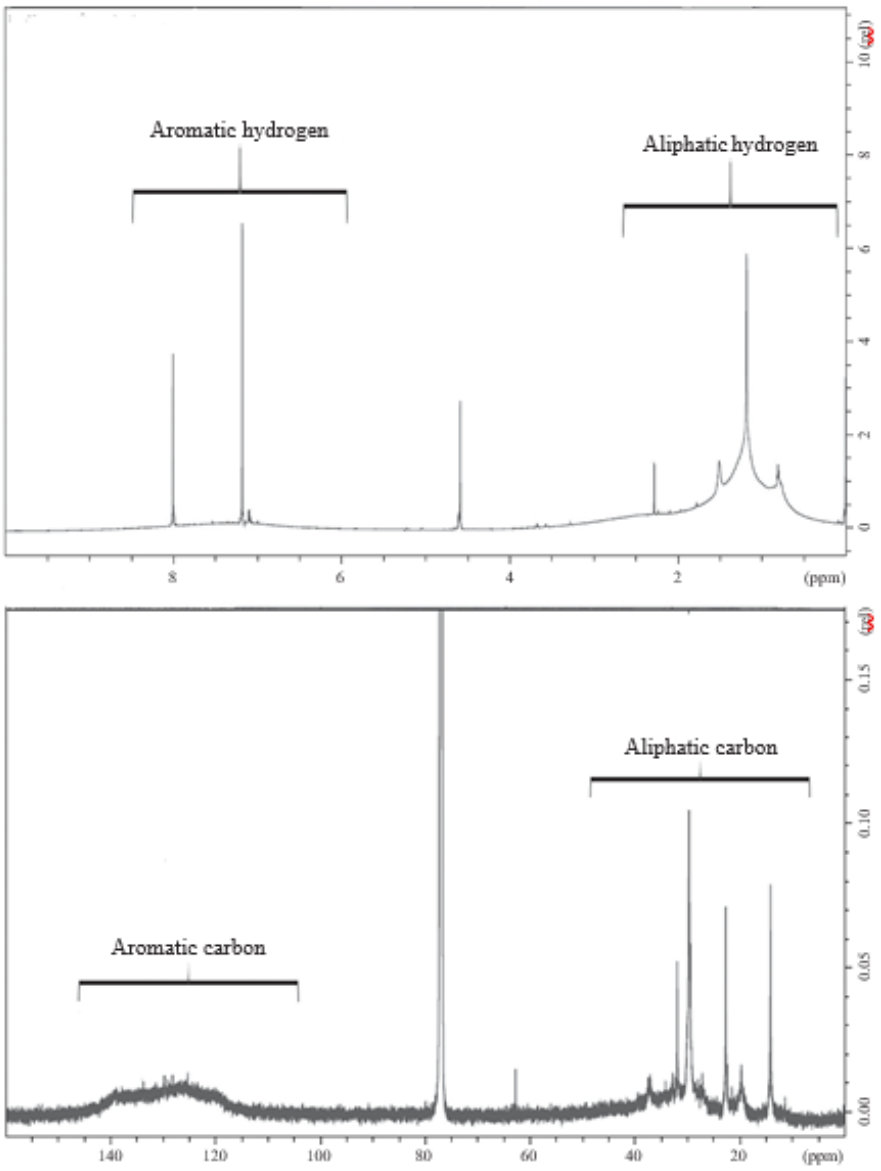

FIGURE 2.9 Typical ^{1}H and ^{13}C of asphaltenes. (From Rezaee, S. et al., Asphaltene characterization, fractionation and chemical properties, In Preparation, 2017b.)

CRUDE OIL AND ASPHALTENE CHARACTERIZATION

come out. This loss only accounts for less than 5% of the initial mass. At temperatures higher than 673 K, depending on the type of asphaltene and fraction, the sample under- goes thermal degradation and loses about 40%–80% of its initial mass. Most of the mass loss happens between 673 K–773 K and once the temperature reaches 773 K,

the weight loss curve becomes a plateau. In the case of having oxygen in the system, the same procedure happens until around 763 K–773 K, at which the combustion of

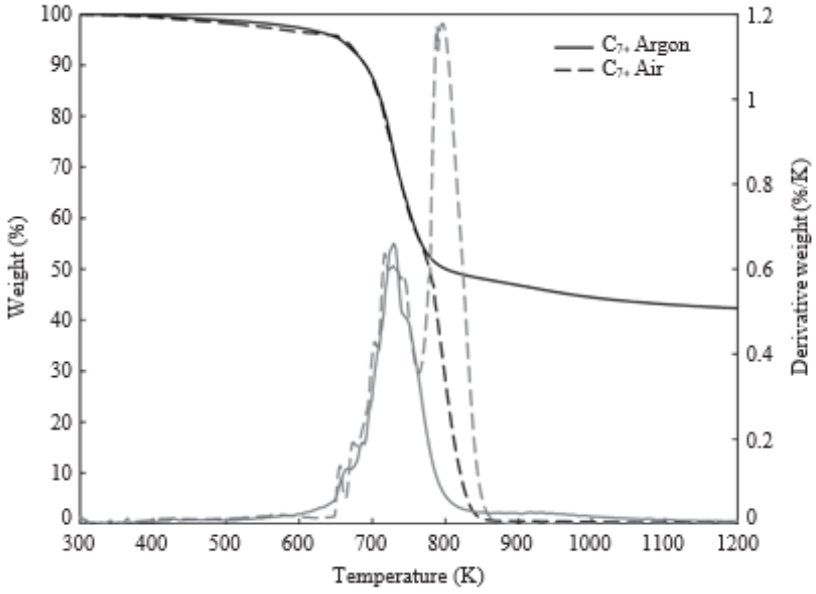

FIGURE 2.10 TGA of C_{7+} asphaltenes extracted from a bitumen in the presence of argon (dash lines) and air (solid lines) with the heating rate of 20 K/min. The peaks (grey lines) show the weight derivative of TGA analysis for both samples. (From Enayat, S. et al., Development of water soluble and photoluminescent carbon based nanoparticles from asphaltenes, In Preparation, 2017b.)

organic matters (mostly char and coke) in the sample starts. At the end, only a very small fraction of the sample's initial weight is left, which is mostly composed of ash and some inorganics such as metal oxides. This residue can be dissolved in an aqueous solution for metal content measurement of the initial sample using different methods such as inductively coupled plasma mass spectroscopy or inductively coupled optical emission spectroscopy (ICP-OES) (Enayat et al. 2017b).

Figure 2.11 shows a thermal behavior comparison between C7+ and C5–7 fractions of asphaltenes extracted from a bitumen in the presence of argon as the carrier gas. There is no significant change in the weight of the C7+ sample up to 673 K. However, above this temperature, the thermal degradation of asphaltene structure starts and the weight of the sample decreases dramatically, which

CRUDE OIL AND ASPHALTENE CHARACTERIZATION

reaches to its maximum rate at 729 K. During the decomposition, most of the relatively weak bonded aliphatic chains are removed, which result in a lower H/C atomic ratio compared to the initial sample. The pyrolysis reaction finishes at 813 K, and the weight reduction curve reaches a plateau.

The C5–7 fraction follows the same behavior until the temperature around 538 K at which the trend starts to deviate from the C7+ thermal behavior. As it is demonstrated,

the thermal degradation of the lighter C5–7 fraction starts at a lower temperature com- pared to the heavier C7+ fraction. Moreover, the amount of the carbonized char left from the C5–7 fraction is almost half of the C7+ fraction (21.5% vs. 42%). Therefore, this TGA comparison between the two fractions can demonstrate that the lighter C5–7 fraction has

more aliphatic chains compared to the heavier C7+ fraction, which ultimately explains the higher solubility of the C5–7 fraction (Enayat et al. 2017b).

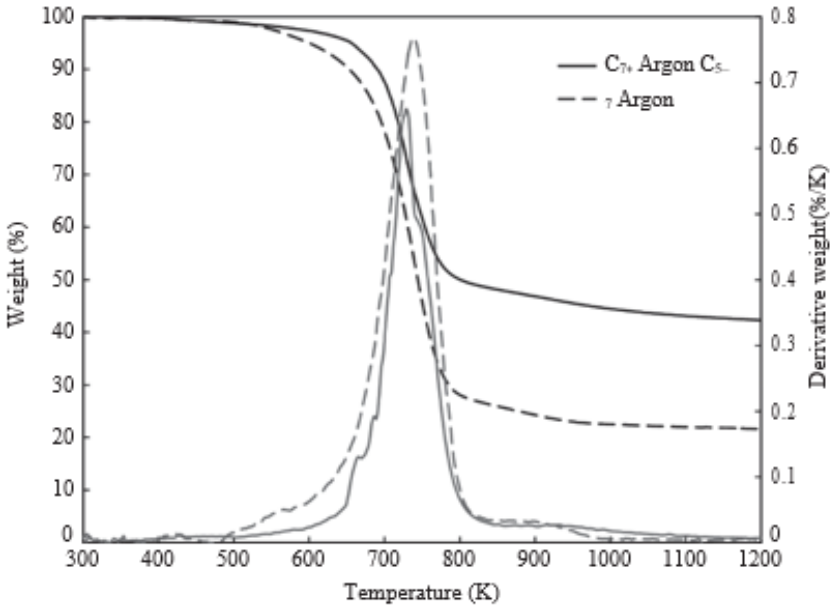

FIGURE 2.11 TGA of C_{7+} asphaltenes extracted from a bitumen (dash line) compared with C_{5-7} fraction (solid line) in the presence of argon. The peaks (grey lines) show the weight derivative of TGA analysis for both samples. (From Enayat, S. et al., Development of water soluble and photoluminescent carbon based nanoparticles from asphaltenes, In Preparation, 2017b.)

CRUDE OIL AND ASPHALTENE CHARACTERIZATION

Another application of the pyrolysis process for the characterization of asphaltenes comes up when the gases proceeding from the pyrolysis chamber are fed to a gas chro- matograph coupled to a mass spectrometer. Because of the large size of asphaltene molecules, their analysis by analytical methods such as FTIR, NMR, and elemental composition, among others, leads us to obtain *bulk* average rather than molecular composition (Behar and Pelet 1984). On the other hand, this large size makes imprac- ticable the use of chromatographic techniques by themselves. However, the addition of a rapid pyrolysis process makes the components of asphaltenes of a suitable size for their gas chromatographic analysis and, by adding a mass spectrometer at the end, the different moieties can be identified and quantified. The resultant technique is known as *pyrolysis-gas chromatography-mass spectroscopy* (py-gc-ms) (Speight 2014)

Speight and Pancirov (1984) showed that a determined fraction of asphaltenes can be divided into subfractions. All of these subfractions contained small polynuclear aromatic systems (one to four rings); however, the distribution of these species was not constant throughout the different fractions of asphaltenes. Another example of the use of pyrolysis in the chromatographic characterization of asphaltenes is the study carried by Behar and Pelet (1984). They found that a low amount of the aliphatic chains of asphaltenes contained more than 30 carbons. With 13C NMR the mean carbon number determined is 4–5, however, it is important to remember that 13C NMR can only report average amounts, contrary to what py-gc-mass spectroscopy is capable to detect.

2.2.2 asPhaltene ProPerties

2.2.2.1 Aromaticity

The study of asphaltenes structure and aromaticity is necessary to understand their self-association and aggregation behavior. Also, aromaticity is one of the important parameters to investigate the stability of the crude oil. Asphaltene aro- maticity range is reported from 0.4 to 0.7 (Bouhadda et al. 2010). If the asphaltene aromaticity is high, there is more tendency for the asphaltenes to aggregate and precipitate. The aggregation of the asphaltene molecules with higher aromaticity happens in lower asphaltene concentration in comparison to the asphaltene with lower aromaticity (León et al. 2000). Besides, the aromaticity of the maltene fraction affects the stability of the crude oil; if the maltene aromaticity is high, it can be a good solvent for the asphaltene and makes the crude oil more stable (Murgich et al. 1996).

Temperature and molecular weight changes influence the asphaltene aroma- ticity. By increasing the temperature and molecular weight of the sample the aromaticity increases (Speight and Moschopedis 1981). At high temperature, the rheology of asphaltene can be changed (Sharma and Yen 1994); some of the long alkyl functional groups in asphaltene structure are separated from the molecule. Also,

CRUDE OIL AND ASPHALTENE CHARACTERIZATION

because of the polymerization and condensation, some products such as carbon–carboids and coke will form which cause the higher degree of aromaticity (Kayukova et al. 2016).

There are different ways to calculate the aromaticity index; based on elemental composition and by FTIR and NMR spectroscopy. Based on elemental analysis, the aromaticity index (relative aromaticity) is equal to the ratio of C/H (McLean and Kilpatrick 1997).

Aromatic compounds have a higher C/H ratios than naphthenes, which in turn have higher C/H ratios than paraffin. The heavier (denser) the crude oil, the higher its C/H ratio.

In a more recent approach, the aromaticity is defined as the ratio of unbonded carbon/total carbon or unbonded carbon/total hydrogen. The unbonded carbons are the carbons in the aromatic rings, and it is assumed that the aromatic carbons do not have any bonding with hydrogen. So, the unbonded carbons are calculated based on the Equation 2.21 (Rezaee et al. 2017b).

$$UC = TC - \frac{TH}{2} \qquad (2.21)$$

where:

UC is the unbonded carbon

TC is the total carbon

TH is the total hydrogen

Another method is based on NMR spectroscopy; this method can provide accurate values (McLean and Kilpatrick 1997). In this method, the aromaticity is

defined as the number of aromatic carbon to the number of total carbon based on the 13C NMR spectrum. The peaks in the 100–170 ppm region are related to aromatic bands and the ones in 10–70 ppm region are related to aliphatic bands (Davarpanah et al. 2015; Calemma et al. 1995). The Aromaticity Index is calculated by the number of aromatic carbons divided by the amount of aromatics plus the amount of aliphatic carbons (Maki et al. 2001; Rogel et al. 2003; Liu and

Li 2015). 13CNMR shows that the asphaltene molecule contains 40% aromatic carbon and 90% of hydrogen is in methylene and methyl groups (Groenzin and Mullins 1999).

Aromaticity can be defined based on the FTIR spectrum as well (Craddock et al. 2015). It is defined as the ratio of absorbance at the 1600 cm−1 band (which corresponds to the aromatic C=C bonds) to the absorbance at 1400 cm−1 band

CRUDE OIL AND ASPHALTENE CHARACTERIZATION

(which

corresponds to aliphatic C—H bonds; Petrova et al. 2013). In addition, there is an

indirect aromaticity index, which is defined based on the ratio of absorbance at the

1600 cm−1 band to the absorbance at 2900 cm−1 band (which corresponds to aliphatic C−H bonds; Rogel et al. 2015).

Figure 2.12 shows the correlation between the result of aromaticity of C5+ asphaltene fractions for three crude oils (P1, P7, and P60) by FTIR and elemental analysis methods. The aromaticity calculated by elemental analysis is the ratio of *UC/TC*, *UC/TC*, and *C/H*. The result shows that there is a good correlation between the aromaticity calculated by the three methods so they can be used as an index to compare the asphaltene fractions structure. Based on the obtained aromaticity factors, one can conclude that the polycyclic aromatic core for the asphaltenes in the crude oil P1 contains less aliphatic chains and more aromatic rings in comparison to the asphaltene in the crude oil P7. Also, asphaltenes of the crude oil P60 have the lowest aromaticity (Rezaee et al. 2017b).

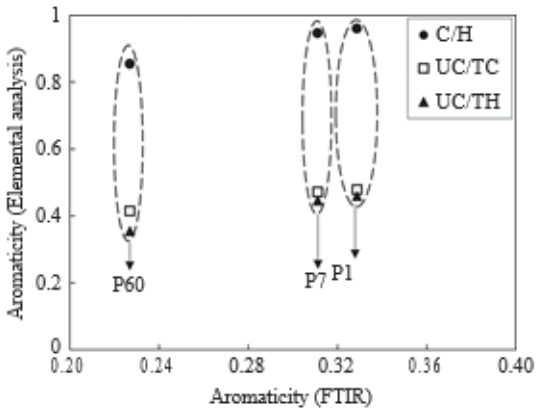

FIGURE 2.12 Aromaticity based on elemental analysis and FTIR spectroscopy. (From Rezaee, S. et al., Asphaltene characterization, fractionation and chemical properties, In Preparation, 2017b.)

In addition to the methods mentioned previously, aromaticity index (AI) can be calculated based on the Equation 2.22 (Koch and Dittmar 2006):

CRUDE OIL AND ASPHALTENE CHARACTERIZATION

$$AI = \frac{DBE_{AI}}{C_{AI}} = \frac{1 + C - O - S - 0.5H}{C - O - S - N - P} \tag{2.22}$$

The Double Bond Equivalent (DBE) is equal to the minimum numbers of C–C doublebonds plus rings in a structure of a molecule, which has heteroatoms.

$$DBE_{AI} = 1 + \frac{1}{2}\left(2(C - O - N - S - P) - (H - N - P) + N + P\right) \tag{2.23}$$

CAI is equal to the number of carbons which will be reduced by the number of heteroatoms (Koch and Dittmar 2006).

2.2.2.2 Molecular Weight

Molecular weight is one of the important parameters used to develop correlations for the physical properties of asphaltenes (León and Parra 2010). Since asphaltenes are a polydisperse distribution of a broad range of molecules with different sizes and molecular characteristics so a distribution of molar masses is expected for its molecular weight (Yarranton 2005). The average monomer asphaltene molecular weight goes from 500 to 1000 g/mol depending on the source of the sample (Molina et al. 2017). The average molecular weight of the aggregates varies from 3000 to 10000 g/mol and some of the aggregate sizes can reach as high as 50000 g/mol (Yarranton 2005).

Asphaltene molecules have the tendency to self-associate into nano-aggregates, which causes some trouble in the molecular weight measurement (Powers et al. 2016). One of the key concepts in asphaltene self-association modeling, developed by Agrawala and Yarranton (2001), is that asphaltene molecules may contain mul-tiple active sites that can act as propagators or single active sites that can act as terminators. In a mixture of asphaltenes and resins, asphaltenes are considered propagators, which serve as links for other similar molecules and form a chain. Resins serve as the terminators and end the chains. Molecular dynamic simulations have shown that the major driving force for the association is the interaction between the aromatic cores of the asphaltene molecules. In addition, the heteroat-oms attached to the aromatic cores have more influence on the association in com- parison to the ones attached to the aliphatic chain. Also, the length and number of chains are not as effective on the aggregation of asphaltenes as the aromatic cores; this last one will affect the aggregation size of asphaltenes (Sedghi et al. 2013).

CRUDE OIL AND ASPHALTENE CHARACTERIZATION

The asphaltene molar mass depends on the solvent, temperature, and concentration. By increasing the concentration and decreasing the temperature and aromatic- ity of the solvent, the asphaltene molar mass increases (Sztukowski 2005). Yarranton (2005) showed that asphaltene aggregation and self-association decrease in a good solvent (such as tetrahydrofuran [THF]) and high temperature.

There are three most common methods for molecular weight (*MW*) measurement; gel permeation chromatography (GPC), vapor pressure osmometry (VPO), and MS. GPC (also called size exclusion chromatography [SEC]) separates molecules by their size, similarly to a molecular sieve process. The separation is strictly based on the size of the sample in solution. There should be no interaction with the column packing (e.g., adsorption, partition, etc.) as in conventional HPLC. The mode of separation is based on the size of the material (usually a polymer). For a correct GPCanalysis, the sample must be dissolved in a suitable solvent (Lambert 1971).

GPC consists of three PSS-SDV (Styrene-divinylbenzene) columns with 100, 1000, and 10000 Å pore sizes. These pores can vary from small to quite large and act as the molecular filters. The larger size molecules will not fit into the smaller pores. Conversely, the smaller molecules will fit into most of the pores and will be retained longer (Lambert 1971).

Figure 2.13 illustrates how the sample is injected into the mobile phase and the path that the sample takes to the detector. The mobile phase normally being used in a GPC method is THF, because of its low refractive index and viscosity, and the calibration standard is based on polystyrene (Hendrickson and Moore 1966).

Inside the GPC, the dissolved sample is injected into a continually flowing stream of solvent (mobile phase). The mobile phase (THF) flows through millions of highly porous, rigid particles (stationary phase) tightly packed together in a column. Data-acquisition accessories control the test automatically, record the results, and calculate the average molecular weight. The most widely used detector today for GPC analysis is the differential refractometer. It is a concentration sensitive detector that simply measures the difference in refractive index between the eluent in the refer-

ence side and the sample + eluent on the sample side. Because the refractive index of polymers is usually constant above molecular weights of about 1,000 g/mol, the detec-

tor response is directly proportional to the sample concentration (Hendrickson and Moore 1966).

GPC can determine several important parameters including number average molecular weight (*Mn*), weight average molecular weight (*MW*), and polydispersity, which is the ratio of *MW/Mn* and is the most fundamental characteristic of a polydisperse system. *Mn* is affected mainly by the low molecular weights of nonassociated molecules in the sample.

CRUDE OIL AND ASPHALTENE CHARACTERIZATION

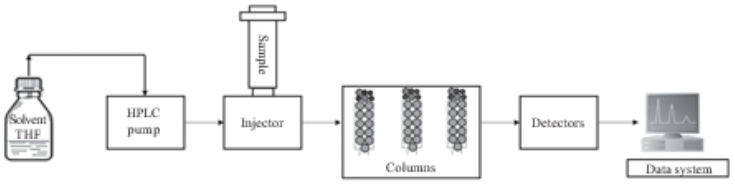

FIGURE 2.13 Schematic of a basic gel permeation chromatography. (Adapted from Walker, J. M. and Rapley, R., *Molecular Biomethods Handbook*, 2nd ed., Humana Press, Totowa, NJ, 2008.)

MW is affected mainly by the weight of the aggregates and the molecular weights of the biggest monomers, and it will influence physical properties of asphaltenes. *MW* is always greater than *Mn* unless the asphaltene aggregates are completely monodisperse. The ratio of *MW* to *Mn* is used to calculate the polydis- persity index (PDI) of a polymer, which provides an indication of aggregation ten- dency of the asphaltene molecule (Buenrostro-Gonzalez et al. 2002). The broader the molecular weight distribution, the larger the PDI. If the PDI value is close to 1.0, the distribution is narrow while larger values mean a broader distribution (Lambert 1971).

Figure 2.14a shows the *Mn* distribution for C5+ asphaltene fractions of crude oil S9 by GPC. As noticed, the distribution changes dramatically by the asphaltene concentration. Based on this result the distribution is broader for higher asphaltene concentration and as the concentration decreases, the curves become narrower. The same observation was reported by Agrawala and Yarranton (2001). By increasing

CRUDE OIL AND ASPHALTENE CHARACTERIZATION

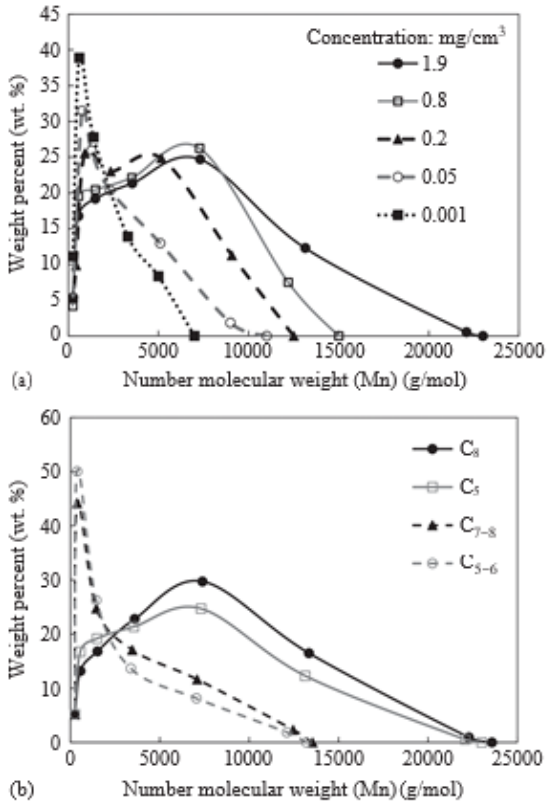

FIGURE 2.14 Asphaltene molecular weight distribution: (a) C_{5+} asphaltene from crude oil S9. (b) Different asphaltene fractions from a light crude oil with the concentration 0.16 wt%. (From Rezaee, S. et al., Asphaltene characterization, fractionation and chemical properties, In Preparation, 2017b.)

the concentration, the molecular weight increases because of the aggregation of the asphaltene molecules, and therefore, the molecular weight shown in this plot is related to the molecular weight of small asphaltene particles and aggregates. Groenzin and Mullins (1999) reported a similar conclusion.

Figure 2.14b shows the *Mn* distribution for different asphaltene fractions (the procedure of fractionation is described in Section 2.2.3). As expected, the molecular weight of the C8+ fraction is the highest, and the distribution is the broadest. The distribution of the molecular weight for C5–6 asphaltene is the narrowest among the asphaltene fractions since the structure of C5–6 asphaltene fraction is more resinous, and its aromaticity is less than a C8+ fraction (Rezaee et al. 2017b).

All of the distributions in Figures 2.14a and b are bimodal, which shows that, at

CRUDE OIL AND ASPHALTENE CHARACTERIZATION

least, there are two different species in the solution. The number of low molecularweight molecules increases in the first peak for the lowest concentration of asphal- tene in Figure 2.14a and the most soluble fraction of asphaltene C5–6 in Figure 2.14b (Rezaee et al. 2017b). Also, Mansoori et al. (2007) showed the same trend for the molecular weight changes for C5+ and C7+ asphaltene.

In addition to the distribution of molecular weight, it is possible to find the average molecular weight of each distribution. The average *Mn* and PDI measured at

1.9 mg/cm3 concentration for the C5+ asphaltene from the crude oil in this example are 1443 g/mol and 3.4, respectively, whereas the average *Mn* and PDI measured at 0.001 mg/cm3 concentration are 710 g/mol and 2.1. The *Mn* reported for the C5+ asphaltene at 1.9 mg/cm3 is an aggregate weight but not the actual *Mn* for an asphal- tene molecule because of the asphaltene self-association (Badre et al. 2006; Rezaee et al. 2017b).

The GPC methodology has some limitations; the most important one is using polystyrene as the standard. According to Sato et al. (2005), hydrocarbons with a pericondensed polyaromatic structure tend to elute later than linear polymers with similar *MW*; therefore, the number-averaged molecular weight determined for asphaltenes is lower than expected. It is considered that the *MW* of asphaltenes determined by this method is not the actual value, but rather a polystyrene equivalent *MW*. Another limitation is that the sample needs to be filtered through a 0.2 μm filter paper to remove some of the aggregrates. As a result, it is not possible to measure asphaltene *MW* in different concentrations by GPC.

Another method to measure asphaltene molecular weight is VPO. It is a common method for the determination of asphaltene molecular weight, though it can- not measure an accurate molar mass of asphaltene in a solvent because of the self-association of the asphaltene molecules, which is considered as its major drawback. The main advantage in comparison to the GPC method is that the molar mass of the asphaltene samples with different concentration can be measured by VPO (Yarranton et al. 2000).

The repeatability of the asphaltene molecular-weight measurements based on the VPO method is approximately ±15%. This method is based on the different vapor pressure created by adding a small amount of solute to a solvent. In this method, two separate thermistors contained a pure solvent, and a drop of solute-solvent are placed in a chamber. Each thermistor shows different temperature because of the

different vapor pressure caused by the various composition of the solute. The difference between the temperatures causes the resistance or voltage to change in proportional relation to the molecular weight of the solute (Barrera et al. 2013).

CRUDE OIL AND ASPHALTENE CHARACTERIZATION

$$\frac{\Delta V}{c_s} = K\left(\frac{1}{M_W} + A_1 c_s + A_2 c_s^2 + \ldots\right) \tag{2.24}$$

where:

ΔV is the voltage difference between the thermistors
c_s is the solute concentration
K is a proportionality constant
A_1 and A_2 are coefficients arising from the nonideal behavior of the solution
M_W is the molecular weight of the sample

The equation at low concentration becomes:

$$\frac{\Delta V}{c_s} = K\left(\frac{1}{M_W} + A_1 c_s\right) \tag{2.25}$$

For an ideal system, the second term is zero, and $\Delta V/cs$ is constant (Peramanu et al. 1999).

VPO shows higher molecular weight in comparison to GPC result because GPC is calibrated based on polystyrene, which does not have the same retention time as crude oil. So, the VPO results are more reliable for lower molecular weights (Peramanu et al. 1999).

Barrera et al. 2013 compared the molecular weight of two asphaltene fractions by VPO: a light cut and a heavy cut. They defined the light cut of asphaltene as the soluble part in a Heptol (*n*-heptane and toluene) solution, and a heavy cut as the precipitated part in the Heptol solution. They showed that the molecular weight of lighter cuts increases less than the heavier cuts by increasing the asphaltene concen- tration. This is caused by the fact that the lighter cuts contain less self-association, whereas the heaviest cuts have more (Barrera et al. 2013).

In addition to VPO and GPC methods, mass spectroscopy is also one of the most commonly used methods for measuring molecular weight. This method is mainly based on the volatilization/ionization of the sample. This is a powerful method to mea- sure the mass-to-charge ratio (*m/z*) of ions to identify and quantify molecules in simple and complex mixtures. In this method, the sample (asphaltene) is vaporized and then ionized by an ion source, which creates molecular ions. These ions will be deflected by electric and magnetic fields. Then, the deflected ions will hit a detector of ions. Based on the strength of the magnetic field, different ions (different *m/z*) will be detected by the ion detector at different times. The computer connected to the mass spectrometer analyzes the data from the detector and produces a plot of *m/z* (on the *x*-axis) against the relative abundance (on the

CRUDE OIL AND ASPHALTENE CHARACTERIZATION

y-axis) of the ions. Assuming that the charge of the ions

is +1 (one electron is lost), it is possible to find the weight percentage of each of the ion fractions based on the relative abundance on the *y*-axis) (Coelho and Franco 2013).

Mass spectroscopy results can be misleading in two conditions; incomplete volatilization because of a low laser power or fragmentation because of an excessive power. Controlling the laser energies can solve the problem of fragmentation. It is possible to control the laser energy by the use of a matrix-assisted laser desorp- tion ionization-time-of-flight method (MALDITOF-MS), which is mainly used to analyze biopolymers and synthetic polymers (Acevedo et al. 2005). In this method, because asphaltenes are dissolved in a diluted solution, it is not necessary to measure the distribution of molecular weight (Hortal et al. 2006; Mullins et al. 2008).

Shinya Sato et al. (2005) compared the data of *MW* obtained by mass spectroscopy (MS) and GPC. They reported that the values of *MW* (MS) is almost the same as *MW* by GPC (standard was polystyrene) for *MW* greater than 900 amu. For the molecular weight less than 900 amu, the difference between the *MW* (MS) and *MW* (GPC) increases (Sato et al. 2005).

There is still a debate on the accuracy of the mass spectroscopy method, although most of the studies proof that the matrix-assisted laser desorption ionization measurements, with the asphaltene diluted in a matrix, give the more reliable results.

2.2.2.2 Wetting Properties

Wettability is defined as the tendency of a fluid to wet a surface, which, talking about oil reservoirs, explains how oil occupies the rock pores. Wetting properties of the rock reservoir have a strong influence on the displacement behavior and the crude oil recovery. The two most widely used parameters to study the wettability behavior are the interfacial tension and the contact angle (Hjelmeland and Larrondo 1986).

Surface tension is one of the major issues in the oil industry because it is needed to predict the capillary pressure of the oil in a porous solid. Also, it influences on the relative gas-to-liquid phase permeability. Surface tension is defined as the attrac- tive force between two phases (a liquid and a solid or a liquid and a gas). When this attractive force is between the two immiscible liquids, it is known as *interfacial tension*. The common units for surface tension are dynes/cm or mN/m, which are equivalent. The surface tension is affected by the temperature and the molecular weight (Speight 2014).

Firoozabadi and Ramey (1988) proposed a correlation for estimating oil–water surface tension as a function of density and reduced temperature. The limitation of using this correlation is that the effect of salt concentration is not considered in the equation.

CRUDE OIL AND ASPHALTENE CHARACTERIZATION

$$\sigma_{hw} = \left[\frac{1.58(\rho_w - \rho_h) + 1.76}{T_r^{0.3125}} \right]^4 \quad (2.26)$$

The contact angle can be measured by Young's equation. This equation considers the equilibrium between the force factors at the oil–water–rock system contact line (Xu 2005):

where:

σ_{hw} is the hydrocarbon/water surface tension in dynes/cm
ρ_w is the density of water in g/cm^3
ρ_h is the density of the hydrocarbon in g/cm^3
T_r is the reduced temperature

The contact angle can be measured by Young's equation. This equation considers the equilibrium between the force factors at the oil–water–rock system contact line (Xu 2005):

$$\sigma_{so} = \sigma_{sw} + \sigma_{wo} \cos \epsilon \quad (2.27)$$

q is the angle at which the fluid–fluid interface meets the surface, and it is defined as the direct measure of the surface wettability. The value of q goes from 0° to 180°. For val- ues between 0° and 75°, it is considered that water is wetting the surface. At q between 75° and 105°, a neutral wettability or an intermediately wet surface happens. When q is greater than 105°, oil is wetting the surface (Rajayi and Kantzas 2011; Speight 2014). is the interfacial energy between solid–oil, solid–water, and water–oil (Xu 2005).

There are several different methods to measure the contact angle (Yuan and Lee 2013), that is, the telescope goniometer (Bigelow et al. 1946), the captive bubble method (Adanson and Gast 1997; Brandon et al. 2003), the dual-drop dual-crystal technique (Rao and Girard 1996), the tilting plate method, the Wilhelmy balance method, the capillary rise at a vertical plate, the capillary tube, the capillary penetration method for powders and granules and the capillary bridge method. In the oil industry, the most widely used methods for measuring the contact angle are the captive bubble and dual-drop dual-crystal techniques (Xu 2005; Rajayi and Kantzas 2011).

In the sessile drop method, a single solid plate is placed in the test cell, which is

CRUDE OIL AND ASPHALTENE CHARACTERIZATION

filled with fluid as its environment, whereas in the dual-drop dual-crystal method, two parallel plates are used in a cuvette that contains the fluid environment. The solid plate is usually made out of quartz or calcite crystals to simulate the reservoir rock surface (Anderson 1986a; Morrow 1990).

The first step for the measurement of the contact angle by sessile drop method is to place the oil droplet on the solid surface by injecting the oil with a U-shaped needle (Figure 2.15). During the process of oil expansion on the solid plate, the measured angle is called the *receding contact angle* (RCA) with respect to water, and during the withdrawal of the oil, the contact angle is defined as the *advancing contact angle* (ACA) with respect to water.

Before measuring ACA, one must wait enough time to reach the equilibrium of the receding contact angle. Six days are needed to reach the equilibrium contact angle for a sample of 0.1 wt% C5+ asphaltene in toluene (Rezaee et al. 2017b). Also, Anderson reported about 1000 h to reach the equilibrated contact angle (Anderson 1986b).

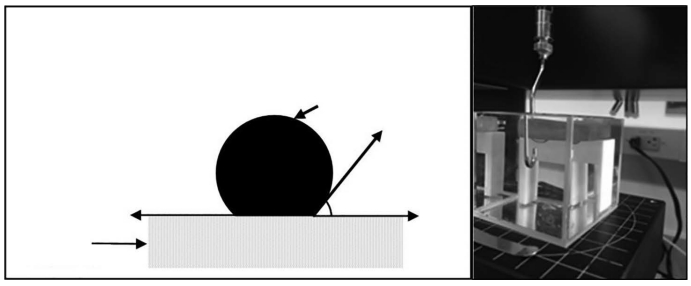

FIGURE 2.15 (a and b) Contact angle at oil–water–solid interface. (From Rezaee, S. et al., Asphaltene characterization, fractionation and chemical properties, In Preparation, 2017b.)

Because of the long time needed to reach equilibrium, Buckley et al. (1997) proposed to age the plate before measuring the contact angle at a temperature higher than 333 K. However, Hopkins et al. (2017) reported that both the aged and non-aged chalk cores were mixed wet in the presence of crude oil.

After the aging process, the bulk oil should be washed by the appropriate solvent. Figure 2.16 shows how washing or soaking with different solvent affects the contact angle measurement.

CRUDE OIL AND ASPHALTENE CHARACTERIZATION

Decane acts as the precipitant, and based on the contact angle when using decane, the plate is considered completely oil wet. Cyclohexane is neither a solvent nor a precipitant for asphaltenes, but based on the asphaltene type, it may act as a puresolvent. Toluene is a good solvent for asphaltenes, but rinsing with toluene can just remove the bulk oil from the surface of calcite, while soaking with toluene may dissolve some the asphaltenes adsorbed to the surface (Buckley et al. 1997).

There are some parameters that affect the wetting properties of crude oil such as physical and chemical properties of the solid surface, crude oil fractions (acidic and basic groups), brine composition (ionic strength, pH) and ambient conditions (e.g., temperature, pressure and dissolved carbon dioxide) (Buckley 1998).

The effect of temperature and pressure on wettability alteration depends on the condition of the test which is under study. Wang and Gupta (1995) showed that pressure does not have a significant effect on contact angle of oil–brine on two substrates of quartz and calcite plates. They also found that by increasing the temperature, calcite becomes more water wet, while quartz becomes more oil wet. Rajayi and Kantzas (2011) demonstrated that the contact angle of bitumen–water decreases (more water wet) as the pressure increased. Najafi-Marghmaleki et al. (2016) investigated the wettability alteration of four carbonate reservoir by temperature. They concluded that temperature and pressure had a negligible effect on wettability alteration of the reservoir with the lowest asphaltene content.

Brine composition has a significant impact on wetting properties of rock reservoirs.

CRUDE OIL AND ASPHALTENE CHARACTERIZATION

Previous studies have shown that potential determining ions, such as Mg2+, Ca2+,

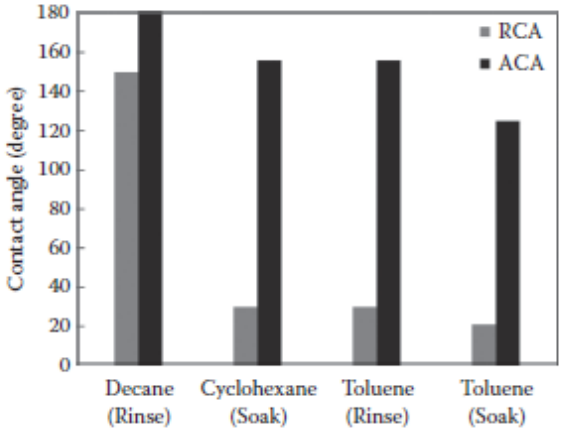

FIGURE 2.16 Effect of washing on RCA and ACA measurement. (From Buckley, J. S. et al., *SPE J*, 2, 107–119, 1997.)

CO 2-, and SO 2- present in the brine, increase the water wetness of the chalk rocks (Puntervold et al. 2007). Puntervold et al. (2007) demonstrated that the water wetness of the chalk reservoir increases with temperature because of the SO 2- affinity to the chalk surface in the presence of Ca2+ and Mg2+. Generosi et al. (2017) studied the effect of Mg2+ on calcite wettability alteration. Based on their result, the surface becomes more water wet by replacing NaCl brine with a solution containing MgSO4 (The organic attraction to the surface of calcite is weaker in the presence of Mg2+). Their result is in agreement with other studies available in the literature. For example, Prabhakar and Melnik (2017) found that Mg2+ and SO 2- ions make the surface of calcite more water wet in case of having an excess of Mg2+ because Mg2+ forms Mg acetate in the presence of oil in the system. Mg acetate is less sticky on the surface of calcite, and therefore, causes the more water wetness condition.

Based on the study by Andersson et al. (2016), calcite surface is more hydrophilic in the presence of divalent transition metal ions (Mn, Fe, Co, Ni, Cu, and Zn). They proposed to use divalent ion Mn for the low temperature and Fe for the high temperature carbonate reservoir in order to enhance oil recovery (Andersson et al. 2016). In addition, different studies have shown the importance of low salinity water injection in enhancing oil recovery (Tang and Morrow 1997; Al Shalabi et al. 2013). However, there are still debates on understanding the mechanism of increasing oil recovery by low salinity water flood (Yousef et al. 2010; Lee et al. 2010; Mahani et al. 2017).

CRUDE OIL AND ASPHALTENE CHARACTERIZATION

Crude oil composition has a significant effect on wettability alteration, which is mainly because of the presence of resins and asphaltenes as the most polar fractions in the crude oil (Anderson 1986a,b). In case of carbonate rocks, the carboxylic acid group is responsible for the adsorption to the positively charged calcite surface. Therefore, it is important to measure the acid number (AN) of the test oil, which shows the amount of acidic compounds (Hopkins et al. 2017). Different studies available in the literature have presented a correlation between acid number and wettability alteration. They also investigated the effect of asphaltene on changing the wettability of reservoir rocks (Morrow 1990; Pedroza et al. 1996; Buckley et al. 1997; Drummond and Israelachvili 2004).

The interactions between the solid plate and oil can be ionic and surface precipitation. Ionic interaction happens when acids and bases ionize at the interface of oil–water or solid–water. Surface precipitation interaction depends on the solvent properties (crude oil media) of asphaltene (Al-Maamari and Buckley 2003). The adsorption of asphaltenes on the solid surfaces depends mostly on the stability of the crude oil (Akhlaq et al. 1996). Figure 2.17 shows the results of RCA and ACA for C5+ asphaltene in toluene.

Based on the results RCA at time zero is approximately 20° and increases until it reaches equilibrium at 38°. It is shown that during the measurement of ACA, a rigid film is formed and remains on the surface of calcite. This film formation around the droplet is not related to the concentration of asphaltene since it was is seen at

0.01 wt% C5+ asphaltene in toluene (Rezaee et al. 2017b). Hjelmeland and Larrondo (1986) showed that a thick rigid film at the brine–oil interface would form, especially at low temperature. The rigid film is formed because the surface active components of asphaltene are adsorbed at the interface of brine–model oil (Buckley et al. 1997). Rezaee et al. (2017b) showed that the rigid film is formed even in the presence of the lightest fraction of asphaltene (C5–6 asphaltene) (refer to Section 2.2.3).

CRUDE OIL AND ASPHALTENE CHARACTERIZATION

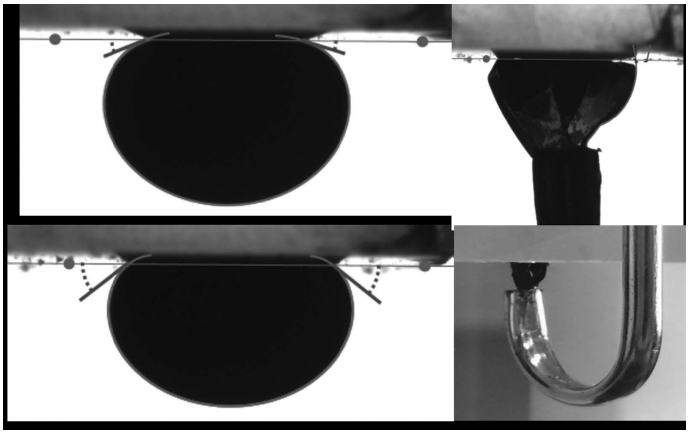

FIGURE 2.17 RCA and ACA measurement for 0.1 wt% C5–6 asphaltene in toluene fromcrude oil S6 at room temperature. (From Rezaee, S. et al., Asphaltene characterization, fractionation and chemical properties, In Preparation, 2017b.) (a) RCA measurement at time zero. (b) Equilibrium RCA after 6 days. (c) ACA measurement, rigid film formation. (d) The rigid film remained after reducing the drop volume.

Hjelmeland and Larrondo (1986) showed that the rigid film formation is temperaturedependent. They observed that the rigid film disappears above 333 K after a short time.

Regarding the comparison of the surface activity of different asphaltene fractions, the only difference was that the rigid film is thicker for the heavier fractions of asphaltene (C8+ asphaltene in comparison to C5–6 asphaltene) (Rezaee et al. 2017b). Rao and Girard (1996) proposed a dual-drop dual-crystal technique to remove the problem of skin formation. In this method, the RCA and ACA are measured by shifting the lower calcite plate. A drop of oil is placed between the two plates, and the RCA and ACA are measured by moving the plates toward each other. In this case, because the volume of the droplet is not changing, there is no rigid film (no asphaltene accumulation in the interface of water–oil) during the advancing contact

CRUDE OIL AND ASPHALTENE CHARACTERIZATION

angle measurement. Also, the results reported by this method are more reproducible in comparison to the other methods (Rao and Girard 1996).

2.2.3 asPhaltene FraCtionation

A common strategy to study the asphaltene characterization is the fractionation based on their solubility. As advantages, this strategy reduces the complexity of the material to study and provides a distribution of properties for the each of the asphaltene fractions. Rogel et al. (2015) fractionated asphaltene into four parts: fraction 1 was extracted with 15/85 CH2Cl2/n-heptane at room temperature; fraction 2 was extracted with 30/70 CH2Cl2/n-heptane at room temperature; fraction 3 was extracted with 100% CH2Cl2 at room temperature; and fraction 4 was extracted with 90/10 CH2Cl2/ methanol. They showed that there is a decrease in the H/C molar ratio from fraction 1 to 3, which is inconsistent with a lower solubility. There was an increase in the H/C ratio in fraction 4. This is caused by the low solubility of this fraction and might be Crude Oil and Asphaltene Characterization partially as a result of the presence of polar functionalities. Also, infrared spectroscopy shows that there is an increase in the carbonyl signal for fraction 4. It also shows that a low amount of hydrogen would cause an increase in aromaticity and the size of the polyaromatic rings in the molecules.

Davarpanah et al. (2015) fractionated the asphaltene into two C5+ and C7+ asphaltenes based on their solubility in n-alkanes. They showed that the aromaticity (defined as the number of aromatic carbon to the total carbon using 13C NMR) of the C7+ fraction is higher than the one for C5+. Also, the number of carbons for the C5+ fraction is higher than the C7+ fraction based on 1H NMR results. The number of carbons per alkyl substituent based on 1H NMR is calculated by the equation:

$$n_{\text{carbon}} = \frac{\left[H_\alpha + \left(H_\beta + H_\gamma\right)\right]}{H_\alpha} \qquad (2.28)$$

where Hα, Hβ, and Hγ refer to the α-hydrogen-to-aromatic ring (2 to 5 ppm region),

CRUDE OIL AND ASPHALTENE CHARACTERIZATION

β-hydrogen-to-aromatic ring (−0.5 to 2 ppm region), and γ-hydrogen-to-aromatic ring (−0.5 to 2 ppm region), respectively. The aromatic hydrogen band refers to the aromatic hydrogens (5 to 10 ppm region). Strausz et al. (2002) separated Athabasca asphaltenes into five fractions using GPC fractionation by separating them with different ratio of solvent (benzene) to sample. The GPC result showed that, by diluting the sample the retention time of the asphaltene in GPC response increases and MW decreases from 17000 to below 12000. Also, they showed that the aromaticity decreases from 48% to 35% by increasing the ratio of solvent. The nitrogen, oxygen, and sulfur content is the same in different fractions.

Östlund et al. (2004) fractionated asphaltenes based on their different polaritiesusing binary mixtures of DCM and n-pentane. In the first step the asphaltene is dissolved in DCM, and it is mixed completely. In the second step, n-pentane is added and mixed for 30 minutes. Then the mixture is centrifuged, and the undissolved asphaltene is separated. This process is repeated three more times, and the asphaltene of each step is separated. They showed that the asphaltene separated in the first step has the highest tendency to flocculate and the highest molecular weight. The heteroatoms content was approximately the same for the four asphaltenes fractions.

Tojima et al. (1998) developed a new method of fractionation by using heptanetoluene and separating the light and heavy C7+ asphaltene fraction. In their method the C7+ asphaltene is separated first, then a toluene-to-heptane a ratio of 65:35 is added to the C7+ asphaltene. In this step, the undissolved asphaltene is separated and named the lowest soluble portion of C7+ asphaltene. As the next step, the soluble asphaltenes remained in toluene solution are recovered by evaporation of the solvent. To separate the most soluble fraction of C7+, the process will be repeated two more times with a toluene-to-heptane ratio of 25:75 and 18:82. Finally, the most soluble fraction of C7+b asphaltene is separated by evaporation of toluene. They showed that the aromaticity of heavier asphaltenes is higher than for the lighter asphaltenes, and it has the most highly condensed polynuclear aromatics. As a result, they concluded that the heavy asphaltenes are considered as peptized material and the light ones are peptizing material.

Rezaee et al. (2017b) proposed a new method for asphaltene fractionation based on the solubility difference of four n-alkanes. The asphaltenes separation is based

CRUDE OIL AND ASPHALTENE CHARACTERIZATION

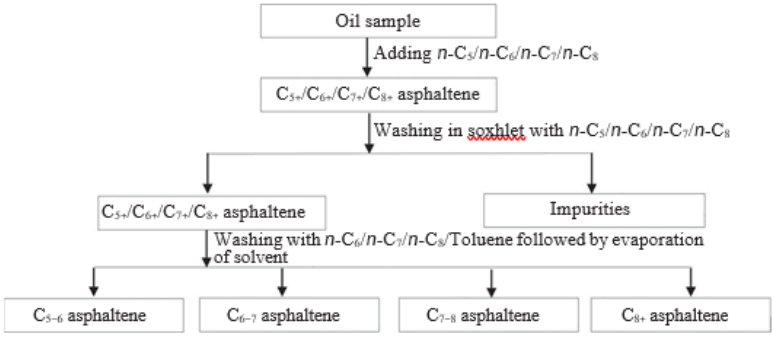

FIGURE 2.18 Asphaltene fractionation; aging time was 48 hours. (From Rezaee, S. et al., Asphaltene characterization, fractionation and chemical properties, In Preparation, 2017b.)

on the IP-143 procedure (ASTM D6560 2005). Figure 2.18 shows the different steps of the asphaltene fractionation.

In this method, the chosen precipitant (*n*-pentane, *n*-hexane, *n*-heptane, and *n*-octane), is added to the crude oil at a 40:1 volume-to-weight ratio (40 cm3 of pre- cipitant per 1 g of oil). The oil is mixed with the precipitant in a glass vial and the vial is sealed to prevent the evaporation of the solvent. The mixture is sonicated once a day for 30 minutes to enhance the mixing of the oil and the precipitant, and the subsequent precipitation of asphaltenes. The aging process of the asphaltene aggre- gates occurs at ambient temperature. After two days, the aging process is completed and the solution is filtered using a 0.2 μm Nylon filter.

In the next step, the filtrate, containing the maltenes fraction, is analyzed by the automated chromatographic columns system described in Section 2.1.2.3.

The filter cake, containing the asphaltenes fraction, is placed inside a Soxhlet appara- tus (Figure 2.19) using a paper thimble and refluxed with the corresponding asphaltene precipitant (*n*-C5, *n*-C6, *n*-C7, and *n*-C8) for two days to purify the asphaltene fraction and remove any co-precipitated material. The solvent plus the impurities are then added to the maltene fraction. The heating rate, condenser cooling rate, and fluid level of the solvent in the Soxhlet apparatus have to be adjusted to maintain the appropriate level of solvent in the Soxhlet and flask. To increase the rate of asphaltenes purification, a motor is installed on top of the condenser column to vertically move the thimble containing the filtered asphaltenes. Using this technique, the diffusion rate of impurities into the wash- ing solvent increases, and therefore, the efficiency of extraction improves.

In the next step, the filter papers containing the purified asphaltenes are washed with toluene to dissolve all asphaltenes. The end point of this step is determined by the color of the toluene in contact with the thimble; the process will stop when tolu- ene is colorless.

In the final step, the solutions of toluene and asphaltenes are transferred to evaporation plates to allow the complete evaporation of toluene at a temperature of 378 K–393 K. The samples are taken to constant weight and the weights of C5+, C6+, C7+, and C8+ asphaltenes are calculated.

CRUDE OIL AND ASPHALTENE CHARACTERIZATION

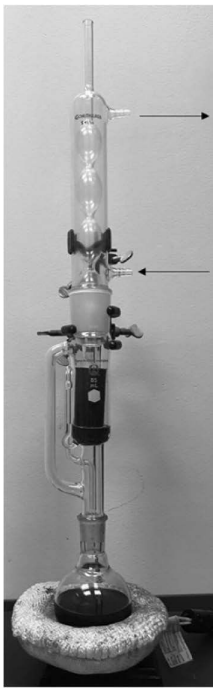

FIGURE 2.19 Asphaltene separation by Soxhlet extraction. (Courtesy of Vargas Research Laboratory, Rice University, Houston, Texas.)

Finally, by subtracting the C6+ asphaltene content from the C5+ asphaltene content, the amount of C5–6 asphaltene is quantified. With the same methodology, the amounts of C6–7 and C7–8 asphaltenes are obtained.

In order to separate C5–6, C6–7, C7–8, and C8+ asphaltene fractions for further analy- ses, it is needed to wash the C5+, C6+, C7+, and C8+ fractions with *n*-C6, *n*-C7, *n*-C8, and toluene, respectively. The final step is to remove the added solvent by evaporation. The residue is the corresponding asphaltene fraction.

Table 2.5 shows the results of the asphaltene fractionation of two light crude oils. Based on the results, the asphaltene distribution is not the same for the two crude oils. Different asphaltene fractions have different chemical compositions and structures (Section 2.2.1.1). Not only asphaltene structure varies from one crude oil to the other, but also the asphaltene subfractions look different.

Although it is not applicable for all asphaltene fractions from different crude oils, some of the subfractions may also look different. In a few cases, the C5–6 asphaltenes are viscous liquid, whereas the C5+ asphaltenes are powdery solid (Figure 2.20).

CRUDE OIL AND ASPHALTENE CHARACTERIZATION

Based on the results described in this chapter, C5–6 asphaltene has the lowest aromaticity and molecular weight, whereas the C8+ has the highest molecular weight and aromaticity (Rezaee et al. 2017b).

TABLE 2.5
Asphaltene Fractionation of Crude Oil S9 and S6

Asphaltene Fraction	Crude Oil S6 Asphaltene Content (wt%)	Crude Oil S9 Asphaltene Content (wt%)
C_{5+} (Total)	2.1	1.0
C_{6+}	1.8	0.8
C_{7+}	1.7	0.6
C_{8+}	1.5	0.5
C_{5-6}	0.3	0.2
C_{6-7}	0.1	0.2
C_{7-8}	0.2	0.1

Source: Rezaee, S. et al., Asphaltene characterization, fractionation and chemical properties, In Preparation, 2017b.

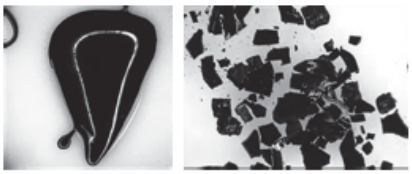

(a) (b)

FIGURE 2.20 (a) C_{5-6} and (b) C_{5+} asphaltenes separated from the crude oil A. (Courtesy of Vargas Research Laboratory, Rice University, Houston, Texas.)

2.3 FINAL REMARKS

In this chapter, the methods and techniques currently used to determine the physical and chemical properties and characteristics of both crude oil and asphaltenes are discussed. Most of the methodologies for crude oil analysis presented here are based on ASTM standards. In other cases, the property is calculated from another property, which was obtained experimentally, under the same ASTM conditions, as in the case of the solubility parameter. Despite the reproducibility and reliability of these tests, the conditions of temperature and pressure at which these tests take place are not representative of the actual conditions of the oil wells. One solution to this problem is the use of more sophisticated equipment, such as the Anton Paar

CRUDE OIL AND ASPHALTENE CHARACTERIZATION

DMA HPM HPHT apparatus to obtain the density at conditions of high temperature and pressure. However, this type of equipment is expensive and not commonly found in laboratories. To provide a solution, mathematical correlations have been proposed. Section 2.1.1.7 describes several equations that can be used to predict properties, such as the solubility parameter, the viscosity, and the molecular weight.

Next, the main methods to characterize crude oils by fractionation are described. Knowing that crude oil is composed of many different types of hydrocarbons and that some of these molecules share similar characteristics, fractionation techniques have been divided into three categories: based on the boiling point of the different groups, based on similar chemical structures, and based on similar polarity. All three methods have pros and cons; the differences are mainly in the use of expensive versus affordable equipment, large versus small amounts of sample and solvent, the need for asphaltene removal, and the time needed to complete the tests. Vargas and coworkers are currently developing a new methodology, based on polarity, which optimizes all these factors mentioned.

The last part of this chapter explains in detail the different methodologies and techniques to determine the properties and chemical composition of asphaltenes. All these properties will be used in further chapters.

REFERENCES

Abdallah, W. A., and Y. Yang. 2012. Raman spectrum of asphaltene. *Energy & Fuels* 26 (11): 6888–6896. doi:10.1021/ef301247n.

Acevedo, S., L. B. Gutierrez, G. Negrin, J. C. Pereira, B. Mendez, F. Delolme, G. Dessalces, and D. Broseta. 2005. Molecular weight of petroleum asphaltenes: A comparison between mass spectrometry and vapor pressure osmometry. *Energy & Fuels* 19 (4): 1548–1560. doi:10.1021/ef040071+.

Adamson, A. W., and A. P. Gast. 1997. *Physical Chemistry of Surfaces*, 6th ed. New York: Wiley. doi:10.1126/science.160.3824.179.

Agrawala, M., and H. W. Yarranton. 2001. An asphaltene association model analogous to linear polymerization. *Industrial & Engineering Chemistry Research* 40 (21): 4664– 4672. doi:10.1021/ie0103963.

Aitani, A. M. 2004. Oil refining and products. In *Encyclopedia of Energy*, 715–729. doi:10.1016/B0-12-176480-X/00259-X.

Akhlaq, M. S., D. Kessel, and W. Dornow. 1996. Separation and chemical characterization of wetting crude oil compounds. *Journal of Colloid and Interface Science* 180 (2): 309–314. doi:10.1006/jcis.1996.0308.

Al-Maamari, R. S. H., and J. S. Buckley. 2003. Asphaltene precipitation and alteration of wetting: The potential for wettability changes during oil production. *SPE Reservoir Evaluation & Engineering* 6 (04): 210–214. doi:10.2118/84938-PA.

Alomair, O., M. Jumaa, A. Alkoriem, and M. Hamed. 2016. Heavy oil viscosity and

CRUDE OIL AND ASPHALTENE CHARACTERIZATION

density prediction at normal and elevated temperatures. *Journal of Petroleum Exploration and Production Technology* 6 (2): 253–263. doi:10.1007/s13202-015-0184-8.

Al-Rawahi, N., G. Vakili-Nezhaad, I. Ashour, and A. Fatemi. 2012. A new correlation for prediction of viscosities of Omani Fahud-field crude oils. In *Advances in Modeling of Fluid Dynamics*, C. Liu (Ed.). InTech.

AlShaikh, M., and J. Mahadevan. 2014. Impact of brine composition on carbonate wettability: A sensitivity study. *Society of Petroleum Engineers*. doi:10.2118/172187-MS.

Al Shalabi, E., Delshad, M. and Sepehrnoori, K., 2013. Does the double layer expansion mechanism contribute to the LSWI effect on hydrocarbon recovery from carbonate rocks? In *Society of Petroleum Engineers*. doi:10.2118/165974-MS.

Ancheyta, J., G. Centeno, F. Trejo, G. Marroquín, J. A. García, E. Tenorio, and A. Torres. 2002. Extraction and characterization of asphaltenes from different crude oils and sol- vents. *Energy & Fuels* 16 (5): 1121–1127. doi:10.1021/ef010300h.

Ancheyta, J., and J. G. Speight. 2007. *Hydroprocessing of Heavy Oils and Residua*. Boca Raton, FL: CRC Press.

Andersson, M. P., K. Dideriksen, H. Sakuma, and S. L. S. Stipp. 2016. Modelling how incorporation of divalent cations affects calcite wettability–implications for biomineralisation and oil recovery. *Scientific Reports* 6 (June): 28854. doi:10.1038/srep28854.

Anderson, W. G. 1986a. Wettability literature survey—Part 2: Wettability measurement.

Journal of Petroleum Technology 38 (11): 1–246.

Anderson, W. G. 1986b. Wettability literature survey—Part 1: Rock/oil/brine interactions and the effects of core handling on wettability. *Journal of Petroleum Technology* 38 (10): 1125–1144. doi:10.2118/13932-PA.

Asemani, M., and A. R. Rabbani. 2016. Oil-oil correlation by FTIR spectroscopy of asphal- tene samples. *Geosciences Journal* 20 (2): 273–283. doi:10.1007/s12303-015-0042-1.

Aske, N. 2002. Characterisation of crude oil components, asphaltene aggregation and emul- sion stability by means of near infrared spectroscopy and multivariate analysis.

ASTM D86. 2016. *Standard Test Method for Distillation of Petroleum Products and Liquid Fuels at Atmospheric Pressure*. ASTM D86-16. West Conshohocken, PA: American Society for Testing and Materials.

ASTM D445. 2017. *Standard Test Method for Kinematic Viscosity of Transparent and Opaque Liquids (and Calculation of Dynamic Viscosity)*. ASTM D445-17. West Conshohocken, PA: American Society for Testing and Materials.

ASTM D1160. 2015. *Standard Test Method for Distillation of Petroleum Products at*

CRUDE OIL AND ASPHALTENE CHARACTERIZATION

Reduced Pressure. ASTM D1160-15. West Conshohocken, PA: American Society for Testing and Materials.

ASTM D1218. 2002. *Standard Test Method for Refractive Index and Refractive Dispersion of Hydrocarbon Liquids*. ASTM D1218-02. West Conshohocken, PA: American Society for Testing and Materials.

ASTM D1747. 2004. *Standard Test Method for Refractive Index of Viscous Materials*. ASTM D1747-99. West Conshohocken, PA: American Society for Testing and Materials.

ASTM D2007. 2007. *Standard Test Method for Characteristic Groups in Rubber Extender and Processing Oils and Other Petroleum–Derived Oils by the Clay–Gel Absorption Chromatographic Method*. ASTM D 2007. West Conshohocken, PA: American Society for Testing and Materials.

ASTM D2502. 2014. *Standard Test Method for Estimation of Mean Relative Molecular Mass of Petroleum Oils from Viscosity Measurements*. ASTM D2502-14. West Conshohocken, PA: American Society for Testing and Materials.

ASTM D2503. 1992. *Standard Test Method for Relative Molecular Mass (Molecular Weight) of Hydrocarbons by Thermoelectric Measurement of Vapor Pressure*. ASTM D2503. West Conshohocken, PA: American Society for Testing and Materials.

ASTM D2709. 1996. *Standard Test Method for Water and Sediment in Middle Distillate Fuels by Centrifuge*. ASTM D2709-96. West Conshohocken, PA: American Society for Testing and Materials.

ASTM D2892. 2016. *16 Standard Test Method for Distillation of Crude Petroleum (15-Theoretical Plate Column*). ASTM D2892-16. West Conshohocken, PA: American Society for Testing and Materials.

ASTM D4006. 2005. *Standard Test Method for Water in Crude Oil by Distillation*. ASTM D4006-81. West Conshohocken, PA: American Society for Testing and Materials.

ASTM D4007. 2002. *Standard Test Method for Water and Sediment in Crude Oil by the Centrifuge Method*. ASTM D4007. West Conshohocken, PA: American Society for Testing and Materials.

ASTM D4287. 2014. *Standard Test Method for High-Shear Viscosity Using a Cone/Plate Viscometer*. ASTM D4287-14. West Conshohocken, PA: American Society for Testing and Materials.

ASTM D4928. 2000. *Standard Test Methods for Determination of Water in Crude Oils by Coulometric Karl Fischer Titration*. ASTM D4928. West Conshohocken, PA: American Society for Testing and Materials.

ASTM D5481. 2013. *Standard Test Method for Measuring Apparent Viscosity at High-Temperature and High-Shear Rate by Multicell Capillary Viscometer*. ASTM D5481-13. West Conshohocken, PA: American Society for Testing and Materials.

ASTM D6304. 2007. *Standard Test Method for Determination of Water in Petroleum Products, Lubricating Oils, and Additives by Coulometric Karl Fischer Titration*. ASTM D6304-

CRUDE OIL AND ASPHALTENE CHARACTERIZATION

07. West Conshohocken, PA: American Society for Testing and Materials.

ASTM D6560. 2005. *Standard Test Method for Determination of Asphaltenes (Heptane Insolubles) in Crude Petroleum and Petroleum Products*. ASTM D6560-05. West Conshohocken, PA: American Society for Testing and Materials.

ASTM D7042. 2016. *Standard Test Method for Dynamic Viscosity and Density of Liquids by Stabinger Viscometer (and the Calculation of Kinematic Viscosity)*. ASTM D7042-16. West Conshohocken, PA: American Society for Testing and Materials.

ASTM D7152. 2011. *Standard Practice for Calculating Viscosity of a Blend of Petroleum Products*. ASTM D7152-11(2016). West Conshohocken, PA: American Society for Testing and Materials.

ASTM D7395. 2007. *Standard Test Method for Cone/Plate Viscosity at a 500 S-1 Shear Rate*. ASTM D7395-07(2012). West Conshohocken, PA: American Society for Testing and Materials.

ASTM D7996. 2015. *Standard Test Method for Measuring Visible Spectrum of Asphaltenes in Heavy Fuel Oils and Crude Oils by Spectroscopy in a Microfluidic Platform*. ASTM D7996-15. West Conshohocken, PA: American Society for Testing and Materials.

Badre, S., C. C. Goncalves, K. Norinaga, G. Gustavson, and O. C. Mullins. 2006. Molecular size and weight of asphaltene and asphaltene solubility fractions from coals, crude oils and bitumen. *Fuel* 85 (1): 1–11. doi:10.1016/j.fuel.2005.05.021.

Barneto, A. G., J. A. Carmona, and M. J. F. Garrido. 2016. Thermogravimetric assessment of thermal degradation in asphaltenes. *Thermochimica Acta* 627–629: 1–8. doi:10.1016/j. tca.2016.02.004.

Barrera, D. M., D. P. Ortiz, and H. W. Yarranton. 2013. Molecular weight and density distribu- tions of asphaltenes from crude oils. *Energy & Fuels* 27 (5): 2474–2487. doi:10.1021/ ef400142v.

Barton, A. F. M. 1991. *CRC Handbook of Solubility Parameters and Other Cohesion Parameters*, 2nd ed. Boca Raton, FL: CRC Press.

Barwise, A. J. G. 1990. Role of nickel and vanadium in petroleum classification. *Energy & Fuels* 4 (6): 647–652. doi:10.1021/ef00024a005.

Beggs, H. D., and J. R. Robinson. 1975. Estimating the viscosity of crude oil systems. *SPE: Journal of Petroleum Technology* 27 (9). doi:10.2118/5434-PA.

Behar, F., and R. Pelet. 1984. Characterization of asphaltenes by pyrolysis and chro- matography. *Journal of Analytical and Applied Pyrolysis* 7 (1–2): 121–135. doi:10.1016/0165-2370(84)80045-5.

Bigelow, W. C., D. L. Pickett, and W. A. Zisman. 1946. Oleophobic monolayers: I. Films adsorbed from solution in non-polar liquids. *Journal of Colloid Science* 1 (6): 513–538. doi:10.1016/0095-8522(46)90059-1.

Biltz, H. 1899. *Practical Methods for Determining Molecular Weights*. Easton, PA: Chemical Publishing Company.

Bird, R. B., W. E. Stewart, and E. N. Lightfoot. 2002. *Transport Phenomena*, 2nd ed. New York: John Wiley & Sons.

Bouhadda, Y., D. Bormann, E. Sheu, D. Bendedouch, A. Krallafa, and M. Daaou. 2007.

CRUDE OIL AND ASPHALTENE CHARACTERIZATION

Characterization of Algerian Hassi-Messaoud asphaltene structure using Raman spectrom- etry and X-ray diffraction. *Fuel* 86 (12–13): 1855–1864. doi:10.1016/j.fuel.2006.12.006.

Bouhadda, Y., P. Florian, D. Bendedouch, T. Fergoug, and D. Bormann. 2010. Determination of Algerian Hassi-Messaoud asphaltene aromaticity with different solid-state NMR sequences. *Fuel* 89 (2): 522–526. doi:10.1016/j.fuel.2009.09.018.

Brandon, S., N. Haimovich, E. Yeger, and A. Marmur. 2003. Partial wetting of chemically patterned surfaces: The effect of drop size. *Journal of Colloid and Interface Science* 263 (1): 237–243. doi:10.1016/S0021-9797(03)00285-6.

Buckley, J. S. 1998. Wetting alteration of solid surfaces by crude oils and their asphaltenes.

Oil & Gas Science and Technology 53 (3): 303–312. doi:10.2516/ogst:1998026.

Buckley, J. S. 1999. Predicting the onset of asphaltene precipitation from refractive index measurements. *Energy Fuels* 13 (2): 328–332. doi:10.1021/ef980201c.

Buckley, J. S., G. J. Hirasaki, Y. Liu, S. Von Drasek, J.-X. Wang, and B. S. Gill. 1998. Asphaltene precipitation and solvent properties of crude oils. *Petroleum Science and Technology* 16 (3–4): 251–285. doi:10.1080/10916469808949783.

Buckley, J. S., X. Xie, Y. Liu, and N. R. Morrow. 1997. Asphaltenes and crude oil wetting-the effect of oil composition. *SPE Journal* 2 (2): 107–119. doi:10.2118/35366-PA.

Buenrostro-Gonzalez, E., S. I. Andersen, J. A. Garcia-Martinez, and C. Lira-Galeana. 2002. Solubility/molecular structure relationships of asphaltenes in polar and nonpolar media. *Energy & Fuels* 16 (3): 732–741. doi:10.1021/ef0102317.

Burke, J. 1984. Solubility parameters: Theory and application. Text. Article. X-Unrefereed. Retrieved from http://cool.conservation-us.org/coolaic/sg/bpg/annual/v03/bp03-04. html.

Buryakovsky, L., N. A. Eremenko, M. V. Gorfunkel, and G. V. Chilingarian. 2005. *Geology and Geochemistry of Oil and Gas*. Amsterdam, the Netherlands: Elsevier.

Calemma, V., P. Iwanski, M. Nali, R. Scotti, and L. Montanari. 1995. Structural characterization of asphaltenes of different origins. *Energy & Fuels* 9 (2): 225–230. doi:10.1021/ef00050a004. Castro, A. T. 2006. NMR and FTIR characterization of petroleum residues: Structural param- eters and correlations. *Journal of the Brazilian Chemical Society* 17 (6): 1181–1185.

doi:10.1590/S0103-50532006000600016.

Ceric, E. 2012. *Crude Oil, Processes and Products*. Sarajevo: IBC.

Chew, J. N., and C. A. Connally Jr. 1959. A viscosity correlation for gas-saturated crude oils, January. Retrieved from https://www.onepetro.org/general/SPE-1092-G.

Coelho, A. V., and C. Franco. 2013. *Tandem Mass Spectrometry—Molecular*

CRUDE OIL AND ASPHALTENE CHARACTERIZATION

Characterization.

London, UK: InTech. doi:10.5772/56703.

Correra, S., M. Merlini, A. Di Lullo, and D. Merino-Garcia. 2005. Estimation of the solvent power of crude oil from density and viscosity measurements. *Industrial & Engineering Chemistry Research* 44 (24): 9307–9315. doi:10.1021/ie0507272.

Craddock, P. R., T. V. Le Doan, K. Bake, M. Polyakov, A. M. Charsky, and A. E. Pomerantz. 2015. Evolution of kerogen and bitumen during thermal maturation via semi-open pyrolysis investigated by infrared spectroscopy. *Energy & Fuels* 29 (4): 2197–2210. doi:10.1021/ef5027532.

Davarpanah, L., F. Vahabzadeh, and A. Dermanaki. 2015. Structural study of sphaltenes from Iranian heavy crude oil. *Oil & Gas Science and Technology—Revue d'IFP Energies Nouvelles* 70 (6): 1035–1049. doi:10.2516/ogst/2012066.

Donaldson, E. C., G. V. Chilingarian, and T. F. Yen. 1985. *Enhanced Oil Recovery, I: Fundamentals and Analyses*, 1st ed. Amsterdam, the Netherlands: Elsevier.

Drummond, C., and J. Israelachvili. 2004. Fundamental studies of crude oil–surface water interactions and its relationship to reservoir wettability. *Journal of Petroleum Science and Engineering* 45 (1): 61–81. doi:10.1016/j.petrol.2004.04.007.

Egbogah, E. O., and J. T. Ng. 1990. An improved temperature-viscosity correlation for crude oil systems. *Journal of Petroleum Science and Engineering* 4 (3): 197–200. doi:10.1016/0920-4105(90)90009-R.

El Ghandoor, H., E. Hegazi, I. Nasser, and G. M. Behery. 2003. Measuring the refractive index of crude oil using a capillary tube interferometer. *Optics & Laser Technology* 35 (5): 361–367. doi:10.1016/S0030-3992(03)00029-X.

Enayat, S., F. Lejarza, M. Tavakkoli, and F. M. Vargas. 2017a. Development of asphaltene coated melamine sponges for water-oil separation. In Preparation.

Enayat, S., M. Tavakkoli, and F. M. Vargas. 2017b. Development of water soluble and photo- luminescent carbon based nanoparticles from asphaltenes. In Preparation.

Ese, M.-H., J. Sjöblom, J. Djuve, and R. Pugh. 2000. An atomic force microscopy study of asphaltenes on mica surfaces. Influence of added resins and demulsifiers. *Colloid and Polymer Science* 278 (6): 532–538. doi:10.1007/s003960050551.

Fan, T., and J. S. Buckley. 2002. Rapid and accurate SARA analysis of medium gravity crude oils. *Energy & Fuels* 16 (6): 1571–1575. doi:10.1021/ef0201228.

Fan, T., J. Wang, and J. S. Buckley. 2002. Evaluating crude oils by SARA analysis. In *Society of Petroleum Engineers Journal*, 1–6. Tulsa, OK. doi:10.2118/75228-MS.

Fedors, R. F. 1974. A method for estimating both the solubility parameters and molar volumes of liquids. *Polymer Engineering & Science* 14 (2): 147–154. doi:10.1002/pen.760140211. Firoozabadi, A., and H. J. Ramey Jr. 1988. Surface tension of water-hydrocarbon systems at reservoir conditions. *Journal of Canadian Petroleum Technology* 27 (03).

doi:10.2118/88-03-03.

CRUDE OIL AND ASPHALTENE CHARACTERIZATION

Gaweł, B., M. Eftekhardadkhah, and G. Øye. 2014. Elemental composition and fourier trans- form infrared spectroscopy analysis of crude oils and their fractions. *Energy & Fuels* 28 (2): 997–1003. doi:10.1021/ef402286y.

Generosi, J., M. Ceccato, M. P. Andersson, T. Hassenkam, S. Dobberschütz, N. Bovet, and

R.

4 L. S. Stipp. 2017. Calcite wettability in the presence of dissolved Mg2+ and SO 2–.

Energy & Fuels 31 (1): 1005–1014. doi:10.1021/acs.energyfuels.6b02029.

Glaso, O. 1980. Generalized pressure-volume-temperature correlations. *Journal of Petroleum Technology* 32 (05): 785–795. doi:10.2118/8016-PA.

González, G., and M. B. C. Moreira. 1991. The wettability of mineral surfaces contain- ing adsorbed asphaltene. *Colloids and Surfaces* 58 (3): 293–302. doi:10.1016/ 0166-6622(91)80229-H.

Groenzin, H., and O. C. Mullins. 1999. Asphaltene molecular size and structure. *The Journal of Physical Chemistry A* 103 (50): 11237–11245. doi:10.1021/jp992609w.

Groysman, A. 2014. *Corrosion in Systems for Storage and Transportation of Petroleum Products and Biofuels: Identification, Monitoring and Solutions*. Dordrecht, the Netherlands: Springer Science & Business Media.

Hansen, C. M. 1967. The three dimensional solubility parameter. *Danish Technical: Copenhagen*, 14.

Hansen, C. M. 2007. *Hansen Solubility Parameters: A User's Handbook*. 2nd ed. Boca Raton, FL: CRC Press.

Hay, G., H. Loria, and M. A. Satyro. 2013. Thermodynamic modeling and process simula- tion through PIONA characterization. *Energy & Fuels* 27 (6): 3578–3584. doi:10.1021/ ef400286m.

Hendrickson, J. G., and J. C. Moore. 1966. Gel permeation chromatography. III. Molecular shape versus elution. *Journal of Polymer Science Part A-1: Polymer Chemistry* 4 (1): 167–188. doi:10.1002/pol.1966.150040111.

Hjelmeland, O. S., and L. E. Larrondo. 1986. Experimental investigation of the effects of tem- perature, pressure, and crude oil composition on interfacial properties. *SPE Reservoir Engineering* 1 (04): 321–328. doi:10.2118/12124-PA.

Hopkins, P. A., I. Omland, F. Layti, S. Strand, T. Puntervold, and Tor Austad. 2017. Crude oil quantity and its effect on chalk surface wetting. *Energy & Fuels* 31 (5): 4663–4669. doi:10.1021/acs.energyfuels.6b02914.

Hortal, A. R., B. Martínez-Haya, M. D. Lobato, J. M. Pedrosa, and S. Lago. 2006. On the determination of molecular weight distributions of asphaltenes and their asggregates in laser desorption ionization experiments. *Journal of Mass Spectrometry* 41 (7): 960–968. doi:10.1002/jms.1056.

CRUDE OIL AND ASPHALTENE CHARACTERIZATION

Huc, A. Y. 2010. *Heavy Crude Oils: From Geology to Upgrading: An Overview*. Paris: Editions TECHNIP.

International Energy Statistics. 2017. Accessed April 21. http://tinyurl.com/ybmoofhe. Jafarinejad, S. 2016. *Petroleum Waste Treatment and Pollution Control*. Cambridge, MA:

Butterworth-Heinemann.

Jewell, D. M., J. H. Weber, J. W. Bunger, H. Plancher, and D. R. Latham. 1972. Ion-exchange, coordination, and adsorption chromatographic separation of heavy-end petroleum dis- tillates. *Analytical Chemistry* 44 (8): 1391–1395. doi:10.1021/ac60316a003.

Jiang, C., S. R. Larter, K. J. Noke, and L. R. Snowdon. 2008. TLC–FID (Iatroscan) analysis of heavy oil and tar sand samples. *Organic Geochemistry* 39 (8): 1210–1214. doi:10.1016/j. orggeochem.2008.01.013.

Karger, B. L., L. R. Snyder, and C. Eon. 1978. Expanded solubility parameter treatment for classification and use of chromatographic solvents and adsorbents. *Analytical Chemistry* 50 (14): 2126–2136. doi:10.1021/ac50036a044.

Kayukova, G. P., A. T. Gubaidullin, S. M. Petrov, G. V. Romanov, N. N. Petrukhina, and

A. V. Vakhin. 2016. Changes of asphaltenes' structural phase characteristics in the pro- cess of conversion of heavy oil in the hydrothermal catalytic system. *Energy & Fuels* 30 (2): 773–783. doi:10.1021/acs.energyfuels.5b01328.

Kitak, T., A. Dumičić, O. Planinšek, R. Šibanc, and S. Srčič. 2015. Determination of solubil- ity parameters of Ibuprofen and Ibuprofen lysinate. *Molecules* 20 (12): 21549–21568.

doi:10.3390/molecules201219777.

Koch, B. P., and T. Dittmar. 2006. From mass to structure: An aromaticity index for high- resolution mass data of natural organic matter. *Rapid Communications in Mass Spectrometry* 20 (5): 926–932.

Krevelen, D. W., and K. Te Nijenhuis. 2009. *Properties of Polymers: Their Correlation with Chemical Structure; Their Numerical Estimation and Prediction from Additive Group Contributions*. Amsterdam, the Netherlands: Elsevier.

Lambert, A. 1971. Review of gel permeation chromatography. *British Polymer Journal* 3 (1): 13–23. Lee, S. Y., K. J. Webb, I. Collins, A. Lager, S. Clarke, M. Sullivan, A. Routh, and X. Wang. 2010. Low salinity oil recovery: Increasing understanding of the underlying mechanisms.

SPE Improved Oil Recovery Symposium, April 24–28, Tulsa, Oklahoma, Society of Petroleum Engineers. doi:10.2118/129722-MS.

León, A. Y., and M. J. Parra. 2010. Determination of molecular weight of vacuum residue and their SARA fractions. *CT&F—Ciencia, Tecnología Y Futuro* 4 (2): 101–112.

León, O., E. Rogel, J. Espidel, and G. Torres. 2000. Asphaltenes: Structural characterization, self-association, and stability behavior. *Energy & Fuels* 14 (1): 6–10.

CRUDE OIL AND ASPHALTENE CHARACTERIZATION

Lewis, I. R., and H. Edwards. 2001. *Handbook of Raman Spectroscopy: From the Research Laboratory to the Process Line*. New York: CRC Press.

Liu, Y. J., and Z. F. Li. 2015. Structural characterisation of asphaltenes during residue hydrotreatment with light cycle oil as an additive. *Journal of Chemistry* 2015: e580950. Lundanes, E., and T. Greibrokk. 1994. Separation of fuels, heavy fractions, and crude oils into compound classes: A review. *Journal of High Resolution Chromatography* 17 (4): 197–202.

Luo, P., X. Wang, and Y. Gu. 2010. Characterization of asphaltenes precipitated with three light alkanes under different experimental conditions. *Fluid Phase Equilibria* 291 (2): 103–110. Mahani, H., A. L. Keya, S. Berg, and R. Nasralla. 2017. Electrokinetics of carbonate/brine inter- face in low-salinity waterflooding: Effect of brine salinity, composition, rock type, and

pH on ζ-potential and a surface-complexation model. *SPE Journal* 22 (01): 53–68. doi:10.2118/181745-PA.

Maki, H., T. Sasaki, and S. Harayama. 2001. Photo-oxidation of biodegraded crude oil and toxicity of the photo-oxidized products. *Chemosphere* 44 (5): 1145–1151.

Mansoori, G. A., D. Vazquez, and M. Shariaty-Niassar. 2007. Polydispersity of heavy organ- ics in crude oils and their role in oil well fouling. *Journal of Petroleum Science and Engineering* 58 (3): 375–390.

McLean, J. D., and P. K. Kilpatrick. 1997. Comparison of precipitation and extrography in the fractionation of crude oil residua. *Energy & Fuels* 11 (3): 570–585.

Microfluidic SARA Analysis | Schlumberger. 2017. Coupling microfluidics and spectroscopy for precise SARA measurements. Accessed April 22. http://www.slb.com/services/characterization/reservoir/core_pvt_lab/fluid_lab_services/microfluidic-analysis.aspx.

Mitra-Kirtley, S., O. C. Mullins, J. F. Branthaver, and S. P. Cramer. 1993. Nitrogen chemis- try of kerogens and bitumens from X-ray absorption near-edge structure spectroscopy.

Energy & Fuels 7 (6): 1128–1134.

Mitra-Kirtley, S., O. C. Mullins, C. Y. Ralston, and C. Pareis. 1999. Sulfur characteriza- tion in asphaltene, resin and oils fractions of two crude oils. *ACS: New Orleans*. http://web.anl.gov/PCS/acsfuel/preprint%20archive/Files/44_4_NEW%20ORLEANS_08-99_0763.pdf.

Molina V., D., E. Ariza, and J. C. Poveda. 2017. Structural differences among the asphaltenes in colombian light crudes from the colorado oil field. *Energy & Fuels* 31 (1): 133–139. Morrow, N. R. 1990. Wettability and its effect on oil recovery. *Journal of Petroleum*

Technology 42 (12): 1–476.

Moschopedis, S. E., and J. G. Speight. 1976. Oxygen functions in asphaltenes. *Fuel* 55 (4): 334–336.

Mullins, O. C. 2008. Review of the molecular structure and aggregation of

CRUDE OIL AND ASPHALTENE CHARACTERIZATION

asphaltenes and petroleomics. *SPE Journal* 13 (01): 48–57.

Mullins, O. C., B. Martínez-Haya, and A. G. Marshall. 2008. Contrasting perspective on asphal- tene molecular weight. This comment vs the overview of A. A. Herod, K. D. Bartle, and

R. Kandiyoti. *Energy & Fuels* 22 (3): 1765–1773.

Mullins, O. C., and E. Y. Sheu. 1999. *Structures and Dynamics of Asphaltenes*. New York: Springer Science & Business Media.

Murgich, J., J. Rodríguez, and Y. Aray. 1996. Molecular recognition and molecular mechan- ics of micelles of some model asphaltenes and resins. *Energy & Fuels* 10 (1): 68–76.

Nadkarni, R. A. 2000. *Guide to ASTM Test Methods for the Analysis of Petroleum Products and Lubricants*. ASTM Manual Series 44. West Conshohocken, PA: ASTM.

Najafi-Marghmaleki, A., A. Barati-Harooni, A. Soleymanzadeh, S. J. Samadi, B. Roshani, and A. Yari. 2016. Experimental investigation of effect of temperature and pressure on contact angle of four Iranian carbonate oil reservoirs. *Journal of Petroleum Science and Engineering* 142: 77–84.

Östlund, J. A., P. Wattana, M. Nydén, and H. S. Fogler. 2004. Characterization of fractionated asphaltenes by UV–vis and NMR self-diffusion spectroscopy. *Journal of Colloid and Interface Science* 271 (2): 372–380.

Otremba, Z. 2000. The impact on the reflectance in VIS of a type of crude oil film floating on the water surface. *Optics Express* 7 (3): 129–134.

Pearson, C. D., and S. G. Gharfeh. 1986. Automated high-performance liquid chromatogra- phy determination of hydrocarbon types in crude oil residues using a flame ionization detector. *Analytical Chemistry* 58 (2): 307–311.

Pedroza, T. M. de, G. Calderon, and A. Rico. 1996. Impact of asphaltene presence in some rock properties. *SPE Advanced Technology Series* 4 (1): 185–191. doi:10.2118/27069-PA.

Peramanu, S., B. B. Pruden, and P. Rahimi. 1999. Molecular weight and specific grav- ity distributions for athabasca and cold lake bitumens and their saturate, aromatic, resin, and asphaltene fractions. *Industrial & Engineering Chemistry Research* 38 (8): 3121–3130.

Permanyer, A., L. Douifi, N. Dupuy, A. Lahcini, and J. Kister. 2005. FTIR and SUVF spectroscopy as an alternative method in reservoir studies. Application to Western Mediterranean oils. *Fuel* 84 (2–3): 159–168.

Permanyer, A., C. Rebufa, and J. Kister. 2007. Reservoir compartmentalization assessment by using FTIR spectroscopy. *Journal of Petroleum Science and Engineering* 58 (3–4): 464–471.

Person, W. B., and G. Zerbi. 1982. *Vibrational Intensities in Infrared and Raman Spectroscopy*.

CRUDE OIL AND ASPHALTENE CHARACTERIZATION

Amsterdam, the Netherlands: Elsevier.

Petrova, L. M., N. A. Abbakumova, I. M. Zaidullin, and D. N. Borisov. 2013. Polar-solvent fractionation of asphaltenes from heavy oil and their characterization. *Petroleum Chemistry* 53 (2): 81–86.

Pomerantz, A. E., D. J. Seifert, K. D. Bake, P. R. Craddock, O. C. Mullins, B. G. Kodalen,

S. Mitra-Kirtley, and T. B. Bolin. 2013. Sulfur chemistry of asphaltenes from a highly compositionally graded oil column. *Energy & Fuels* 27 (8): 4604–4608.

Powers, D. P. 2014. Characterization and asphaltene precipitation modeling of native and reacted crude oils. University of Calgary. Retrieved from http://theses.ucalgary.ca/ handle/11023/1873.

Powers, D. P., H. Sadeghi, H. W. Yarranton, and F. G. A. van den Berg. 2016. Regular solu- tion based approach to modeling asphaltene precipitation from native and reacted oils: Part 1, molecular weight, density, and solubility parameter distributions of asphaltenes. *Fuel* 178: 218–233.

Prabhakar, S., and R. Melnik. 2017. Wettability alteration of calcite oil wells: Influence of smart water ions. *Scientific Reports* 7 (1): 17365. doi:10.1038/s41598-017-17547-z.

Puntervold, T., S. Strand, and T. Austad. 2007. New method to prepare outcrop chalk cores for wettability and oil recovery studies at low initial water saturation. *Energy & Fuels* 21 (6): 3425–3430. doi:10.1021/ef700323c.

Rajayi, M., and A. Kantzas. 2011. Effect of temperature and pressure on contact angle and interfacial tension of quartz/water/bitumen systems. *Journal of Canadian Petroleum Technology* 50 (06): 61–67.

Rao, D. N., and M. G. Girard. 1996. A new technique for reservoir wettability characteriza- tion. *Journal of Canadian Petroleum Technology* 35 (01). https://www.onepetro.org/ journal-paper/PETSOC-96-01-05.

Rezaee, S., R. H. Doherty, M. Tavakkoli, and F. M. Vargas. 2017a. Crude oil characterization, fractionation and SARA analysis. In Preparation.

Rezaee, S., M. Tavakkoli, R. H. Doherty, and F. M. Vargas. 2017b. Asphaltene characteriza- tion, fractionation and chemical properties. In Preparation.

Riazi, M. R. 2005. *Characterization and Properties of Petroleum Fractions*. West Conshohocken, PA: ASTM International.

Riazi, M. R., and G. N. Al-Otaibi. 2001. Estimation of viscosity of liquid hydrocarbon sys- tems. *Fuel* 80 (1): 27–32.

Riedeman, J. S., N. Reddy Kadasala, A. Wei, and H. I. Kenttämaa. 2016. Characterization of asphaltene deposits by using mass spectrometry and Raman spectroscopy. *Energy & Fuels* 30 (2): 805–809.

Riley, B. J., C. Lennard, S. Fuller, and V. Spikmans. 2016. An FTIR method for the analysis of crude and heavy fuel oil asphaltenes to assist in oil fingerprinting. *Forensic Science International* 266: 555–564.

Rogel, E., O. León, E. Contreras, L. Carbognani, G. Torres, J. Espidel, and A. Zambrano. 2003. Assessment of asphaltene stability in crude oils using conventional

CRUDE OIL AND ASPHALTENE CHARACTERIZATION

techniques. *Energy & Fuels* 17 (6): 1583–1590.

Rogel, E., M. Roye, J. Vien, and T. Miao. 2015. Characterization of asphaltene fractions: Distribution, chemical characteristics, and solubility behavior. *Energy & Fuels* 29 (4): 2143–2152.

Sato, S., T. Takanohashi, and R. Tanaka. 2005. Molecular weight calibration of asphaltenes using gel permeation chromatography/mass spectrometry. *Energy & Fuels* 19 (5): 1991–1994.

Savage, P. E., M. T. Klein, and S. G. Kukes. 1988. Asphaltene reaction pathways. 3. Effect of reaction environment. *Energy & Fuels* 2 (5): 619–628.

Sedghi, M., L. Goual, W. Welch, and J. Kubelka. 2013. Effect of asphaltene structure on asso- ciation and aggregation using molecular dynamics. *The Journal of Physical Chemistry B* 117 (18): 5765–5776.

Sharma, A., H. Groenzin, A. Tomita, and O. C. Mullins. 2002. Probing order in asphaltenes and aromatic ring systems by HRTEM. *Energy and Fuels* 16 (2): 490–496.

Sharma, M. K., and T. F. Yen. 1994. *Asphaltene Particles in Fossilfuel Exploration, Recovery, Refining, and Production Processes*. New York: Springer.

Shimadzu excellence in science. 2017. PONA Analysis (GC): SHIMADZU (Shimadzu Corporation). *SHIMADZU* (*Shimadzu Corporation*). Accessed April 22. http://www.shimadzu.com/an/industry/machineryautomotive/fuel_battery0403020.htm.

Sieben, V. J., A. J. Stickel, C. Obiosa-Maife, J. Rowbotham, A. Memon, N. Hamed,

J. Ratulowski, and F. Mostowfi. 2017. Optical measurement of saturates, aromatics, resins, and asphaltenes in crude oil. *Energy & Fuels* 31 (4): 3684–3697. doi:10.1021/acs.energyfuels.6b03274.

Silva, R. C., P. R. Seidl, S. M. C. Menezes, and M. A. G. Teixeira. 2004. 1H and 13C NMR for determining average molecular parameters of asphaltenes from vacuum residue distillation. *Annals of Magnetic Resonance* 3: 63–67.

Silverstein, R. M., F. X. Webster, D. J. Kiemle, and D. L. Bryce. 2014. *Spectrometric Identification of Organic Compounds*. Hoboken, NJ: John Wiley & Sons.

Simanzhenkov, V., and R. Idem. 2003. *Crude Oil Chemistry*. Boca Raton, FL: CRC Press.
Speight, J. G. 2014. *The Chemistry and Technology of Petroleum*, 5th ed. Boca Raton, FL:

CRC Press.

Speight, J. G., and S. E. Moschopedis. 1981. On the molecular nature of petroleum asphaltenes. In *Chemistry of Asphaltenes*, 1–15. Advances in Chemistry 195. Washington, DC: American Chemical Society. doi:10.1021/ba-1981-0195.ch001.

Speight, J. G., and R. J. Pancirov. 1984. Structural types in petroleum asphaltenes as deduced from pyrolysis/gas chromatography/mass spectroscopy. *Liquid Fuels Technology* 2 (3): 287–305.

CRUDE OIL AND ASPHALTENE CHARACTERIZATION

Stefanis, E., and C. Panayiotou. 2008. Prediction of Hansen solubility parameters with a new group-contribution method. *International Journal of Thermophysics* 29 (2): 568–585.

Strausz, O. P., P. Peng, and J. Murgich. 2002. About the colloidal nature of asphaltenes and the MW of covalent monomeric units. *Energy & Fuels* 16 (4): 809–822.

Sztukowski, D. M. 2005. Asphaltene and solids-stabilized water-in-oil emulsions. Retrieved from http://adsabs.harvard.edu/abs/2005PhDT 171S.

Tang, G. Q., and N. R. Morrow. 1997. Salinity, temperature, oil composition, and oil recovery by waterflooding. *SPE Reservoir Engineering* 12 (04): 269–276.

The World Factbook. Central Intelligence Agency. 2017. www.cia.gov/library/publications/ the-world-factbook. Accessed April 21, 2017.

Thomas, R. 2016. *Practical Guide to ICP-MS: A Tutorial for Beginners*, 3rd ed. Boca Raton, FL: CRC Press.

Tojima, M., S. Suhara, M. Imamura, and A. Furuta. 1998. Effect of heavy asphaltene on sta- bility of residual oil. *Catalysis Today* 43 (3–4): 347–351.

U.S. Energy Information Administration. 2017. U.S. Energy Facts. Accessed April 19. Retrieved from https://www.eia.gov/energyexplained/?page=us_energy_home.

Vargas, F. M., and W. G. Chapman. 2010. Application of the one-third rule in hydrocarbon and crude oil systems. *Fluid Phase Equilibria* 290 (1–2): 103–108.

Vazquez, M., and H. D. Beggs. 1980. Correlations for fluid physical property prediction.

Journal of Petroleum Technology 32 (06): 968–970.

Walker, J. M., and R. Rapley. 2008. *Molecular Biomethods Handbook*, 2nd ed. Totowa, NJ: Humana Press.

Wang, F., T. J. Threatt, and F. M. Vargas. 2016. Determination of solubility parameters from density measurements for non-polar hydrocarbons at temperatures from (298–433) K and pressures up to 137 MPa. *Fluid Phase Equilibria* 430: 19–32.

Wang, J., and J. S. Buckley. 2001. A two-component solubility model of the onset of asphal- tene flocculation in crude oils. *Energy & Fuels* 15 (5): 1004–1012.

Wang, W., and A. Gupta. 1995. Investigation of the effect of temperature and pressure on wettability using modified pendant drop method. In *Society of Petroleum Engineers*. doi:10.2118/30544-MS.

Wiehe, I. A., and K. S. Liang. 1996. Asphaltenes, resins, and other petroleum macromol- ecules. *Fluid Phase Equilibria* 117 (1): 201–210.

Wilt, B. K., W. T. Welch, and J. G. Rankin. 1998. Determination of asphaltenes in petro- leum crude oils by fourier transform infrared spectroscopy. *Energy & Fuels* 12 (5): 1008–1012.

Woods, J., J. Kung, D. Kingston, L. Kotlyar, B. Sparks, and T. McCracken. 2008. Canadian crudes: A comparative study of SARA fractions from a modified HPLC separation

CRUDE OIL AND ASPHALTENE CHARACTERIZATION

technique. *Oil & Gas Science and Technology—Revue de l'IFP* 63 (1): 151–163.

The World Factbook—Central Intelligence Agency. 2017. Accessed April 21. Retrieved from https://www.cia.gov/library/publications/the-world-factbook/rankorder/2244rank.html.

Wu, H., and M. R. Kessler. 2015. Asphaltene: Structural characterization, molecular func- tionalization, and application as a low-cost filler in epoxy composites. *RSC Advances* 5 (31): 24264–24273.

Xu, W. 2005. Experimental Investigation of Dynamic Interfacial Interactions at Reservoir Conditions. Louisiana State University. http://etd.lsu.edu/docs/available/etd-04112005-141253/.

Yarranton, H. W. 2005. Asphaltene self-asssociation. *Journal of Dispersion Science and Technology* 26 (1): 5–8.

Yarranton, H. W., H. Alboudwarej, and R. Jakher. 2000. Investigation of asphaltene associa- tion with vapor pressure osmometry and interfacial tension measurements. *Industrial & Engineering Chemistry Research* 39 (8): 2916–2924.

YingShi, H., Y. HongQing, Z. XiaoPing, J. Guitarte, X. ChengGang, L. WeiMin, C. Xiang, and G. HongZhi. 2012. Cased hole formation testing in challenging operational condi- tions reveals reservoir fluids distribution: South China sea case study. In *IPTC 2012: International Petroleum Technology Conference*.

Yousef, A. A., S. Al-Saleh, A. U. Al-Kaabi, and M. S. Al-Jawfi. 2010. Laboratory investigation of novel oil recovery method for carbonate reservoirs. Canadian Unconventional Resources and International Petroleum Conference, October 19–21, Calgary, Alberta, Canada, Society of Petroleum Engineers. doi:10.2118/137634-MS.

Yuan, Y., and T. R. Lee. 2013. Contact angle and wetting properties. In *Surface Science Techniques*, G. Bracco and B. Holst (Eds.), 51:3–34. Berlin, Germany: Springer.

Zhao, Y., F. Wei, and Y. Yu. 2010. Effects of reaction time and temperature on carbonization in asphaltene pyrolysis. *Journal of Petroleum Science and Engineering* 74 (1–2): 20–25.

CHAPTER

2

CHARACTERISTICS OF CONVENTIONAL OIL AND GAS RESOURCES

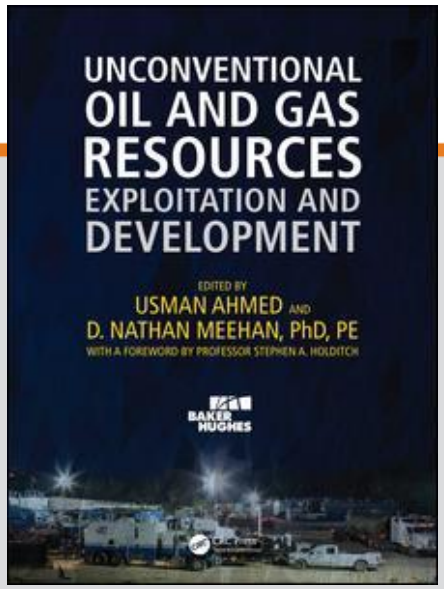

This chapter is excerpted from

Unconventional Oil and Gas Resources Exploitation and Development

by Usman Ahmed, D. Nathan Meehan

Learn more

CHARACTERISTICS OF CONVENTIONAL OIL AND GAS RESOURCES

Characteristics of Unconventional Oil and Gas Resources

"The pessimist complains about the wind. The optimist expects it to change. The leader adjusts the sails."

John Maxwell

Foreword

The adjustments to the unconventional resource exploitation and development sail starts here.

Chapter 2 discussed the difference between unconventional resources and conventional resources. Here, discussions

are presented to characterize unconventional oil and gas resources. We start the discussion by reviewing the

unconventional resources in general, followed by addressing the unconventional resource triangle, which then leads us to discuss the shale resources. This is followed by an overview of tight oil and gas and coalbed methane (also referred to as coal seam gas, or CSG, in Australia).

3.1 Introduction to Unconventional Resources

Some definitions change with time. The depths that correspond to deep water for oil and gas have increased over time as technologies and capabilities have been enhanced. Similarly, the definition of tight oil has changed, as has the meaning of unconventional in relation to reservoirs. For

our purposes, we often describe reservoirs as shales, when they may be, in fact, a combination of marls, mudstones, or even carbonates. This chapter presumes the reader has

some familiarity with both conventional and tight oil and gas principles as we discuss unconventional reservoirs. For this purpose we can use practical and approximate definitions based on the types of wells and completions required.

n Conventional reservoirs can be developed with vertical wells and do not need

CHARACTERISTICS OF CONVENTIONAL OIL AND GAS RESOURCES

large hydraulic fracture stimulation treatments. If used, a conventional well's hydraulic fracturing treatment is typically less than a 100-ft. wing length and has a cost that is less than 10% of total well costs. Using horizontal wells in conventional reservoirs may significantly improve performance if the reservoir is

naturally fractured, is thin, or has important gravity features such as a gas-oil or water-hydrocarbon contact. Transient flow behavior in such wells is often a practical approach for characterizing the reservoir.

n Tight reservoirs require large hydraulic fracture stimulation treatments whose half-wing length is hundreds of feet, which can cost a significant portion of total well costs. Tight

reservoirs produce at negligible to uneconomical rates without stimulation. Horizontal wells with multiple hydraulic fracture stages may improve production; however, operators rarely use dozens of such stages in typical tight reservoirs. Transient flow periods in such wells may be over many months.

n Unconventional reservoirs require long (3,000 to 10,000 ft.) horizontal wells with dozens of hydraulic fracture stages for commercial production. The proximity of

the fracture stages results in stress interference and some degree of improvement in the aggregate matrix permeability. This arises from multiple mechanisms that can include slippage of critically stressed fractures, movement along slowly slipping faults, and complex hydraulic fracture geometry. Transient flow behavior in

such wells is highly complex. Diffusion may ultimately be an important contributor to production.

3.1.1 Shale Reservoirs as Unconventional Plays

According to the US Geological Survey, production from unconventional reservoirs exists in geographically extensive accumulations (USGS report). Unconventional

reservoir deposits generally lack well-defined hydrocarbon/ water contacts and include coalbed methane, some tight sandstone reservoirs, chalks, and self-sourced oil and gas in shale accumulations. The assessment methodology and

production practices for unconventional reservoirs vary from those used for conventional resources. General categories of unconventional petroleum include:

n Deep gas

n Shallow biogenic gas

n Heavy oil and/or natural bitumen

n Shale gas and oil

n Gas hydrates

CHARACTERISTICS OF CONVENTIONAL OIL AND GAS RESOURCES

n Coalbed methane

While the level of maturity of these unconventional resources varies, oil and gas production from shale reservoirs is growing at a phenomenal rate. The type of shale production being discussed is generally conventional oil or gas produced from relatively deeply buried shales that are produced in a manner

roughly similar to conventional wells. We refer to this as shale oil and shale gas. The term *oil shale* is widely applied to petroleum extracted from shallow rocks with very high kerogen content. Many of the rocks referred to as oil shales are not shales and theses rocks are often physically mined rather than having the hydrocarbons produced through wellbores. Oil shales typically contain solid or ultraviscous hydrocarbon material in their pores. While some oil shales can be burned directly, most require some sort of extractive

process, coupled with upgrading, to yield oil like hydrocarbons. Oil shales are not discussed in this book.

3.1.2 So, What Is a Shale Anyway?

Shales are the most abundant types and volumes of rocks in sedimentary basins worldwide. Shales are the most abundant sources of hydrocarbons for oil and gas fields and due to their low permeabilities form the hydrocarbon seal for many fields. A conventional oil or gas field needs a

source, a reservoir (usually porous sandstones or carbonates such as limestone or dolomite), a trap (such as a structural closure, sealing fault, or pinchout), and a seal. The source

is necessary for hydrocarbons to exist and some pathway is necessary for these hydrocarbons to migrate. The reservoir porosity was usually water filled at the time of deposition, allowing the hydrocarbons to migrate through the porosity due to having lower density than the water. The trap and seal are necessary to prevent continued migration (to keep the hydrocarbons in place) and to allow the reservoir to accumulate and store oil or gas. As a result, geologists and geochemists have studied shales extensively with most

of their historical effort focused on shale's source rock potential. The fact that many shales still contain significant amounts of natural gas is no surprise to drillers and geologists. It is routine to observe natural gas "shows" while drilling through shales, occasionally in significant volumes.

But while it may be clear to most readers what porous sandstone or carbonate rock is like (the rocks that form most oil and gas reservoirs), shales remain somewhat of a mystery.

There are multiple definitions of what constitutes shale.

CHARACTERISTICS OF CONVENTIONAL OIL AND GAS RESOURCES

A geologist once mentioned that the way to differentiate between siltstone and shale was to put it in your mouth. If it tastes gritty, it is a siltstone. If it tastes smooth or oily, it is shale. For the record, the authors do not recommend putting any rocks in your mouth!

Shales are sedimentary rocks composed of clastics (portions of older rocks) comprised of silts, muds, and clays. Geological definitions of shales typically reference their grain size as being clay-like (less than 1/256th mm diameter particles).

Silts are also defined based on grain sizes (between 1/16th and 1/256th mm) and are positioned between clays and sands. Very fine silts can be primarily composed of quartzitic materials that are lacking in typical clay minerals. Clay minerals often include kaolinite, montmorillonite-smectite, illite, and chlorite. There are dozens of pure clays, with most clays being mixtures of multiple pure clays. One important clay type in oilfield operations is bentonite, a typical weighting component of drilling mud. Another physical property often used in defining shales is their tendency to split into thin sheets or slabs (fissility). Muds are simply mixtures of water and very fine silt, clay, and soil particles. Mudstones are hardened muds that may not show fissility unless desiccated. While most shales are clastics, significant carbonate components can be present in shales. The formations we refer to as *shale gas* or *shale oil plays* are often layers of shales and layers of silts and/or carbonates.

The depositional environment of shales that are resource plays is typically a low-energy one that allows very fine- grained particles that will constitute future shales to be deposited. High-energy deposits such as channel sands and turbidites will also lead to shale deposition. The low depositional environments associated with marine shales means that their geological and petrophysical properties

change relatively slowly over large distances compared with the higher levels of heterogeneities in many sandstones and carbonates. Petrophysicists take advantage of this when analyzing logs of varying vintages and from varying suppliers by normalizing log responses in marine shales.

Very fine-grained, organic material (usually from plant materials) is often deposited concurrently with the silt, mud, and clay matter that will eventually form shales. Total organic carbon (TOC) is the weight-percent of organic carbon in the shale (and does not include carbon from carbonates for example). Because many shales have relatively high organic carbon content, under certain heat

and temperature conditions, shales can serve as source rocks for oil and gas reservoirs. The organic content originated with living material, ultimately from plant, animal, and bacterial matter such as algae, plankton, or decomposed plant materials. After death, the materials decompose, and the decomposition products can form new polymers to form kerogen. Diagenesis is controlled primarily by biological

and chemical activity associated with mineralogy and redox conditions. Complex thermal transformations characterize subsequent kerogen transformation.

CHARACTERISTICS OF CONVENTIONAL OIL AND GAS RESOURCES

The word kerogen was originated by Professor Crum Brown (of the University of Edinburgh, Scotland) and referred specifically "…to the carbonaceous matter in shale that gives rise to crude oil in distillation" (Brown 1979). Kerogen now refers more broadly to all of the solid organic material in sedimentary rocks; kerogen is generally insoluble in water or organic solvents due to their high molecular weights. Bitumen refers to the insoluble portion.

Kerogen may be formed under various circumstances from this organic matter, which can be broken down into lighter organic materials under heat and pressure. Most oil and gas produced originated with such shales as sources with a few exceptions.

Shales generally have extremely low permeability due to their very fine grain size. Permeabilities are so low in most

shales that excellent seals for oil and gas fields can be formed by shales. Drillers and mud loggers have long known that many shales contain significant quantities of natural gas, because natural gas discoveries are commonplace during drilling through shales. While some shales are rich in heavy hydrocarbons (oil shales), this discussion focuses on shales that are likely to contain natural gas or oil.

It is important to note that the type of shale production being discussed here is generally conventional oils or gas produced from relatively deeply buried shales that are produced in a manner roughly similar to conventional wells. We refer to this as shale oil and shale gas. The term *oil shale* is widely applied to petroleum extracted from shallow rocks with very high kerogen content. Many of the rocks referred to as oil shales are not actually shales—these rocks are often physically mined rather than having the hydrocarbons produced through wellbores. Oil shales contain typically solid or ultraviscous hydrocarbon material in their pores. While some oil shales

can be burned directly, most require some sort of extractive process coupled with upgrading to yield oil like hydrocarbons. Oil shales are not discussed here.

Shale gas production has been recorded for over a century in the Devonian age formations in the Appalachian basin. More than 20,000 wells have been drilled in these shallow shales. Older (and deeper) Devonian shales include the Marcellus formation, which is now a major focal point for the application of advanced technology. Because we have

known about these shales and their hydrocarbon potential for decades, if not more than a century, why has it taken so long to produce them? The answer is clear: the technology to drill, evaluate, complete, and produce these shale plays has only been available for a decade (at best), and many advances have been made in just the last few years.

CHARACTERISTICS OF CONVENTIONAL OIL AND GAS RESOURCES

3.1.3 Shales as Resource Plays

A resource play is a relatively large hydrocarbon accumulation that occurs over a broad geological area. In a resource play, the geological risk of encountering the hydrocarbon bearing strata is nearly certain within the play area. A resource play may nonetheless have wide variability in well performance; however it is often the case that such variability cannot easily be predicted in advance or even correlated to conventional measurements (e.g., porosity, thickness). Resource plays have alternately been described as statistical plays, in which an operator must drill a large number of wells and can expect fairly repeatable results if enough wells are drilled.

Tier one criteria used in defining resource plays include the following characteristics taken from the Society of Petroleum Evaluation Engineers (SPEE) Monograph 2011:

1. Exhibits a repeatable statistical distribution of estimated ultimate recoveries (EURs).

2. Offset well performance is not a reliable predictor of undeveloped location performance.

3. Continuous hydrocarbon system that is regional in extent.

4. Free hydrocarbons (non-sorbed) are not held in place by hydrodynamics.

The SPEE provides certain statistical guidelines for the evaluation of resource plays that require each of the prior criteria to be met. Many shale gas reservoirs are considered to be resource plays, with both geological and engineering data supporting the criteria. It cannot be proven that a given

area is a resource play until a significant number of wells have been drilled—and enough performance data is analyzed—to justify the conclusion. From those criteria, the most important criterion is the first one, which is the repeatable statistical distribution of EURs. Having a statistical distribution of EURs is characteristic of many reservoirs. If the mean measurement (and other measures of the statistical distributions) varies significantly spatially, especially if the variance is, in some way,

correlated to readily identifiable geological data (such as TOCs, thickness, etc.), the play is unlikely to be a true resource play.

CHARACTERISTICS OF CONVENTIONAL OIL AND GAS RESOURCES

The second criterion implies heterogeneity in well performance. This is true of many non-resource plays, including many carbonate reservoirs, so it is not sufficient. The importance is that reasonably obtainable measurements (such as kh) do not predict well performance changes. This truly complicates matters when operators assume the second criterion is "true" and decide not to go to the expense of obtaining well logs. As we will see in Chapter 8, formation evaluation tools for shale gas wells are available that can produce detailed geological and mineralogical information including clay types, TOC, silica content, etc. Such data might be highly predictive of well performance and could even indicate ways to improve well completions and future drill site selections. If such logs are not run and analyzed, the operator will conclude that there is no way to explain variability other than the "statistical" nature of the play.

The third and fourth criteria are generally present in all productive shale gas plays. Tier two criteria (the next tier of criteria) include:

5. Requires extensive stimulation to produce at economic rates.

6. Produces little in-situ water (except for coalbed methane and tight oil reservoirs).

7. Does not exhibit an obvious seal or trap.

8. Low permeability (< 0.1 md) shale bulk permeabilities are typically less than 0.001 md.

Shale gas plays generally satisfy each of these criteria easily. As the plays form seals for conventional reservoirs, they do not have to have a separate trap. Thus, a syncline may easily be as productive as an anticline in shale. The permeabilities of shale gas reservoirs are often well below 0.01 md and generally require stimulation. Shale gas reservoirs have such low permeabilities that free water production is rare; highly fractured shales could allow water from deeper zones to be produced.

3.1.4 Shale as Reservoirs?

While shales are known to be the principal sources for conventional hydrocarbon plays as well as seals, shales can also be the reservoir and trap. Most of the gas created in such reservoirs would be thermogenic in origin, although some shales

CHARACTERISTICS OF CONVENTIONAL OIL AND GAS RESOURCES

(e.g., the Antrim) have significant quantities of biogenic gas. Gas is stored in shales either as free gas in the pore spaces or adsorbed onto the organic material or surface walls in the shale.

Thermogenic methane was formed when organic matter was compressed at very high pressures for a very long time. Just as in oil formation, thermogenic methane is a cracking process that transforms organic particles carried in the clastic material, which then forms the origin of shales. The nature of the organic material and time and pressure dictate what is formed in thermogenic processes. Thermogenic gas can contain significant quantities of heavier hydrocarbons.

Biogenic methane can be formed by microorganisms that chemically break down organic matter. Biogenic methane is generally formed at shallow depths in anoxic environments. While most of this methane escapes to the atmosphere, some can be trapped and buried at depth. Modern landfills can also form biogenic methane. Biogenic methane is essentially unrelated to the processes that form oil—biogenic gas primarily contains methane with very few heavier hydrocarbons. A standard measure of whether a gas is thermogenic or biogenic can be determined by gas geochemistry. Thermogenic gas has less carbon 13 compared to the predominant carbon 12 than do biogenic gases.

3.1.5 Role of Geochemistry

Many tools are used to analyze and study shales. The total organic carbon (TOC) is typically determined by calculating the difference between total organic carbon and the carbonate carbon concentration. While both of the latter measurements are generally made with cuttings or core samples, petrophysical estimates of TOC can provide excellent and continuous estimates of TOC.

Pyrolysis of organic matter in shales involves heating samples to extract volatile hydrocarbons (referred to as S1), thermogenic hydrocarbons (S2), and the carbon dioxide released up to a fixed temperature (S3). The methodology to make these measurements involves pulverizing a small sample of rock and heating it to increasing temperatures. These values (S1 through S3) are used in calculating several common geochemical values including the hydrogen and oxygen indices (HI and OI). The temperature above which no further hydrocarbons are released by pyrolysis is referred to as Tmax and provides a common measure of organic matter. The indices are defined as follows:

HI = (100S_2)*Y*TOC

with units of milligrams hydrocarbons per gram of organic carbon and

CHARACTERISTICS OF CONVENTIONAL OIL AND GAS RESOURCES

OI = (100S_3)/TOC

with units of milligrams CO2 /gram organic carbon.

Geochemists use these values to assess the shale's source rock potential along with the hydrocarbon generation potential and also to describe the types of kerogen. The authors of Chapter

8 point out the value of the S1/TOC ratio and demonstrate that values in excess of 100 milligrams hydrocarbons/gram of

organic carbon are very positive for the production potential of shale oil and shale gas.

Vitrinite reflectance is another widely used measurement associated with shales. Plants take in CO2 and water to generate carbohydrates and polymers that form plant material such as cellulose and lignins. It is this plant material that (with time, temperature, and pressure) ultimately creates oil or natural gas. Vitrinite is a shiny material formed by the thermal alteration of such organic matter; it is present in most kerogens and coals. Vitrinite reflectance is often used to describe the maturity of coals. For example, lignite is a coal with low thermal maturity and reflectance, and anthracite is a highly reflective and more mature coal.

Coalification of peat is strongly analogous chemically and physically to the maturation of kerogen. Vitrinite reflectance can be used in conjunction with TOC values, pyrolysis data, etc. Vitrinite reflectivity is typically measured with an oil-immersion microscope and a device for measuring reflected light. Comparisons are made with reference standards to define the reflectance in oil, R0. While R0 is a measure of thermal maturity, its significance is a function of the type of kerogen being analyzed. Nonetheless, low values of R0 indicate immature kerogen. As R0 increases, the indicated maturity levels suggest oil generation, gas generation with condensates (wet gases), and, ultimately, dry gases at high levels of thermal maturity. At such levels, sufficient time and temperature will have cracked heavier organic molecules.

Different types of kerogen are usually described based on their relative amounts of hydrogen, carbon, and oxygen. Each type of kerogen has varying tendencies to form oil, gas, and coal. The reasons for the different chemical compositions include the type of organic material present (including plankton, algae, spores, pollen, diatoms, etc.) and the chemical processes to which the material was exposed.

While not as routinely used in shale oil and shale gas evaluations, geoscientists often make use of the organic carbon isotope ratios, and atomic carbon nitrogen

CHARACTERISTICS OF CONVENTIONAL OIL AND GAS RESOURCES

ratios, to analyze shale depositional histories and in related studies. Geochemistry can be a powerful tool for reservoir engineers in many areas besides the analysis of unconventional reservoirs.

3.2 Workflow to Address Unconventional Resource Development

As we have noted, classical unconventional resource definitions include coalbed methane (CBM), tight oil and gas reservoirs, and shale oil and gas. Sometimes heavy oil development is lumped with unconventional resources. We choose to place heavy oil in a different category, because the others, as a group, have a lot of similarity in the technology and development requirements that heavy oil does not.

Cost-effective development of the three unconventional resources (listed previously) can follow a certain life-cycle approach, which is a six-step, phased approach that addresses exploration, appraisal, development, production, rejuvenation, and abandonment phases. In the life-cycle approach, we acknowledge the subtle differences between the three groups of unconventional resources and how these factors affect the overall understanding of the reservoir. From this, we can extrapolate the exploitation strategy (placement of wells and stimulation locations and all aspects associated with the process followed by a rejuvenation phase). Field case studies suggest that using such a process can positively affect the recovery factor, while the increased operational efficiency garnered from the process can reduce cost, depending on the scale and scope of the project. Finally, well-thought-out field understanding and development design alone is not good enough without a continued commitment of resources (people, tools, and software). Of these resource commitments, typically the hardest one to meet is securing the proper unconventional resources expertise. Over the last decade, an increased understanding about unconventional resource development has come about in North America, which is now prime to be potentially disseminated as long as we take the time to understand the difference of the new basin and its associated challenges (Ahmed 2014).

There are subtle differences between the three unconventional resources, even though they still follow a similar workflow process as illustrated in **Fig. 3.1** (an entire chapter on workflow is dedicated within Chapter 5). Therefore, as we illustrate the resource triangle, we will then follow with a detailed characterization of the shale oil and gas. Then, we dedicate sections to tight oil and gas and CBM to illustrate the subtle differences in the characterization of both, even though the workflow and development process remain unchanged.

CHARACTERISTICS OF CONVENTIONAL OIL AND GAS RESOURCES

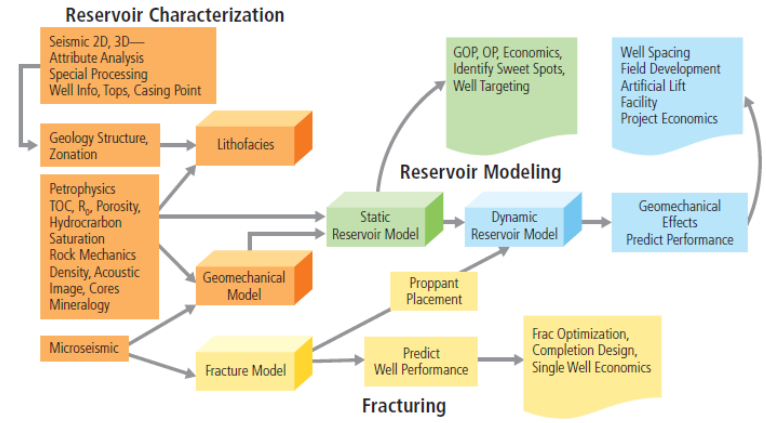

Fig. 3.1—Workflow process and outline for unconventional resources exploitation and development. (From Vassilellis et al. 2011.)

3.1 The Unconventional Resource Triangle

The resource triangle concept was used by Masters (1979) as a method to find large gas fields and build a company in the 1970s. **Fig. 3.2** illustrates the principle of the resource triangle. In the resource triangle, conventional gas is located at the top with better reservoir characteristics and quality,

is associated with conventional technology and ease of development, but exists in small volumes (Holditch 2006). As we navigate further down the triangle, past tight gas and coalbed methane (CBM), shale gas (and gas hydrates) are found at the bottom of the triangle. Progression to

the bottom of the triangle is associated with permeability and reservoir quality decreasing, the technology needed to develop increasing (i.e., becoming more complex), and difficulty of development increasing; however large volumes of these resources can be found. The concept of the resource triangle applies to every hydrocarbon-producing basin in the world. Martin et al. (2008) validated the resource triangle concept using a computer program, database, and software they developed. They also expanded the resource triangle to include liquid and solid hydrocarbons adding heavy oil and oil shale, and referencing work from Gray (1977). Shale resource development is at the bottom left signifying that the resource base is huge (documented in Chapter 4) with decreasing reservoir quality requiring deployment of increasing and demanding technology.

3.2 Characteristics of Shale Oil and Gas

In addition to Section 3.1, in this section we will use the work done by others to characterize shale oil and gas as an unconventional reservoir contained in fine-grained, organic rich, sedimentary rocks, including shale, but composed

of mud containing other minerals like quartz and calcite (US DOE 2009; Warlick 2010; US EIA 2011). A number of formations broadly referred to by industry as *shale*, may contain very little shale lithology and/or mineralogy, but are

considered to be shale by grain size only. Passey et al. (2010) describes shale as extremely fine-grained particles, typically less than 4 microns in diameter, but that may contain variable amounts of silt-sized particles (up to 62.5 microns). No two

CHARACTERISTICS OF CONVENTIONAL OIL AND GAS RESOURCES

shales are alike and they vary areally and vertically within a trend and even along horizontal wellbores (King 2010). Not only will shales vary from basin to basin, but also within the same field (Economides and Martin 2007). These reservoirs are continuous hydrocarbon accumulations that persist over very large geographic areas. Shale hydrocarbon accumulations can range from dry gas to wet gas to condensate, and to all oil phases as seen in the Eagle Ford development. The challenge in developing shale resources is not just to find oil and gas, but to also find the best areas,

or sweet spots, that can result in the best production and recovery (Jenkins and Boyer 2008).

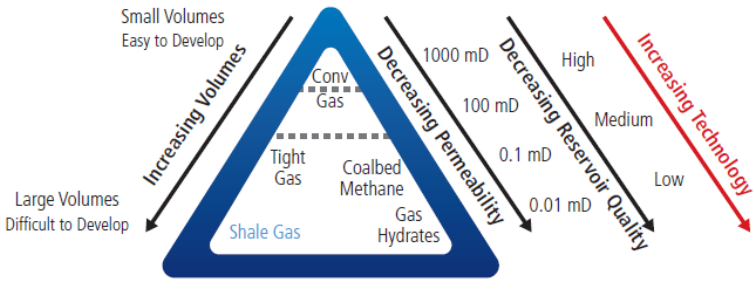

Fig. 3.2—The Unconventional Resource Triangle: The concept of the resource triangle applies to every hydrocarbon-producing basin in the world. (Holditch 2006 after Masters 1979 and Gray 1977.)

CHARACTERISTICS OF CONVENTIONAL OIL AND GAS RESOURCES

Shale reservoirs have no trap like conventional gas reservoirs, and do not contain a gas and/or water contact. Shales are the source rock, which also now acts as the reservoir, where the total or partial volume of oil and gas (hydrocarbon) remains. Shales are the source rock for most of the hydrocarbons.

The key to success with shale is to find the shale plays where the remaining hydrocarbons were not expulsed and did not migrate into conventional formations and are now economically viable for development. A note of caution: not all shales are source rocks and not all shale source rocks still hold the accumulated hydrocarbon.

In terms of the flow behavior, we have already mentioned in the coalbed methane section that shale has more similarity with coalbed methane than tight sedimentary rocks and is illustrated further below.

Natural matrix permeability in shales is extremely low, often in the nano-darcy range. Measurement of shale permeability is difficult and the results are probably inaccurate. In this extreme low-permeability environment, gas (hydrocarbon) flow through the matrix is extremely limited and insufficient for commercial production. Various authors have estimated that a gas molecule will move no more than 10 to 50 feet per year through shale matrix rock. Shale porosities are also relatively low ranging from less than 5 to 12%. Shale reservoirs require hydraulic fracturing to produce commercial amounts of gas. Shale reservoirs with oil resources tend

to have relatively higher permeability and porosity, yet still very low. The porosity is still fairly low; therefore, hydraulic fracturing is still required in this type of shale reservoir to create a path for the oil to flow.

A number of different reservoir parameters that are not necessarily deemed important for conventional gas are still significant for assessing economic viability, development, and well completion techniques for shale production.

This includes the following parameters that we must now consider for shale reservoirs:

- Total organic carbon (TOC) content, kerogen type, and thermal maturity (also referred to as, and measured as, vitrinite reflectance, R0)
- Mineralogy/lithology, brittleness, existence of natural fractures, and stress regime
- Multiple locations and types of oil and gas storage in the reservoir
- Thermogenic or biogenic systems
- Depositional environment, thickness, porosity, and pressure

Though not a parameter, the characteristic steep production decline profile is an important aspect here.

CHARACTERISTICS OF CONVENTIONAL OIL AND GAS RESOURCES

The discussion, next, briefly covers each of these parameters along with the unique aspects of shale, to provide an understanding of the parameters' significance in play analysis and development.

Organic materials, microorganism fossils, and plant matter provide the required carbon, oxygen, and hydrogen atoms needed to create natural gas and oil. TOC is the amount of material available to convert into hydrocarbons (depending on kerogen type) and represents a qualitative measure of source rock potential (Jarvie et al. 2007). This measure is commonly expressed as a *percent by weight*, but it is also sometimes expressed as *percent by volume* (volume

% approximately twice that of weight %). Oil and gas

Table 3.1—Types of kerogen and the hydrocarbon potential by environment, type, and origin. (From Holditch 2011.)

Types of Kerogen and Their Hydrocarbon Potential				
Environment	Kerogen Type	Kerogen Form	Origin	HC Potential
Aquatic	I	Alginite	Algal bodies	Oil
			Structureless debris of algal origin	
	II	Amorphous Kerogen	Structureless planktonic material, primarily of marine origin	
Terrestrial		Exinite	Skins of spores and pollen, cuticles of leaves, and herbaceous plants	
	III	Vitrinite	Fibrous and woody plant fragments and structureless colloidal humic matter	Gas, some oil
				Mainly gas
	IV	Inertinite	Oxidized, recycled woody debris	None

CHARACTERISTICS OF CONVENTIONAL OIL AND GAS RESOURCES

source rocks typically have greater than 1.0% TOC. TOC richness can range from poor at < 1%, to fair at 1 to 2%, to good-to-excellent at 2 to 10% (PESGB 2008). TOC is not the same as kerogen content, because TOC includes both kerogen and bitumen. TOC measurements in shale are determined from wireline logs and by direct measurement from cores and drill cuttings. Kerogen is a solid mixture of organic chemical compounds that make up a portion of the organic matter in sedimentary rocks. Kerogen is insoluble in normal organic solvents because of the huge molecular weight of its component compounds. The soluble portion

is known as bitumen. There are basically four types of kerogen, three of which can generate hydrocarbons. Type I generates oil, Type II wet gas, and Type III dry gas (Holditch 2011). Understanding the kerogen type helps to predict the hydrocarbon type in a play. **Table 3.1** shows the types of kerogen and their hydrocarbon generating potential.

Thermal maturity measures the degree to which a formation has been exposed to high heat needed to break down organic matter in hydrocarbons. As temperature increases with the increasing depth in the earth's crust, heat causes generation of hydrocarbons and can ultimately destroy them. Typical temperature ranges at which oil and gas are generated are shown on **Fig. 3.3**. The oil window is 60 to 175°C (140-to-350°F) and the gas window is 100 to 300°C (212 to 570°F). The position of oil and gas windows within a basin is dependent on the type of organic matter and heating rate. Thermal maturity is a function of both time and temperature (Holditch 2011). Understanding the level of thermal maturity, or indeed whether the shale is thermally mature at all, is key to understanding shale resource

CHARACTERISTICS OF CONVENTIONAL OIL AND GAS RESOURCES

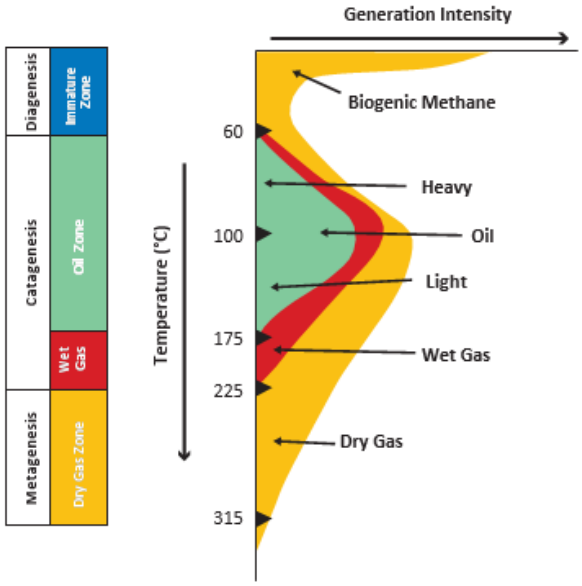

Fig. 3.3—Typical temperature range at which oil and gas are generated. (From Holditch 2011.)

potential (PESGB 2008). Also, higher thermal maturity leads to the presence of nanopores, which contribute to additional porosity in the shale matrix rock (Kuuskra et al. 2011).

Vitrinite reflectance, R_o%, the most commonly used technique for source rock thermal maturity determination, measures the intensity of the reflected light from polished vitrinite particles (a maceral group formed by lignified, higher-land plant tissues, such as leaves, stems, and roots) in shale under a reflecting microscope. Increased reflectance is caused by aromatization of kerogen and loss of hydrogen (Jarvie et al. 2007). **Fig. 3.4** is the thermal maturation scale. Dry gas occurs when R_o is greater than 1.0%, wet gas when R_o is between 0.5 and 1.0%, and oil when R_o is between 0.5 and 1.3% (Kuuskraa et al. 2011).

Mineralogy and lithology are important for:

CHARACTERISTICS OF CONVENTIONAL OIL AND GAS RESOURCES

1. Quantifying TOC.

2. Reducing porosity uncertainty.

3. Identifying shale lithofacies.

4. Indicating variations in mechanical rock properties including brittleness.

Assisting in planning well hydraulic fracturing a

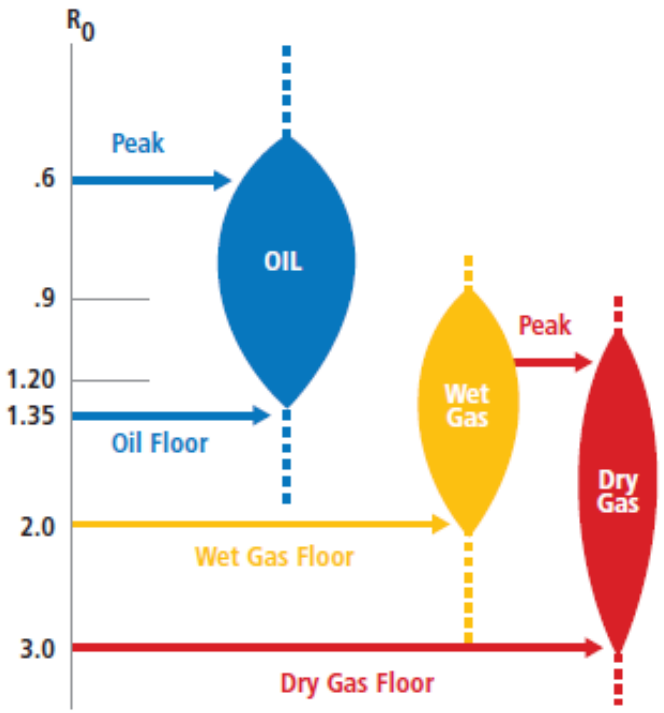

Fig. 3.4—Thermal maturation scale. (From Kuuskra et al. 2011.)

CHARACTERISTICS OF CONVENTIONAL OIL AND GAS RESOURCES

Most shale reservoirs can be chemostratigraphically classified into three primary lithofacies—siliceous mudstone (such as the Barnett), calcareous mudstone lithofacies, and organic mudstone lithofacies. Additional lithofacies have been identified in some reservoirs based on their unique characteristics. Lithology and mineralogy information is obtained from conventional and pulsed neuron log responses, laboratory analysis of cores and cuttings, and mineral spectroscopy analyses. TOC is quantified by the amount and vertical distribution of kerogen, kerogen type, level of maturity, and mineral spectroscopy plus core analysis. Log-derived and computed geomechanical properties include minimum horizontal stress (SHMin), Poisson's ratio, Young's modulus, fracture migration, and static mechanical properties.

Brittleness indicators that are used for identifying best interval to initiate a fracture and location at the vertical from which to drill horizontal laterals are computed from mineralogy and geomechanical brittleness and hardness (Jacobi et al. 2009; LeCompte et al. 2009; Pemper et al. 2009; Mitra et al. 2010).

Geomechanics considerations are significant in the development of unconventional resources in general, not just shale resources. Comments here are also applicable to coalbed methane and tight gas and oil formations. The stress regime in a basin must be considered during well drilling, fracturing, and production. Well orientation is dictated by in-situ stress systems and wellbore stability during drilling. In general, initiating a fracture depends on the stresses around the wellbore—both from the geologically produced tectonic effects and from changes in stresses produced by the fracture growth. Fractures are difficult to initiate where total rock stresses are very high. A major consideration during shale production is the stress evolution accompanying drawdown and depletion activity. It is now well established that reservoir pressure changes have an effect on both the stress magnitudes and direction in the sub-surface (Addis and Yassir 2010; King 2010).

Presence, location, and orientation of natural fractures in shale are significant with respect to the hydraulic fracturing process. In these naturally fractured reservoirs, well placement for initial development is dictated by two sub-surface factors:

1. Location and orientation of natural fracture sets, orientation of the most conductive natural fracture set, and in-situ stress magnitudes and directions

2. Propagation direction of hydraulic fractures from the wellbore and the intersection of natural fracture system (Addis and Yassir 2010)

CHARACTERISTICS OF CONVENTIONAL OIL AND GAS RESOURCES

Table 3.2—Free gas, sorbed gas, and dissolved gas storage methods.

Shale Gas Type →	Free Gas	Sorbed Gas	Dissolved Gas
↓ Storage	In the rock matrix porosity	Adsorbed (chemically bound) to the organic matter (kerogen) and mineral surfaces within the natural fractures	In the hydrocarbon liquids present in the bitumen
	In the natural fractures	Absorbed (physically bound) to the organic matter (kerogen) and mineral surfaces within the matrix rock	

One purpose of hydraulic fracturing is to connect the existing natural fractures to create a complex network of pathways that enable hydrocarbons to enter the wellbore (King 2010; Jenkins and Boyer 2008). For shale gas, the gas (free and sorbed) is stored in three ways in a shale reservoir, as described in **Table 3.2**.

To obtain the total amount of gas in place (GIP), free gas, sorbed gas, and dissolved gas must be added together. Free gas is the *initial flush* production that occurs early, during the first few years of the life of a well. The absorbed gas volume is often significantly more than the free gas stored in the matrix porosity. Gas contents can exceed apparent free gas-filled porosity by

6 to 8 times where organic content is high (Warlick 2010). However, sorbed gas is produced by diffusion or desorption and does not occur until later in the field life after the reservoir pressure has declined. It is generally accepted that sorbed gas does not have an appreciable effect on shale field economics (because it is not produced early in well life), but sorbed gas can constitute a significant part of GIP in some shale reservoirs.

Dissolved gas is only a small part of GIP in most shale reservoirs.

Most shale gas wells produce only dry gas (90% methane) and essentially little water. A notable exception to this is the Eagle Ford where part of the play produces dry gas, part wet gas, and another part produces shale oil. It is understood, based on operator experience, that the emerging Utica shale basin is similar to the Eagle Ford with dry gas, wet gas, and oil areas. The Antrim and New Albany shale do produce formation water. Concerns about water production handling, treating,

re-use, or disposal due to flowback water from fracturing is discussed in Chapter 17.

Shale gas and oil wells display a rather unique decline profile character. Shale gas wells typically exhibit gas storage and flow characteristics uniquely tied to geology and physics (Rushing et al. 2008). Initial production rates are relatively low, in the 2-10+ MMcfd range (horizontal wells), and these rates decline rather rapidly.

However, it seems that a well producing around less than 100 Mcfd would be approaching the economic limit. Shale oil wells have exhibited initial productivity rates in the range of 250 to

CHARACTERISTICS OF CONVENTIONAL OIL AND GAS RESOURCES

2,000 BOPD. Some examples of typical decline type curves are shown as **Fig. 3.5** for Barnett shale gas, in **Fig. 3.6** for Eagle Ford shale gas, in **Fig. 3.7** for Bakken shale oil, and in **Fig.**

3.8 for Eagle Ford shale oil.

Shale natural gas is either *biogenic* in origin, formed by the action of biologic organisms breaking down organic material within the shale, or of *thermogenic* origin formed at depth and high temperatures. Relatively few biogenic gas systems are producing economic gas within the United States. The Antrim shale in Michigan is one of those systems. Another is the New Albany shale of Illinois and Indiana. Wells producing from the biogenic Antrim and New Albany shales have relatively low production rates, e.g., 135 Mcfd; however, they will produce for a long time: 20+ years. In many cases large quantities of water are produced before, or as, any gas is produced. Gas production is closely tied to dewatering the system (like coalbed methane) to gain economic production. Geochemistrical analysis indicates that the water is usually fairly fresh.

The majority of producing shale gas reservoirs in the US are thermogenic systems. Thermogenic gas occurs as a result of primary thermal cracking of the organic matter into a gaseous phase. Secondary thermal cracking of remaining liquids also occurs. Thermal maturity in these reservoirs determines the type of hydrocarbon that will be generated. Gas produced in a thermogenic environment will be relatively dry (Economides and Martin 2007). Reservoir pressure is one of the key parameters to how well conventional gas (and oil) reservoirs perform.

Pressure controls production rates and is used along with boundary conditions to predict recovery. Shale reservoirs range from normally pressured to highly overpressured. The higher pressured shale reservoirs, like the Haynesville, have higher initial production (IP) and higher recovery than others. Higher reservoir pressures do have an effect on the hydraulic fracturing designs; especially selection of appropriate proppants, as higher reservoir pressure can crush some types of proppants.

Depositional environment of shale is important, particularly whether it is marine or non-marine. Marine-deposited shale tends to have lower clay content and be high in brittle materials, such as quartz, feldspar, and carbonates. Because of

CHARACTERISTICS OF CONVENTIONAL OIL AND GAS RESOURCES

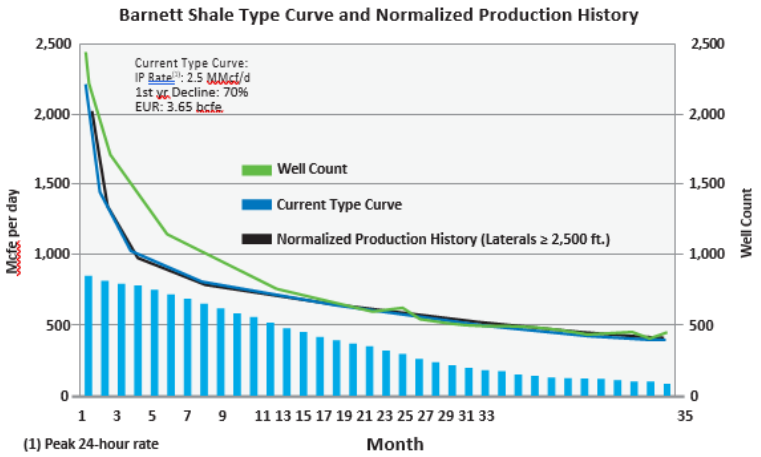

Fig. 3.5—Barnett shale gas. (From EIA 2011.)

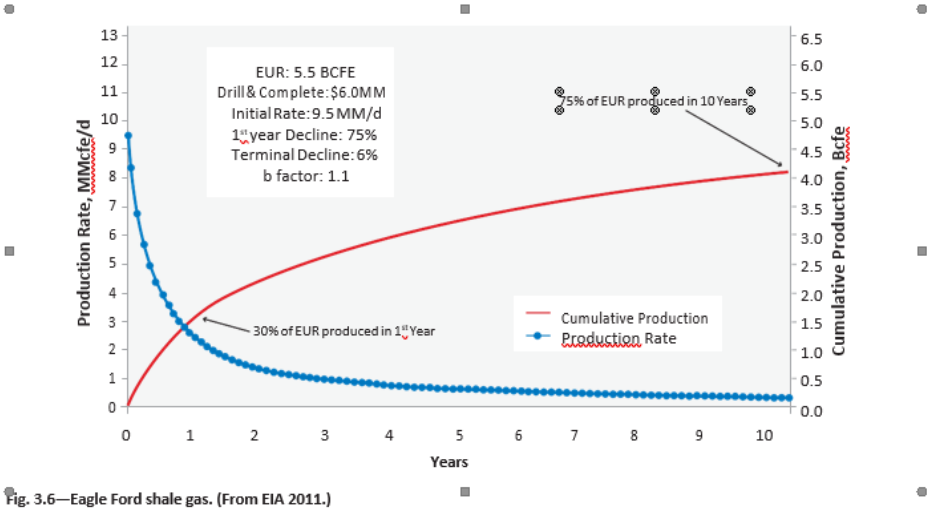

Fig. 3.6—Eagle Ford shale gas. (From EIA 2011.)

this mineralogy, marine-deposited shales respond favorably to hydraulic fracturing. Non-marine deposited shale, i.e., lacustrine and fluvial, tend to be higher in clay, more ductile, and less responsive to hydraulic fracturing. Transgressive systems (also called onlap systems, due to a transgression) are characterized by higher TOC and quartz and less clay. Shale deposited during transgressive systems not only responds favorably to hydraulic fracturing, but also can have higher hydrocarbon recoveries. Alternatively, regressive systems are characterized by lower TOC and quartz and higher clay content. Shales deposited during regression are less responsive to hydraulic fracturing and have lower

CHARACTERISTICS OF CONVENTIONAL OIL AND GAS RESOURCES

hydrocarbon recoveries. Thus, depositional environment for shale can be important along with thickness and reservoir pressure.

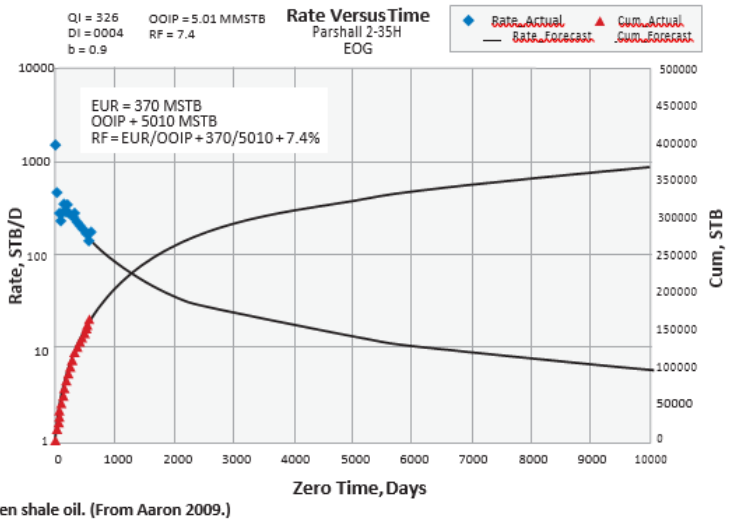

Fig. 3.7—Bakken shale oil. (From Aaron 2009.)

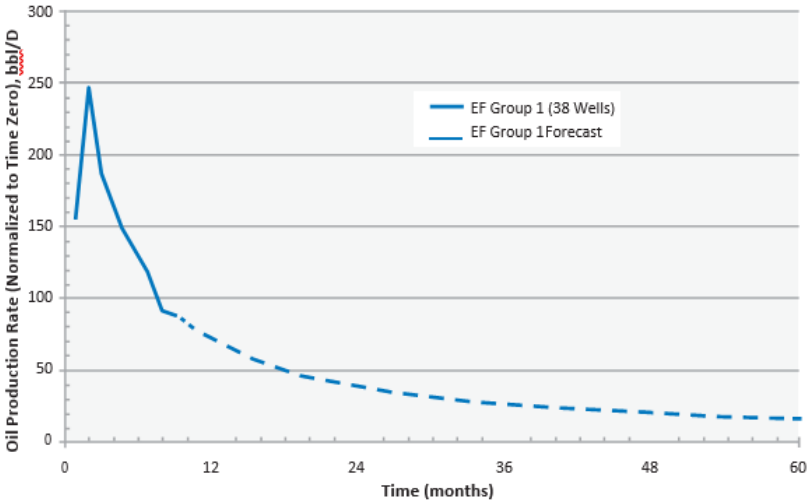

Fig. 3.8—Eagle Ford shale oil. (From Martin et al. 2011.)

CHARACTERISTICS OF CONVENTIONAL OIL AND GAS RESOURCES

3.5 Specific Considerations for Tight Oil and Gas

"In the 1970s the US government decided that the definition of a tight gas reservoir is one in which the expected value of permeability to gas flow would be less than 0.1 md. This definition was a political definition that has been used to determine which wells would receive federal and/or state tax credits for producing gas from tight reservoirs," (Holditch 2006). Holditch wrote that the tight gas definition is a function of a number of physical and economic factors.

Another definition of a tight gas reservoir is "a reservoir that cannot be produced at economic flow rates nor recover economic volumes of natural gas unless the well is stimulated by a large hydraulic fracture treatment or produced by the use of a horizontal wellbore or multilateral wellbores," (Holditch 2006; Shrivastava and Lusatia 2011). Other authors say that flow rate—rather than permeability—should be the measure of what is termed a tight gas reservoir. Certainly that approach has merit, since some reservoirs with 10+md permeability are being fractured and the flow rate is being increased.

There are no "typical" tight oil and gas reservoirs. They can be:

- Deep or shallow
- High-pressure or low-pressure
- High-temperature or low-temperature
- Blanket or lenticular
- Stratigraphic, structural, and channel-influenced
- Homogeneous or naturally fractured
- Single layer or multiple layers
- Sandstone or carbonate
- Shale oil and gas—at times defined as tight oil and gas

Additionally, coal seam gas (CSG)—also referred to as coalbed methane—can be included in this category.

Unlike shale gas and coalbed methane, the hydrocarbons found in tight reservoirs are sourced in another formation, migrate, and then are trapped (like conventional

CHARACTERISTICS OF CONVENTIONAL OIL AND GAS RESOURCES

gas) in the formation where they are found. Discrete gas and water contacts are usually absent, but wells may produce water. Microscopic study of pore and permeability relationships indicates the existence of two varieties of tight oil and gas reservoirs. One variety is *tight* because of the fine grain size of the rock. The second variety is *tight* because the rock is relatively tightly cemented, diagnetically altered, and has pores that are poorly connected by small pore throats and capillaries. What have we learned about the tight oil and gas development in the US? Based on our observations and available statistics from a number of sources, the following conclusions can be drawn and information gathered:

- Tight gas wells must be fracture-stimulated to produce commercially.
- Average well spacing is now (following several field development iterations) 5 to 10 acres in the lenticular formations (Pinedale Anticline, and Piceance).
- Formation thickness ranges from 600 to 6,000 ft.
- Formation depth ranges from 4,700 to 20,000 ft.
- Multiwells pads contain wells that are S-shaped, directional, or vertical (Pinedale Anticline and Piceance).
- Some wells are horizontal and multilateral (Texas Panhandle, Anadarko basin).
- Well IPs range from < 3 to 20 MMcfd.
- Production is dry gas, wet gas, and water.
- Tight gas formations producing water require deliquification (also called dewatering), in particular for coalbed methane.
- Wells exhibit high decline rates in the first few years of production.
- A high number of wells are required to develop shale (low per well EUR).

The four tight gas basins that produce most of the US tight gas are the Pinedale Anticline, Anadarko, Piceance, and Deep Bossier. Step-by-step procedures to effectively develop these tight oil and gas fields have been documented by Ahmed and Jones (1981); Abou-Sayed and Ahmed (1984); Ahmed and Cannon (1985).

Table 3.3 is a comparison of these US tight gas basins.

All tight wells, gas in particular, display the unique decline curve profile similar to shale but not as drastic. **Fig. 3.9** shows several modeled production profiles of various tight gas well scenarios compared to the profile for a conventional gas well plotted from actual measurements obtained from a productive field. Plots show that the initial rates and EUR per well are significantly less than those for conventional gas wells.

CHARACTERISTICS OF CONVENTIONAL OIL AND GAS RESOURCES

Table 3.3—Comparison of the four significant US tight basins. (Source from Warlick 2010.)

BASIN	Depth, ft.	Thickness, ft.	IP, MMcfd	EUR/Well, Bcf	Production	Well Spacing, ac	Formation	Well Cost, $MM	TRR, Tcf
Pinedale Anticline	7,000–14,000	5,000–6,000	9	6.5	Gas + Water	5	Lenticular, Stacked	3	73
Piceance	6,500–9,000	1,500–4,500	3	3–8	Dry Gas + Water	10 (fr 160)	Lenticular, Stacked	1.5–4.0	7
Anadarko	4,700–13,000	3,500–3,600	10–15	7.0	Wet Gas	80	Granite Washes	7.0–8.5	6
Deep Bossier	16,300	600	15–20	1.5–2.0	Dry Gas, No Water	20	Lenticular	7.6–11.0	6

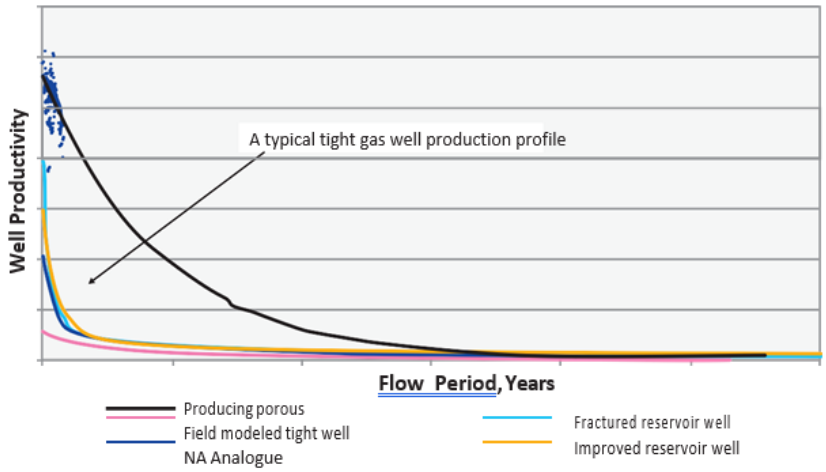

Fig. 3.9—Modeled typical tight gas production profiles compare to a conventional gas well. (Al Kindi et al. 2011.)

CHARACTERISTICS OF CONVENTIONAL OIL AND GAS RESOURCES

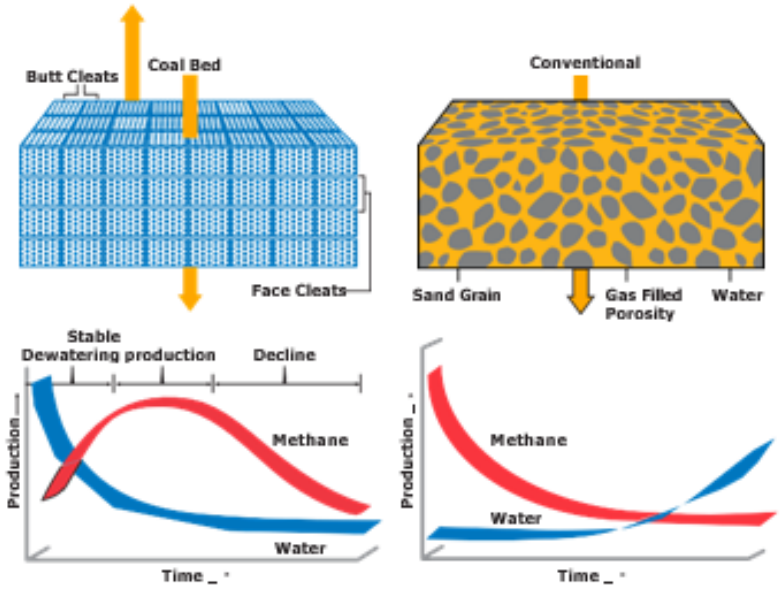

Fig. 3.10 —The flow channels (cleat system) and the production mechanism via dewatering. (From Brown 2002.)

production is controlled by desorption of the gas from the coal matrix as reservoir pressure drops due to long-term water production.

The rate of desorption on the other hand is controlled by macerals (the microscopically recognizable components of coal, analogous to minerals in inorganic rocks), which, in turn, can define the percentage of vitrinite. Vitrinite reflectance values indicate when the coal has reached the gas-generating phase (**Fig. 3.11**), and a rank of class A, a high-volatile bituminous coal (**Table 3.4** for coal rank classes).

Other relevant parameters for further detailed understanding include *cation exchange capacity* (to detect and quantify hydratable clay fractions), *petrographic analysis* (to define pore or flow that channels like the butt and face cleats) and *geophysical logging* (to measure in-situ inferences) allow

CHARACTERISTICS OF CONVENTIONAL OIL AND GAS RESOURCES

the estimation of almost all the above parameters in italics as discussed in detail by Ahmed and Newberry (1988).

Fig. 3.12 illustrates a desorption isotherm suggesting the potential production rate and ultimate recovery over a certain pressure and temperature regime while **Fig. 3.13** illustrates the various items that define the adsorption Isotherm (the amount of gas that the coal in question can adsorb as stored methane gas.

CHARACTERISTICS OF CONVENTIONAL OIL AND GAS RESOURCES

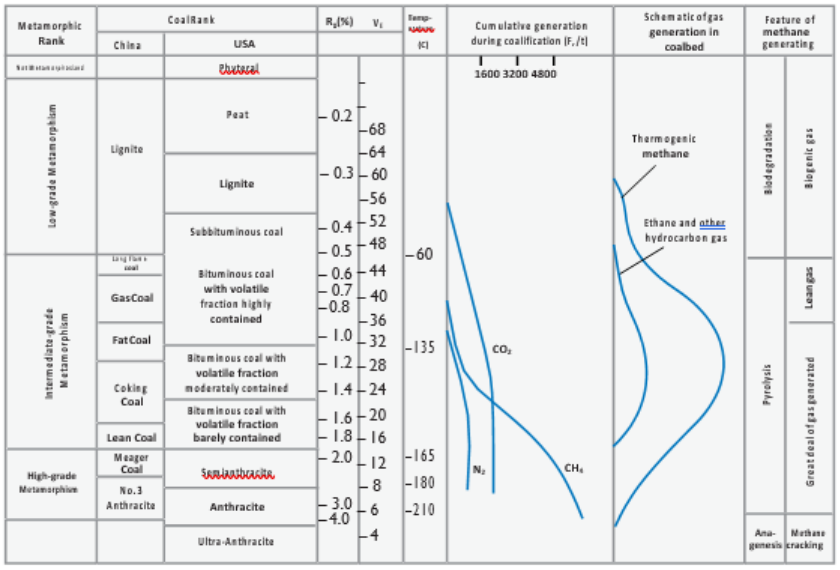

Fig. 3.11—Coal rank and hydrocarbon generation potential (after Qin and Zeng 1995 in Unconventional Petroleum Geology).

Table 3.4—Vitrinite reflectance limits (in oil) and A, S, T, and M coal rank classes.

Rank	Maximum Reflectance %
Sub-Bituminous	Less than 0.47
High Volatile Bituminous C	0.47-0.57
High Volatile Bituminous B	.057-0.71
High Volatile Bituminous A	0.71-1.10
Medium Volatile Bituminous	1.10-1.50
Low Volatile Bituminous	1.50-2.05
Semi-Anthracite	2.05-3.00 (approx.)
Anthracite	Greater than 3.00

CHARACTERISTICS OF CONVENTIONAL OIL AND GAS RESOURCES

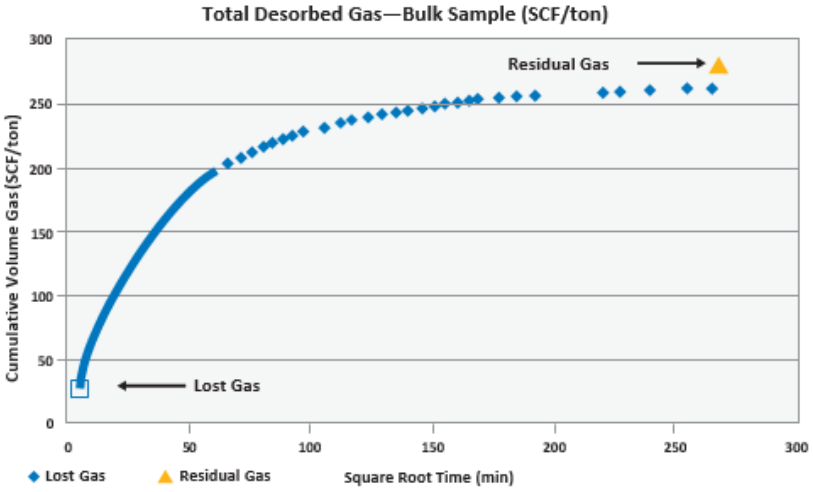

Fig. 3.12—Example of a desorption isotherm as measured in the laboratory environment. (From Waechter et al. 2004.)

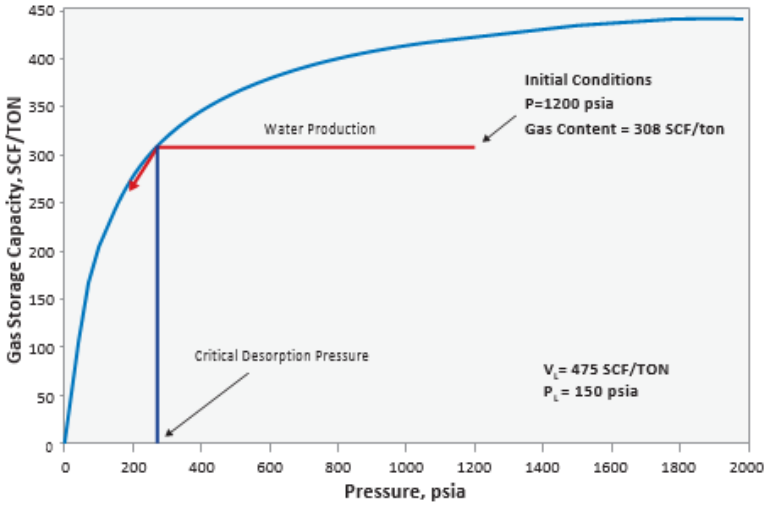

Fig 3.13—A typical adsorbtion isotherm. (From Aminian, West Virginia University.)

CHARACTERISTICS OF CONVENTIONAL OIL AND GAS RESOURCES

3.7 References

Aaron, J.C. 2009. Determination of Recovery Factor in the Bakken Formation, Mountrail County, ND. Paper SPE 133719 presented at the SPE Annual Technical Conference and Exhibition. New Orleans, Louisiana. 4–7 October. http://dx.doi.org/10.2118/133719-STU.

Abou-Sayed A., Ahmed U., and Jones, A. 1982. A Step-by- Step Procedure to Hydraulic Fracture Treatment Design, Implementation and Analysis for Tight Gas Sands. Paper SPE 10829 presented at the SPE Unconventional Gas Recovery Symposium. Pittsburgh, Pennsylvania. 16–18 May. http://dx.doi.org/10.2118/10829-MS.

Addis, M.A. and Yassir, M., 2010. An Overview of Geomechanical Engineering Aspects of Tight Gas Sand Developments, Paper SPE 136919, presented at the 2010 SPE/ DGS Annual Technical Symposium and Exhibition. Al-Khabor, Saudi Arabia. 4–7 April.

Ahmed, U. 2014. Optimized Shale Resource Development: Balance between Technology and Economic Considerations. Paper SPE 169984 presented at the SPE Energy Resources Conference. Trinidad and Tobago. 9–11 June. http://dx.doi.org/10.2118/169984-MS.

Ahmed, U., Abou-Sayed, A., and Jones, A. 1981. Systematic Approach to Massive Hydraulic Fracture Treatment Design. Society of Petroleum Engineers, DOE.

Ahmed, U., Johnston, D., and Colson, L. 1991. An Advanced and Integrated Approach to Coal Formation Evaluation. Paper SPE Paper 22736 presented at the SPE Annual Technical Conference and Exhibition. Dallas, Texas. 6–9 October. http://dx.doi.org/10.2118/22736-MS.

Ahmed, U., Newberry, B., and Cannon, D. 1985. Hydraulic Fracture Treatment Design of Wells with Multiple Zones. Paper SPE 13857 presented at the SPE/DOE Low Permeability Gas Reservoirs Symposium. Denver, Colorado. 19–22 March. http://dx.doi.org/10.2118/13857-MS.

Ahmed, U., Schatz, J.F., Holland, M.T., et al. 1982. State-of-the- Art Hydraulic Fracture Stimulation Treatment for Western Tight Sand Reservoir. Paper SPE 11184 presented at the SPE Annual Technical Conference and Exhibition. New Orleans,

CHAPTER

3

PETROLEUM DATA ANALYTICS

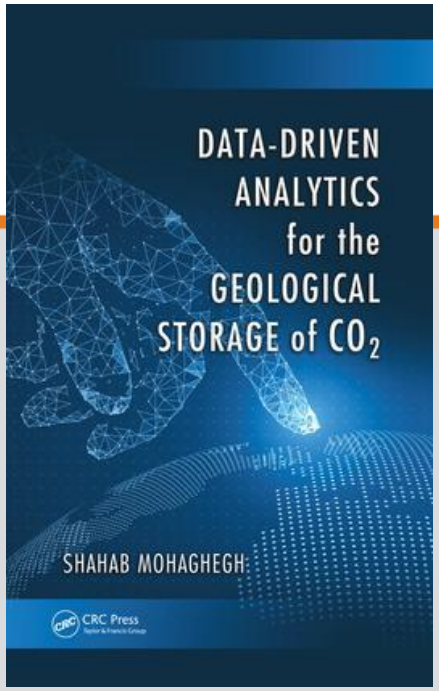

This chapter is excerpted from

Data-Driven Analytics for the Geological Storage of CO2

by Shahab Mohaghegh

Learn more

PETROLEUM DATA ANALYTICS

Excerpted from *Data-Driven Analytics for the Geological Storage of CO2*

Shahab D. Mohaghegh

The realization that much value can be extracted from the data routinely collected (much of it is left unused) during drilling, completion, stimulation, workover, injection, and production operations in the upstream exploration and production (E&P) industry has resulted in a growing interest in the application of data-driven analytics in our industry. Related activities that had been regarded as exotic academic endeavors have now come to the forefront and are attracting much attention. New startups are entering the marketplace, some with good products and expertise, and others purely based on marketing gimmicks and opportunistic intuitions.

Petroleum data analytics (PDA) is the application of data-driven analytics and big data analytics in the upstream oil and gas industry. It is the application of a combination of techniques that make the most of the data collected in the oil and gas industry in order to analyze, model, and optimize production operations. Since the point of departure for this technology is data rather than physics and geology, it provides an alternative to the conventional solutions that have been used in the industry for the past century. Petroleum data analytics lends itself, very favorably to numerical simulation and modeling of carbon storage in geological formations since very large amounts of data can be generated from such numerical models.

The techniques that are incorporated in the author's work to perform the types of analysis, modeling, and optimization that are presented in this book include artificial intelligence, machine learning and data mining, and, more specifically, artificial neural networks, evolutionary optimization, fuzzy set theory. The following sections in this chapter provide some brief explanations on each of these techniques. Much more can be learned about these technologies by digging deeper into the references that are provided at the end of the book.

2.1 Artificial Intelligence

Artificial intelligence (AI) is the area of computer science focusing on creating machines that can engage in behaviors that humans consider intelligent. The ability to create intelligent machines has intrigued humans since ancient times, and today, with the advent of the computer and 50 years of research into AI programming techniques, the dream of smart machines is becoming a reality. Researchers are creating systems which can mimic human thoughts, understand speech, beat the best human chess player, win challenging "Jeopardy" contests, and countless other feats never before possible.

AI is a combination of computer science, physiology, and philosophy. It is a broad topic, consisting of different fields, from machine vision to expert systems. The element that the fields of AI have in common is the creation of machines that can

PETROLEUM DATA ANALYTICS

"think." In order to classify machines as "thinking," it is necessary to define intelligence. To what degree does intelligence consist of, for example, solving complex problems, or making generalizations and relationships? And what about perception and comprehension?

AI may be defined as a collection of analytic tools that attempts to imitate life. AI techniques exhibit an ability to learn and deal with new situations. Artificial neural networks, evolutionary programming, and fuzzy logic are among the paradigms that are classified as AI. These techniques possess one or more attributes of "reason," such as generalization, discovery, association, and abstraction. In the last two decade AI has matured into a set of analytic tools that facilitate solving problems that were previously difficult or impossible to solve. The trend now is the integration of these tools, as well as with conventional tools such as statistical analysis, to build sophisticated systems that can solve challenging problems. These tools are now used in many different disciplines and have found their way into commercial products. AI is used in areas such as medical diagnosis, credit card fraud detection, bank loan approval, smart household appliances, automated subway system controls, self-driving cars, automatic transmissions, financial portfolio management, robot navigation systems, and many more.

In the oil and gas industry these tools have been used to solve problems related to drilling, reservoir simulation and modeling, pressure transient analysis, well log interpretation, reservoir characterization, and candidate well selection for stimulation, among other things.

2.2 Data Mining

As the volume of data increases, human cognition is no longer capable of deciphering important information from it by conventional techniques. Data mining and machine learning techniques must be used in order to deduce information and knowledge from the raw data that resides in the databases. Data mining is the process of extracting hidden patterns from data. With a marked increase in the amount of data that is being routinely collected, data mining is becoming an increasingly important tool to transform collected data into information. Although the incorporation of data mining in the E&P industry is relatively new, it has been commonly used in a wide range of applications, such as marketing, fraud detection, and scientific discovery. Data mining can be applied to datasets of any size. However, while it can be used to uncover hidden patterns in the data that has been collected, obviously it can neither uncover patterns that are not already present in the data, nor uncover patterns in the data that has not been collected.

Data mining (sometimes referred to as knowledge discovery in databases, or KDD) has been defined as "the nontrivial extraction of implicit, previously unknown, and potentially useful information from data." It uses artificial intelligence, machine learning, statistical, and visualization techniques to discover and present knowledge in a form which is easily comprehensible to humans.

Data mining has been able to attract the attention of many in the fields of

PETROLEUM DATA ANALYTICS

scientific research, business, the banking sector, intelligence agencies, and many others from the early days of its inception. However, its use has not always been as easy as it is now. Data mining is used by businesses to improve marketing and to understand the buying patterns of clients. Attrition analysis, customer segmentation, and cross selling are the most important ways through which data mining is showing new ways in which businesses can multiply their revenue.

Data mining is used in the banking sector for credit card fraud detection by identifying the patterns involved in fraudulent transactions. It is also used to reduce credit risk by classifying a potential client and predicting bad loans. Data mining is used by intelligence agencies such as the FBI and CIA to identify threats of terrorism. After the 9/11 incident, data mining has become one of the prime means with which to uncover terrorist plots.

In the popular article, "IT Doesn't Matter" (5) Nicholas Carr argued that the use of IT is nowadays so widespread that any particular organization does not have any strategic advantage over the others due to the use of IT. He concludes that IT has lost its strategic importance. However, it is the view of the author that in today's E&P landscape data mining has become the sort of tool that can provide a strategic and competitive advantage for those that have the foresight to embrace it in their day-to-day operations. It is becoming more and more evident that NOCs (National Oil Companies) and IOCs (International Oil Companies), and independent operators can create strategic advantages over theirs competitors by making use of data mining to obtain important insights from the collected data.

2.2.1 Steps Involved in Data Mining

There are various steps that are involved in mining data, including the following:

1. *Data integration*: The reality is that in today's oil and gas industry data is never in the form that one needs in order to perform data mining. Usually there are multiple sources for data, and the data exists in several databases. Data needs to be collected and integrated from different sources in order to be prepared for data mining.

2. *Data selection*: Once the data is integrated it is usually used for a specific purpose. The collected data needs to be studied and the specific parts of the data that lend themselves to the task at hand in an organization should be selected for the given data mining project. For example, human resources data may not be needed for a drilling project.

3. *Data cleansing*: The data that has been collected is usually not clean and may contain errors, missing values, noise, or inconsistencies. Different techniques need to be applied to the selected data in order to get rid of such anomalies.

4. *Data abstraction and summarization*: The data that has been collected, especially if it is operational data, may need to be summarized while keeping the main essence of its behavior intact. For example, if pressure and temperature data is collected via a permanent down-hole gauge at one-second frequency, it may need to be summarized or abstracted into minute data before use in a specific data-mining project.

5. *Data transformation*: Even after cleaning and abstraction, data may not be ready for mining. Data usually needs to be transformed into forms appropriate for mining.

PETROLEUM DATA ANALYTICS

The techniques used to accomplish this include smoothing, aggregation, normalization, and so on.

6. *Data mining*: Machine learning and techniques such as clustering and association analysis are among the many different techniques used for data mining. Both descriptive and predictive data mining may be applied to the data. The objectives of the project will determine the type of data mining and the techniques used in it.

7. *Pattern evaluation and knowledge presentation*: This step involves visualization, transformation, and removing redundant patterns from the patterns generated.

8. *Decisions/Use of discovered knowledge*: Use of the acquired knowledge to make better decisions is the essence of this last step.

2.3 Artificial Neural Networks

Much has been written about artificial neural networks. There are books and articles that can be accessed for a deep understanding of the topic and all relevant algorithms. The objective here is to provide a brief overview, sufficient to enable an understanding of the topics presented in this book, and make them easy to follow. For a more detailed understanding of this technology, it is highly recommended that the reader refer to the books and articles referenced here.

Neural network research can be traced back to a paper by McCulloch and Pitts in 1943 (6). In 1958 Frank Rosenblatt invented the "Perceptron" (7). Rosenblatt proved that, given linearly separable classes, a perceptron will, in a finite number of training trials, develop a weight vector that will separate the classes (a pattern classification task). He also showed that his proof holds independent of the starting value of the weights. Around the same time Widrow and Hoff (8) developed a similar network called "Adeline." Minsky and Papert (9) in a book called "Perceptrons" pointed out that the theorem obviously applies to those problems that the structure is capable of computing. They showed that elementary calculations such as simple "exclusive or" (XOR) problems cannot be solved by single-layer Perceptrons. Rosenblatt (7) also studied structures with more layers and believed that they could overcome the limitations of simple Perceptrons. However, there was no learning algorithm known that could determine the weights necessary to implement a given calculation. Minskey and Papert doubted that one could be found and recommended that other approaches to artificial intelligence should be pursued. Following this discussion, most of the computer science community left the neural network paradigm for twenty years (10). In the early 1980s Hopfield was able to revive neural network research. Hopfield's efforts coincided with development of new learning algorithms such as back- propagation. The growth of neural network research and applications has

been phenomenal since this revival.

2.3.1 Structure of a Neural Network

PETROLEUM DATA ANALYTICS

An artificial neural network is an information-processing system that has certain performance characteristics in common with biological neural networks. Therefore, it is appropriate to briefly describe a biological neural network before offering a detailed definition of artificial neural networks.

All living organisms are made up of cells. The basic building blocks of the nervous system are nerve cells, called neurons. Figure 2.1 shows a schematic diagram of two bipolar neurons. A typical neuron contains a cell body where the nucleus is located, dendrites, and an axon. Information in the form of a train of electro-chemical pulses (signals) enters the cell body from the dendrites. Based on the nature of this input the neuron will activate in an excitatory or inhibitory fashion, and provides an output that will travel through the axon and connects to other neurons where it becomes the input to the receiving neuron. The point between two neurons in a neural pathway, where the termination of the axon of one neuron comes into close proximity with the cell body or dendrites of another, is called a synapse. Signals traveling from the first neuron initiate a train of electro-chemical pulses (signals) in the second neuron.

It is estimated that the human brain contains on the order of 10–500 billion

neurons (11). These neurons are divided into modules, and each module contains about 500 neural networks (12). Each network may contain about 100,000 neurons, where each neuron is connected to hundreds to thousands of other neurons. This architecture is the main driving force behind the complex behavior that comes so natural to us. Simple tasks such as catching a ball, drinking a glass of water, or walking in a crowded market require so many complex and coordinated calculations that sophisticated computers are unable to undertake the task, and yet it is done routinely by humans without a moment of thought.

This becomes even more interesting when one realizes that neurons in the human brain have a cycle time of about 10–100 milliseconds, while the cycle time of a typical desktop computer chip is measured in nanoseconds (about 10 million times faster than the human brain). The human brain, although a million times slower than common desktop PCs, can perform many tasks orders of magnitude faster than computers because of its massively parallel architecture.

PETROLEUM DATA ANALYTICS

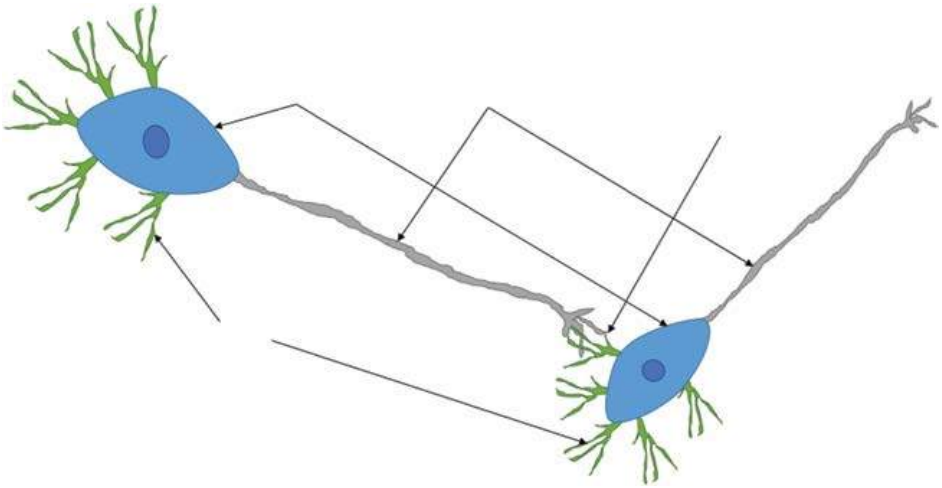

FIGURE 2.1 Schematic diagram of two bipolar neurons

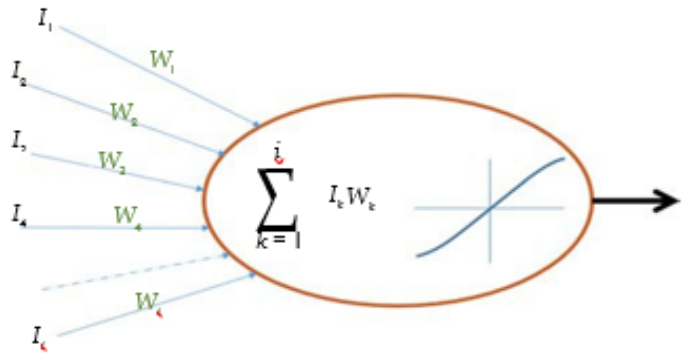

FIGURE 2.2
Schematic diagram of an artificial neuron or a processing element.

PETROLEUM DATA ANALYTICS

Artificial neural networks are a rough approximation and simplified simulation of the process explained above. An artificial neural network can be defined as an information-processing system that has certain performance characteristics similar to biological neural networks. They have been developed as a generalization of mathematical models of human cognition or neural biology, based on the following assumptions:

1. Information processing occurs in simple processing elements, called neurons.
2. Signals are passed between neurons over connection links.
3. Each connection link has an associated weight, which, in a typical neural network, multiplies the signal being transmitted.
4. Each neuron applies an activation function (usually non-linear) to its net input to determine its output signal (13).

Figure 2.2 is a schematic diagram of a typical neuron (processing element) in an artificial neural network. The output from other neurons is multiplied by the weight of the connection and enters the neuron as input. Therefore an artificial neuron has many inputs and only one output. The inputs are summed and subsequently applied to the activation function, and the result is the output of the neuron.

2.1.2 Mechanics of Neural Networks Operation

An artificial neural network is a collection of neurons that are arranged in specific formations. Neurons are grouped into layers. In a multilayer network there is usually an input layer, one or more hidden layers and an output layer. The number of neurons in the input layer corresponds to the number of parameters that are being presented to the network as input. The same is true for the output layer. It should be noted that neural network analysis is not limited to a single output and that neural networks can be trained to build data-driven models with multiple outputs. The neurons in the hidden layer or layers are mainly responsible for feature extraction.

An increase in the number of hidden neurons provide increased dimensionality and accommodate tasks such as classification and pattern recognition. Figure 2.3 is a schematic diagram of a fully connected three- layer neural network. There are many kinds of neural network. Neural network scientists and practitioners have provided different classifications to describe these. One of the most popular classifications is based on training methods, whereby neural networks can be divided into two major categories, namely supervised and unsupervised neural networks. Unsupervised neural networks, also known as self-organizing maps, are mainly clustering and classification algorithms. They have been used in the oil and gas industry to interpret well logs and to identify lithology. They are called unsupervised simply because no feedback is provided to the network by the person that is training the neural network. The network is asked to classify the input vectors into groups and clusters. This requires a certain degree of redundancy in

PETROLEUM DATA ANALYTICS

the input data and hence the notion that redundancy is knowledge (14).

Most of the practical and useful neural network applications in the upstream oil and gas industry are based on supervised training algorithms. During a supervised training process both input and output are presented to the network to permit learning on a feedback basis. A specific architecture, topology, and training algorithm are selected and the network is trained until it converges to an acceptable solution. During the training process, the neural network tries to converge to an internal representation of the system behavior. Although by definition neural networks are model-free function approximators, some people choose to call the trained network a "neuro- model." In this book our preferred terminology is "data-driven" model.

The connections correspond roughly to the axons and synapses in a biological system, and they provide a signal transmission pathway between the nodes. Several layers can be interconnected. The layer that receives the inputs is called the input layer. It typically performs no function other than buffering

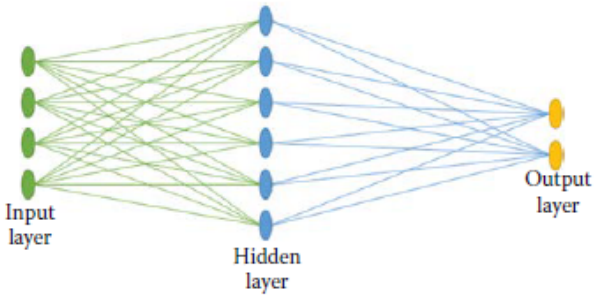

FIGURE 2.3
Schematic diagram of a three-layer neuron network.

PETROLEUM DATA ANALYTICS

of the input signal. In most cases, the calculation performed in this layer is a normalization of the input parameters so that parameters such as porosity (which is usually represented as a fraction) and initial pressure (usually in thousands of psi) would be treated equally by the neural network at the start of the training process. The network outputs are generated from the output layer. Any other layers are called hidden layers because they are internal to the network and have no direct contact with the external environment. Sometimes they are likened to a "black box" within the network system. However, just because they are not immediately visible does not mean that one cannot examine the function of those layers. There may be zero to several hidden layers in a neural network. In a fully connected network every output from one layer is passed along to every node in the next layer.

In a typical neural data-processing procedure, the database is divided into three separate portions called training, calibration, and verification sets. The training set is used to develop the desired network. In this process (depending on the training algorithm that is being used), the desired output in the training set is used to help the network adjust the weights between its neurons or processing elements. During the training process the question arises of when to stop the training? How many times should the network go through the data in the training set in order to learn the system behavior? When should the training stop? These are legitimate questions, because a network can be over trained. In the neural-network-related literature, over- training is also referred to as memorization. Once the network memorizes a dataset, it would be incapable of generalization. It will fit the training dataset quite accurately, but suffers in generalization. The performance of an over- trained neural network is similar to a complex non-linear regression analysis. Over-training does not apply to some neural network algorithms simply because they are not trained using an iterative process. Memorization and over-training are applicable to those networks that are historically among the most popular ones for engineering problem solving. These include back-propagation networks that use an iterative process during training.

In order to avoid over-training or memorization, it is a common practice to stop the training process every so often and apply the network to the calibration dataset. Since the output of the calibration dataset is not presented to the network (during the training), one can evaluate the network's generalization capabilities by how well it predicts the calibration set's output. Once the training process is completed successfully, the network is applied to the verification dataset.

During the training process each artificial neuron (processing element) handles several basic functions. First, it evaluates input signals and determines the strength of each one. Second, it calculates a total for the combined input signals and compares that total to some threshold level. Finally, it determines what the output should be. The transformation of the input to output – within a neuron – takes place using an activation function. Figure 2.4 shows two of the commonly used activation (transfer) functions.

PETROLEUM DATA ANALYTICS

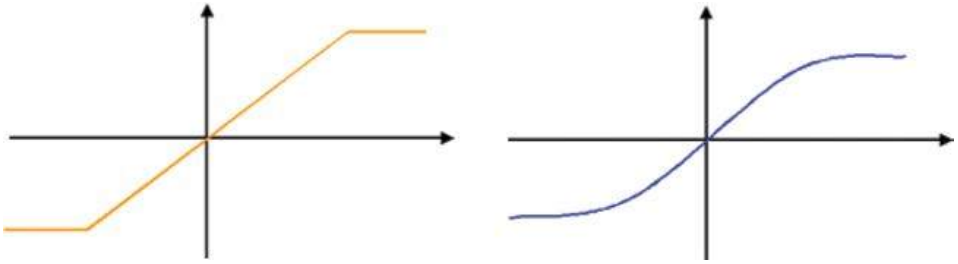

Piecewise linear activation function

Sigmoid or logistic activation function

FIGURE 2.4

Commonly used activation functions in artificial neurons.

All the inputs come into a processing element (in the hidden layer) simultaneously. In response, the neuron either "fires" or "doesn't fire," depending on some threshold level. The neuron will be allowed a single output signal, just as in a biological neuron – many inputs, one output. In addition, just as things other than inputs affect real neurons, some networks provide a mechanism for other influences. Sometimes this extra input is called a bias term, or a forcing term. It could also be a forgetting term, when a system needs to unlearn something (15).

Each input is initially assigned a random relative weight (in some advanced applications – based on the experience of the practitioner – the relative weight assigned initially may not be random). During the training process the weight of the inputs is adjusted. The weight of the input represents the strength of its connection to the neuron in the next layer. The weight of the connection will affect the impact and influence of that input. This is similar to the varying synaptic strengths of biological neurons. Some inputs are more important than others in the way they combine to produce an impact. Weights are adaptive coefficients within the network that determine the intensity of the input signal. The initial weight for a processing element could be modified in response to various inputs and according to the network's own rules for modification.

Mathematically, we could look at the inputs and the weights on the inputs as vectors, such as *I*1, *I*2, *I*3, *I*4 … *In* for inputs and as *W*1, *W*2, *W*3, *W*4 … *Wn* for weights. The total input signal is the dot, or inner, product of the two vectors. Geometrically, the inner product of two vectors can be considered a measure of their similarity. The inner product is at its maximum if the vectors point in the same direction. If the vectors point in opposite directions (180°), their inner product is at its minimum.

Signals coming into a neuron can be positive (excitatory) or negative (inhibitory). A positive input promotes the firing of the processing element, whereas a negative input tends to keep the processing element from firing. During the training process

PETROLEUM DATA ANALYTICS

some local memory can be attached to the processing element to store the results (weights) of previous computations. Training is accomplished by modification of the weights on a continuous basis until convergence is reached. The ability to change the weights allows the network to modify its behavior in response to its inputs, or to learn. For example, suppose a network is being trained to correctly calculate the initial production from a newly drilled well. At the early stages of the training the neural network calculates the initial production from the new well to be 150 bbls/day, whereas the actual initial production is 1000 bbls/day. On successive iterations (training), connection weights that respond to an increase in initial production (the output of the neural network) are strengthened, and those that respond to a decrease are weakened until they fall below the threshold level and the correct calculation of the initial production is achieved. In the back-propagation algorithm (16) (one of the most commonly used supervised training algorithms in upstream oil and gas operations) the network output is compared with the desired output – which is part of the training dataset – and the difference (error) is propagated backward through the network. During this back-propagation of error the weights of the connections between neurons are adjusted. This process is continued in an iterative manner. The network converges when its output is within acceptable

proximity of the desired output.

2.1.1 Practical Considerations during the Training of a Neural Network

There is a substantial amount of art involved in the training of a neural network. In this section of the book the objective is to share some personal experiences that have been gained throughout many years of developing data-driven models for oil- and gas-related problems. These are mainly practical considerations and may or may not agree with similar practices in other industries, but they have worked very well for the author over the past two decades.

Understanding how machines learn is not complicated. The mathematics associated with neural networks, including how they are built and trained, is not really complex (16). It includes vector calculus and the differentiation of some normal functions. However, being a good reservoir or production engineer and a capable petroleum engineering modeler is essential for building and effectively utilizing the data-driven models that are covered in this book. In order to be a capable petroleum data scientist, while it is necessary to be a competent petroleum engineer, it is not a requirement to have degrees in mathematics, statistics, or machine learning.

In order to develop functional data-driven models there is no need to be an expert in machine learning or artificial neural networks. What is required, though, is an ability to understand the fundamentals of this technology and eventually become an effective user and practitioner of it. Although such skills are not taught as part of any petroleum engineering curriculum at universities, acquiring such skills is not a far-reaching task, and any petroleum engineer with a bachelor's degree should be able to master it with some training and effort. It is important to understand and subscribe to the philosophy of machine learning. This means that, although as an engineer you have learned to solve problems in a particular way, you need to

PETROLEUM DATA ANALYTICS

understand and accept that there is more than one way to solve engineering-related problems.

The technique that engineers have used to solve problems follows a well- defined path of identifying the parameters involved and then constructing the relationships between the parameters (using mathematics) to build a model. The philosophy of solving a problem using machine learning is completely different. Given that in machine-learning algorithms such as artificial neural networks, models are built using data, the path to follow in order to solve an engineering problem differs from that you learned as a petroleum engineer. To solve problems using data, you have to be able to teach an open computer algorithm about the problem and its solutions. This process is called supervised learning. You have to create (actually collect) a large number of records (examples) that include the inputs (parameters involved) and the outputs (the solution you are trying to solve for). During training, these records (the coupled input–output pairs) are presented to the machine-learning algorithm, and by repetition (redundancy sometimes plays a positive role in this process) the machine will eventually learn how the problem is solved. The algorithm does this by building an internal representation of the mapping between inputs and outputs.

In the previous section of this book, the fundamentals of this technology

were covered. In this section, some practical aspects of this technology will be briefly discussed. These practical aspects will help a data-driven modeler learn how to train good and useful neural networks. The neural network training includes several steps, which are also covered here.

2.3.3.1 Selection of Input Parameters

Since all models are wrong, the scientist cannot obtain a "correct" one by excessive elaboration. On the contrary, following William of Occam,* the scientist should seek an economical description of natural phenomena. Just as the ability to devise simple but evocative models is the signature of the great scientist, over-elaboration and over-parameterization are often the mark of mediocrity (17). In order not to over-parameterize our neural network model we need to use the right number of variables.

Selection of the input parameters that are going to be used to train a neural network from the variables (potential inputs) that have been assimilated in the database is not a trivial procedure. A database generated for a given project usually includes a very large number of parameters, all of which are potential input parameters to the neural networks that are going to be trained for the data-driven model. They include static parameters and dynamic parameters,

* Occam's razor is a problem-solving principle devised by William of Ockham (c.

PETROLEUM DATA ANALYTICS

1287–1347). The principle states that, among competing hypotheses, the one with the fewest assumptions should be selected. In the absence of certainty, the fewer assumptions that are made, the better. as well as similar parameters for several offset wells. These parameters are designated as columns in a flat file that is eventually used to train data-driven models (neural networks).

Not all of the parameters that are included in the database are used to train the neural networks. Actually, it is highly recommended that the number of parameters that are used to build (train, calibrate, and validate) the neural network be limited. This limitation of the input parameters should not be interpreted as the other parameters not playing any role in forming or calculating the output of the model. The elimination of some of the parameters and the use of some others to build the data-driven model simply means that a subset of the parameters play such an important role in the determination of the model output that they overshadow (or sometimes implicitly represent) the impact of other parameters. In other words a model can be developed using only these parameters and safely ignoring others.

Only a subset of these parameters should therefore be selected and used as the input to the data-driven models. Experience with developing successful data-driven models has shown that the process of selecting the parameters that must be used as input to the model needs to satisfy the following three criteria:

• The impact (influence) of all the exiting parameters (in the database) on the model output should be identified and ranked. Then the top "*x*" percent of these ranked parameters should be used as input in the model. This is easier said than done. There are many techniques that can be used to help the data-driven modeler in identifying the influence of parameters on a selected output. These techniques can be as simple as linear regression and as complex as fuzzy pattern recognition.* Some use principal component analysis (18) to accomplish this task.

• In the list of input parameters that are identified to be used in the training of the neural network, there must exist parameters that can validate the physics and/or the geology of the model. If such parameters are already among the highly ranked parameters in the previous step, then great, otherwise, the data-driven modeler must see to it that they are included in the model. Being able to verify that the data-driven model has understood the physics and honors it is an important part of data-driven modeling.

• In many cases the data-driven model is developed in order to optimize production. Identification of optimized choke setting during production is a good example of such a situation. In such cases, parameters that are needed to optimize production should be included in the set of input parameters. If the optimization

* This is a proprietary algorithm developed by Intelligent Solutions, Inc. and used in their Data Driven Modeling software application called IMprove™ (www.IntelligentSolutionsInc.com). parameters are already among the highly ranked parameters in the previous step, then great, otherwise, the data-driven modeler must see to it that they are included in the model.

The machine learning literature includes many techniques for this purpose. In these publications the technology is referred to as "feature selection."

PETROLEUM DATA ANALYTICS

2.3.3.2 Partitioning the Dataset

Data in the spatio-temporal database is transferred into a flat file once a superset of parameters are selected to be used in the training of the neural networks. The data in the flat file needs to be partitioned into three segments: training, calibration, and validation. As will be discussed in the next section, the way these segments are treated determines the essence of the training process. In this section, the characteristics of each of these data segments and their use and purpose are briefly discussed.

In general, the largest of the three segments is the training dataset. This is the data that is used to train the neural network and create the relationships between the input parameters and the output parameter. Everything that one wishes to teach a data-driven model must be included in the training dataset. One must realize that the range of the parameters as they appear in the training set determines the range of the applicability of the data-driven model. For example, if the range of permeability in the training set is between 2 and 200 mD, one should not expect the data-driven model to perform reasonably well for a data record with permeability values less than 2 mD and higher than 200 mD. This is due to the well-known fact that most machine-learning algorithms, neural networks included, demonstrate great interpolative capabilities, even if the relationship between the input parameters and the output(s) is highly non-linear. However, machine-learning algorithms are not known for their extrapolative capabilities. As we mentioned in Section 2.3.1, the input parameters are connected to the output parameter through a set of hidden neurons. The strength of the connections between neurons (between input neurons and hidden neurons, between hidden neurons with one another if such connections exists, and between hidden neurons and output neurons) is determined by the weight associated with each connection. During the training process, the optimum weight of each connection is determined through an iterative learning process. During the training process, the weights between the neurons (also known as synaptic connections) in a neural network find their optimum value. Collection of these optimum values forms the coefficient matrices that are used to calculate the output parameter. Therefore, the role of the training dataset is to help the modeler determine the strength between the neurons in a neural network. Convergence of a network to a desirable set of weights that will translate to a well-trained and smart neural network model depends on the information content of the training dataset. When the neural networks are being trained for data-driven model purposes, the size of the training dataset may be as high as 80% or as low as 40% of the entire dataset. This percentage is a function of the number of records in the database.

The calibration dataset is not used directly during the training process, and it actually plays no direct role in changing the weights of the connections between the neurons. The calibration dataset is a blind dataset that is used after every epoch of training* in order to test the quality and the goodness of the trained neural network. In many circles this is also called the "test" set. The calibration dataset is essentially a watch dog that observes the training process and decides when to stop the training process, because the network is only as good as its prediction of the calibration dataset (a randomly selected dataset that is actually a blind dataset).

Therefore, after every epoch of training (when the network gets to see all the records in the training dataset, once) the weights are saved and the network is tested against the calibration dataset to see if there has been any improvement of network predictive performance against this blind dataset. This test of network predictive capabilities is performed after every epoch to monitor its generalization

PETROLEUM DATA ANALYTICS

capabilities. Usually one or more metrics such as *R*2, the correlation coefficient, or the mean square error (MSE) are used to calculate the network's generalization capabilities. These metrics are used to determine how closely the set of synaptic connection weights will enable the calculation of the outputs as a function of the input parameters by comparing the output values computed by the neural networks against those measured in the field (the actual or real outputs) and used to train the neural network. As long as this metric is improving for the calibration dataset, it means that the training can continue and the network is still learning. When the neural networks are being trained for data-driven modeling purposes, the size of the calibration dataset is usually between 10% and 30% of the entire dataset,

depending on the size of the database.

The last, but arguably the most important, dataset (segment) is the validation or verification dataset. This dataset plays no role during training or calibration of the neural network. It has been selected and put aside from the very beginning to be used as a blind dataset. It literally sits on the sidelines and does nothing until the training process is over. This blind dataset validates the generalization capabilities of the trained neural network. While having no role to play during the training and calibration of the neural network, this dataset validates the robustness of the predictive capabilities of the neural network. The data-driven model that will result from the neural network that is being trained is as good as the outcome of the validation or verification dataset. When neural networks are being trained for data-driven modeling purposes, the size of the validation (verification) dataset is usually between 10%

and 30% of the entire dataset, depending on the size of the database.

* An epoch of training is completed when all the data records in the training set have been passed through the neural network and the error between neural network output and the actual field measurements are calculated.

Since the database is being partitioned into three datasets, it is important to make sure that the information content of each dataset is comparable to the others. If they differ, and often they will, then it would be best that the training set have the largest, most comprehensive information content of the three datasets. This will ensure a healthy training behavior and will increase the likelihood of training a good and robust neural network. Information content and its relationship with entropy within the context of information theory is an interesting subject that those involved with data-driven analytics and machine learning should understand (19).

2.3.3.3 Structure and Topology

The structure and topology of a neural network is determined by several factors, and hypothetically can have an infinite number of possible forms. However, almost all of them include a combination of factors, such as the number of hidden layers, the number of hidden neurons in each hidden layer, the combination of the activation functions, and the nature of the connections between neurons. In this section the objective is to briefly discuss some of the most popular structures and

PETROLEUM DATA ANALYTICS

specifically those that have shown success when used in the development of data-driven models for oil- and gas-related applications. In other words, the intention is not to turn this chapter of the book into a neural network tutorial, but rather to present practices that have proven successful during the development of data-driven models in the past for the author and can be used as a "rule of thumb" for those entering the world of data-driven modeling.

As far as the connection between neurons is concerned, the structures that

have been used most successfully in data-driven models are fully connected neural networks. In fully connected networks every input neuron is connected to every hidden neuron, and every hidden neuron is also connected to the output neuron; this network is called a fully connected network, as shown in Figures 2.5 through 2.7.

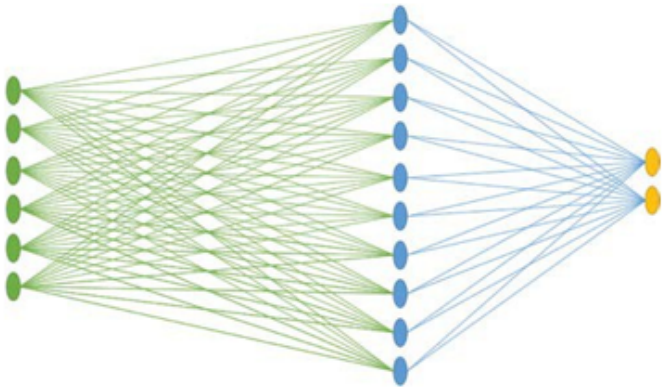

FIGURE 2.5
A fully connected neural network with one hidden layer that includes 11 hidden neurons, seven input neurons and one output neuron.

PETROLEUM DATA ANALYTICS

I

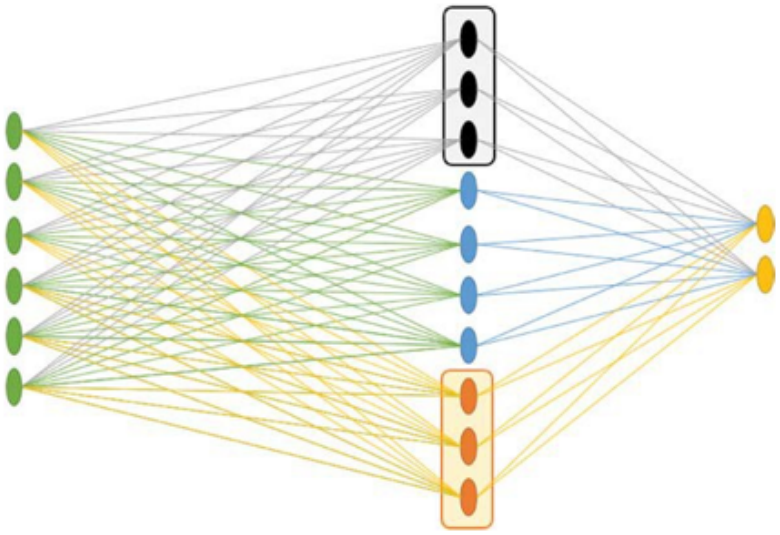

FIGURE 2.6

A fully connected neural network with one hidden layer that includes three different sets of activation functions along its 11 hidden neurons, seven input neurons and one output neuron.

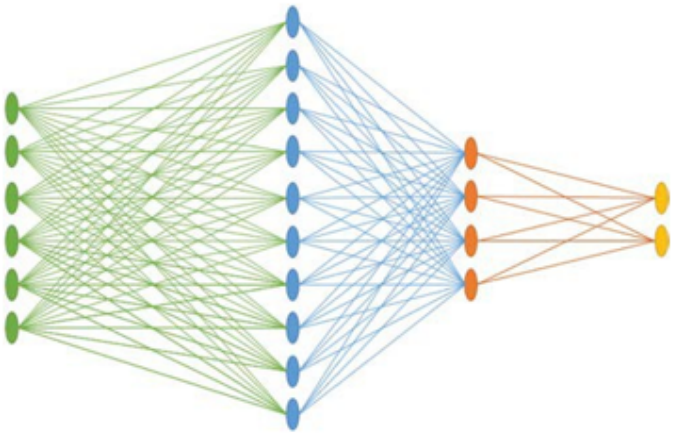

FIGURE 2.7

A fully connected neural network with two hidden layer that includes 11 and seven hidden neurons, respectively, as well as seven input neurons and one output

PETROLEUM DATA ANALYTICS

Figure 2.5 shows the most simple and also the most popular type of neural network for the development of data-driven models that form the main engines of the data-driven model. This is a simple, three-layer, fully connected neural network. The three layers are the input layer, the hidden layer, and the output layer. Furthermore, while the number of output neurons in the output layer can be more than one, our experience with data-driven

models has shown that, except in some specific situations, a single output neuron in the output layer performs best.

Furthermore, after experience with a large number and variety of network structures, the author's experience has shown that if you are not able to train a good network* using a simple structure as shown in Figure 2.5, your chances of achieving a good neural network with any other structure will be slim. In other words, it is not the structure of the neural network that will make or break the success of your efforts in training a data-driven model, rather it is the quality and information content of the database that determines your chances of being successful in developing a neural network, and by the same token, a data-driven model. If you see persistent issues in developing the data-driven model (the networks cannot be trained properly or do not have good predictive capabilities), you need to revisit your database rather than playing around with the structure and the topology of your neural network. In the author's opinion, when practitioners of machine learning (specifically in the upstream oil and gas industry) concentrate their efforts, and naturally the presentation of their data-driven modeling efforts, on the neural network structure and how it can be modified in order to control the training of the model, one must take that as an indication of naivety and a lack of substance and skill of the practitioner in machine learning technology, and not an indication of expertise. You will find that an expert in the art and science of machine learning will concentrate most on the information content and details of the dataset being used to train the neural network, as long as the very basic issues (the number of hidden layers and hidden neurons, the learning rate and momentum, etc.) of the structure of the neural network have been reasonably determined to be solid. The details of the structure and topology of a neural network can have an enhancing impact on the results,

but it will not make or break your data-driven model.

Sometimes, changing some of the activation functions can help in fine- tuning a neural network's performance, as shown in Figure 2.6. In this figure the hidden neurons are divided into three segments and each set of hidden neurons can be assigned a different activation function. Some details about activation functions were covered in previous sections. The author does not recommend that the initial structure of a neural network model be designed as shown in Figure 2.6; rather, if need be, the structure in Figures 2.6 and 2.7 may be used to enhance the performance of a network that has shown serious promise to be a good network, but its enhancement requires some fine-tuning. Once the structure of the neural network has been determined, it is time to decide upon the learning algorithm. By far the most popular learning (training) algorithm is "error back-propagation" (16) (or simply referred to as "back-propagation"). In this learning algorithm the

PETROLEUM DATA ANALYTICS

network calculates

* What constitutes a "good network"? A good network is a network that can be trained and calibrated and validated. It can learn well and has robust predictive capabilities. The rest is very problem dependent.

a series of outputs based on the current values of the weights (strength of the connections between neurons – synaptic connections) and compares its calculated outputs for all the records with actual (measured) outputs (what it is trying to match).

The calculated error between the network output and the measured values (also known as the target) is then back-propagated throughout the network structure with the aim of modifying the synaptic weights between neurons as a function of the magnitude of the calculated error. This process is continued until the back-propagation of the error and modification of the connection weights no longer enhances the network performance.

Several parameters are involved and can be modified during this training process to impact the progression of the network training. These parameters include the network's learning rate and the momentum for the weights between each set of neurons (layers), as well as the nature of the activation function. However, just as mentioned before, none of these factors will make or break a neural network; rather they can be instrumental in fine-tuning the result of a neural network. The information content of the database (which is essentially domain expertise related to petroleum engineering and geosciences) is the most important factor in the success or failure of a data-driven model.

2.3.3.1 Training Process

Since neural networks are known to be universal function approximators, hypothetically speaking they are capable of complete replication (reproduction) of the training dataset. In other words, given enough time and a large enough number of hidden neurons, a neural network should be able to reproduce the outputs of the training set from all the inputs, with 100% accuracy. This is something that one expects from a statistical approach or mathematical spline curve-fitting process. Such a result from a neural network is highly *undesirable,* and must be avoided. This is due to the fact that a neural network that is so accurate on the training set has literally memorized all the training records and has next to no predictive value.

This is the process that is usually referred to as over-training or over-fitting, and in the artificial intelligence lingo is referred to as "memorization" and must be avoided. An over-trained neural network memorizes the data in the training set and can reproduce the output values, almost identically, and does not learn it. Therefore, it cannot generalize and will not be able to predict the outcome of new data records. Such a model (if it can actually be called a model) is merely a statistical curve fit and has no value whatsoever.

Some of the geo-statistical techniques that are currently used by many commercial software applications to populate geo-cellular models are examples of such a technique (using neural networks as a curve fitting technique). Some of the most

PETROLEUM DATA ANALYTICS

popular geo-modeling software applications that are quite cognizant of this fact have incorporated neural networks as part of their tools. However, a closer look at the way neural networks have

been implemented in these software applications reveals that they are merely a marketing gimmick, and these software applications incorporate them as statistical curve-fitting techniques, which make neural network as useless as other geo-statistical techniques.

One of the roles of the calibration dataset is to prevent over-training. It is good practice to observe the network behavior during the training process in order to understand whether the neural network is in the process of converging to a solution or it needs attention from the modeler. There is much that can be learned from this observation. A simple plot of MSE versus the number of training epochs displays the neural network's training and convergence behavior. Furthermore, if the MSE is plotted for both the training dataset and the calibration dataset (after every training epoch), much can be learned from their side-by-side behavior. Several examples of such plots are shown in Figures 2.8 and 2.9.

Figures 2.8 and 2.9 include three sets of examples, each. Each example includes two graphs. The ones on the left show MSE vs. number of epochs for the calibration dataset, and the ones on the right show MSE vs. number of epochs for the training dataset. Please remember that training and calibration datasets are completely independent and have different sizes. Normally, the training dataset includes 80% and the calibration dataset includes 10% of the complete dataset. Each pair of graphs in Figures 2.8 and 2.9 represents the training process of one neural network.

During a healthy training process, the error in the calibration dataset (two-dimensional graphs on the left side of Figures 2.8 and 2.9) that is playing no role in changing the weights in the neural network is expected to behave quite similarly to the error in the training dataset (two-dimensional graphs on the right side of Figures 2.8 and 2.9). Several examples of a healthy training process are shown in Figure 2.8. In the plots shown in Figure 2.8 MSE is plotted vs. number of training epochs.

If the graphs in Figure 2.8 are plots that are being updated in real time, then the modeler can observe the error behavior of the training progress in real time and decide whether the training process should continue or should be stopped so that some modifications can to be made to the network structure or datasets. Actions such as this may be necessary once it is decided that the training process has entered a potential dead-end (lack of convergence) and there will be no more learning.

A healthy training process is defined as one where continuous, effective learning is taking place and the network is getting better with each epoch of training. One indication of such a healthy training process is the similarity of the behavior in the two plots, as shown in Figure 2.8. In the three examples shown in this figure, the error in both calibration and training sets has similar slope and behavior. This is important, because the calibration dataset is blind and independent of the training set, and such similarities in the error behavior indicate an effective partitioning of the datasets.

PETROLEUM DATA ANALYTICS

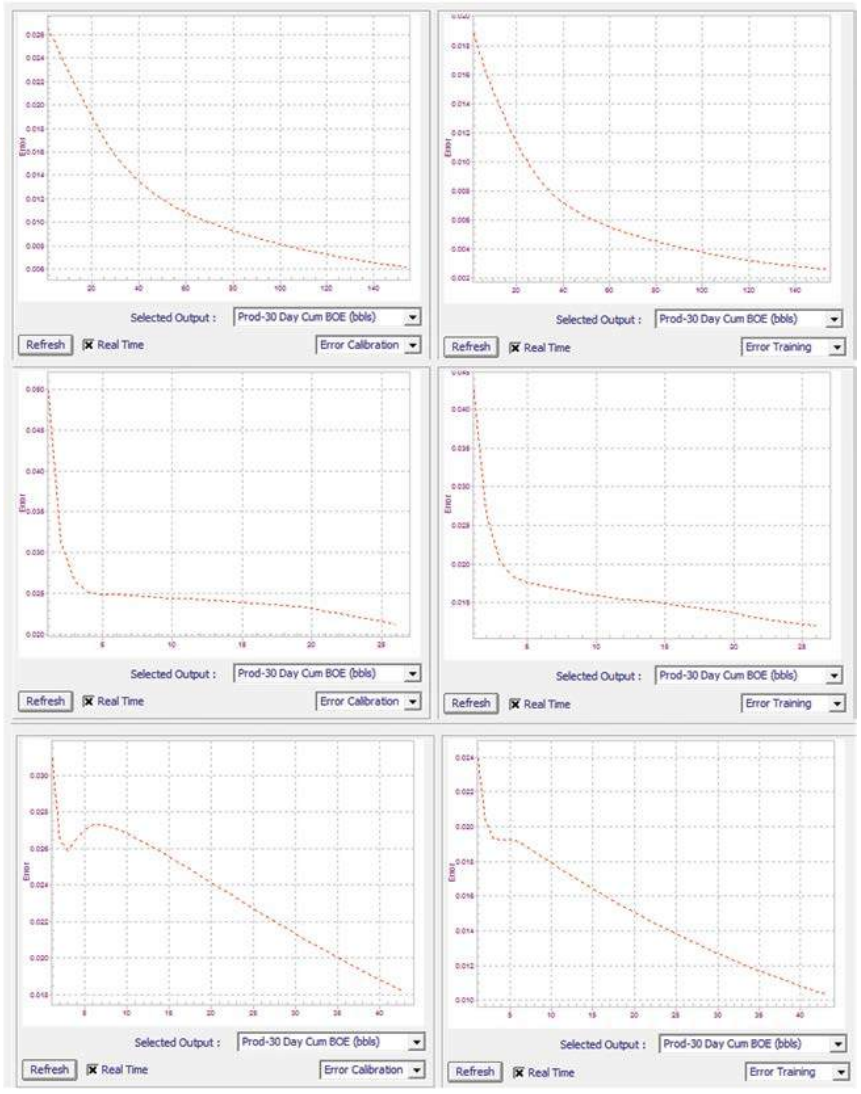

FIGURE 2.8

Plot of mean square error as a function of number of training epochs. The plot on the left shows the error for the calibration dataset and the plot on the right shows the error for the training dataset. Shown are three examples of a training process that is progressing in a satisfactory manner, when the behavior of the errors mirrors one another.

PETROLEUM DATA ANALYTICS

On the other hand, an unhealthy training process is one in which the behavior of the error in the training and calibration datasets differs and sometimes starts moving in opposite directions. Figure 2.9 shows three examples of unhealthy error behavior. That said, it also should be mentioned that given the nature of how gradient decent algorithms such as

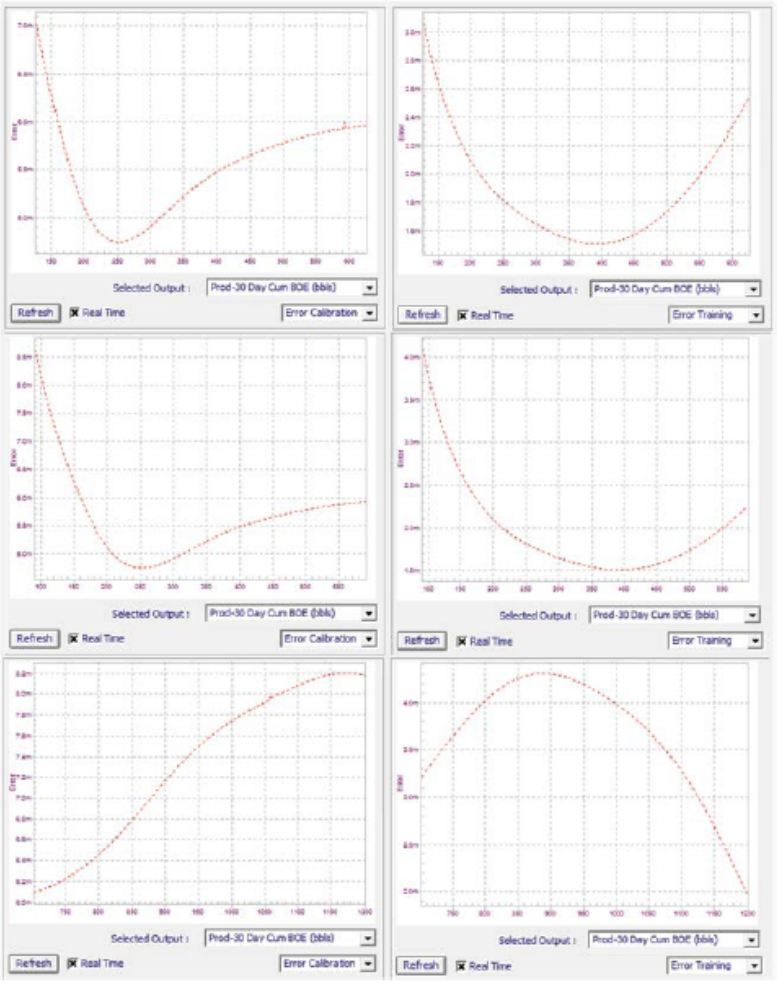

FIGURE 2.9
Plot of mean square error as a function of number of training epochs. The plot on the left shows the error for the calibration dataset and the plot on the right shows the error for the training dataset. Shown are three examples of a training process that are *not* progressing in a satisfactory manner, when the behavior of the errors is different, with opposite slopes.

PETROLEUM DATA ANALYTICS

back-propagation work, it is expected, from time to time, that a difference in error behavior between these two datasets will be observed, but will be temporary. In such cases, if you give the algorithm enough time, it will correct itself and the error behavior will begin to get healthier. This is of course a function of the problem being solved and the prepared dataset that is being used and must be carefully observed and judged by the modeler.

At this point in time, a legitimate question that can be asked is "What would make a training behavior unhealthy and how can it be overcome?" For example, if the best network that is saved is the one with the best (highest) *R*2 and/or lowest value of MSE for the calibration dataset, how can we try to avoid an early (premature) convergence? A premature convergence is defined as a situation where the error in the training dataset is decreasing while the opposite trend is observed in the error of the calibration dataset, as shown in Figure 2.9. The answer to this question relies on the information content of the training, the calibration and the validation datasets, as mentioned in the previous section. In other words, one of the reasons why such phenomena can take place is the way the database has been partitioned. To clarify this point an example is provided. The example is demonstrated using Figures

2.10 through 2.12. In these figures you can see that the largest value of the field measurement (*y* axis) for the output (30 days cumulative production in barrels of oil equivalent (BOE)) in the training dataset is 3850 bbls (Figure 2.10) while the largest value of the field measurement for the output in the validation dataset is 4550 bbls (Figure 2.12). Clearly, the model is not being trained on any field measurements with values larger than 3850 bbls. Therefore, the model not learning about the combined set of conditions is the reason for such a large

PETROLEUM DATA ANALYTICS

FIGURE 2.10
Cross plot of observed (measured) output versus neural network prediction for the training dataset. The largest field measurement is 3850 bbls.

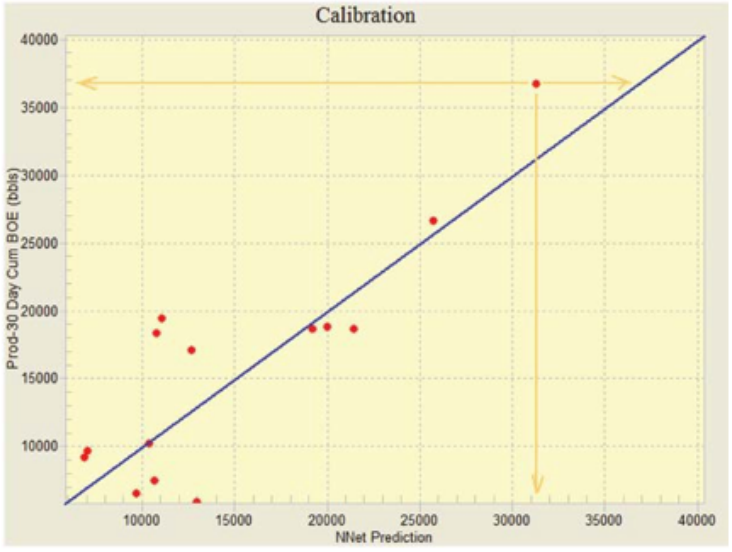

FIGURE 2.11
Cross plot of observed (measured) output versus neural network prediction for the calibration dataset. The largest field measurement is 3700 bbls.

PETROLEUM DATA ANALYTICS

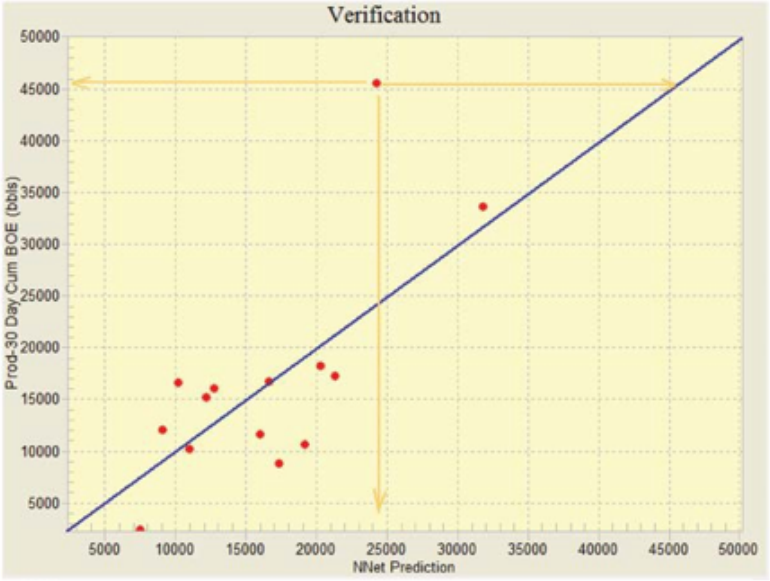

FIGURE 2.12
Cross plot of observed (measured) output versus neural network prediction for the validation dataset. The largest field measurement is 4550 bbls.

value of 30 days cumulative production. This is a clear consequence of inconsistency in the information content of the training, the calibration, and the validation datasets, which needs to be avoided.*

2.3.3.1 Convergence

In the context of data-driven models, convergence is referred to as the point when the modeler or software intelligent agent that oversees the training process decides that a better network cannot be trained and therefore the training process must end. As you may note, this is a bit different from the way convergence is defined in mathematically iterative procedures. Here, it is not advisable to identify a small enough delta error for the convergence since such an error value may never be achieved. The acceptable error in data-driven models is very much a problem-dependent issue.

In data-driven models the best type of convergence criterion is the highest *R*2 or lowest MSE for the calibration dataset. It is important to note that, in many cases, these values can be a bit misleading (although they remain the best measure), and it is recommended to visually inspect the results for all the wells in the field, individually, before making a decision of whether to stop the training or continue the search for a better data-driven model.

CHAPTER

4

ENGINEERING THE FLUID

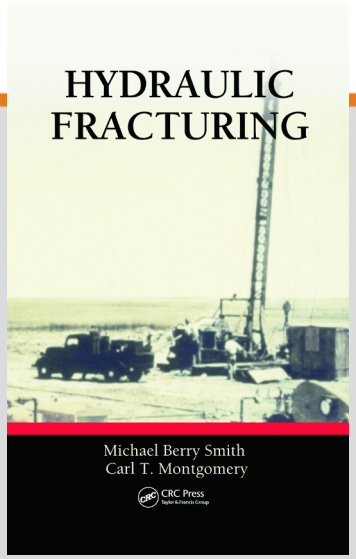

This chapter is excerpted from

Hydraulic Fracturing

by Michael Berry Smith, Carl Montgomery

Learn more

ENGINEERING THE FLUID

Introduction

The selection of a proper fracturing fluid is all about choices. It begins with choosing the pad volume where one must consider what and how much pad is required to create the desired fracture geometry. This is followed by choosing how much viscosity the fluid needs to have to

- Provide sufficient fracture width to ensure proppant entrance into the fracture.
- Provide a desired net pressure to either treat some desired height growth or prevent breaking out into some undesirable zone, for example, water.
- Provide carrying capability to transport proppant from the wellbore to the fracture tip.
- Control fluid loss. In cases where a gel filter cake cannot form, the fracturing fluid viscosity (i.e., *C*l) may be the main mechanism for fluid loss control.

This choice system continues when it comes to selecting the appropriate fluid system for a propped or acid frac treatment. The considerations include the following:

- Safe: The fluid should expose the on-site personnel to a minimal danger.
- Environmentally friendly: The composition of the fluid should be as "green" as possible.
- Breaker: The fluid must "break" to a low viscosity so that it can flow back and allow cleanup of the fracture.
- Cost effective: The fluid must be economical and not drive the treat- ment cost to an unacceptable level.
- Compatibility: The fluid must not interact and cause damage with the formation mineralogy and/or formation fluids.
- Cleanup: The fluid should not damage the fracture conductive of the fracture or, to prevent water blocks, change the relative permeability of the formation. This becomes very important in low-pressure wells or wells that produce very dry gas.
- Easy to mix: The fluid system must be easy to mix even under very adverse conditions.
- Fluid loss: The fluid needs to help control fluid loss. An ideal fluid should have fluid loss flexibility.

In summary, an ideal fracturing fluid would be the one that would have an easily measured controllable viscosity, would have controllable fluid loss characteristics, would not damage the fracture or interact with the formation fluid, would be completely harmless and inert, and would cost less than 4.00 USD/gal.

ENGINEERING THE FLUID

Unfortunately, this is currently not possible, so compromises have to be made. Typically, cost is the driving force and choices are made, which can be disastrous to the productivity index (PI) of the well.

Of these factors, the fluid viscosity is the major fluid-related parameter for fracture design. However, *how much viscosity needed is often overestimated*. Excessive viscosity increases costs, raises treating pressure, which may cause undesired height growth, and can reduce fracture conductivity since many of the chemicals used to increase viscosity leave residue that damages the proppant permeability.

The need for a precise value of viscosity is also over engineered. This can be seen from the basic equations where treating pressure, and thus fracture width, is proportional to viscosity raised to the ¼ power (for a Newtonian fluid).

$$p_{net} \propto \frac{E'^{3/4}}{L^{?}}[\mu Q L]^{1/4} + P_{tip}$$

Thus, a 100% error in viscosity results in an error of about 19% in calculat- ing fracture width. This error would, of course, lead to an error in the fluid volume requirements for a particular job. However, further assuming that 1/2 of the fracturing fluid leaks off to the formation reduces the 19% error in width to only a 9.5% error in fluid volume requirements. While such an error is not desirable, it does illustrate that precise viscosity data are not a requirement for treatment design, which is fortunate since the measurement of the viscosity of fracturing fluids is such a difficult task. This complexity combined with multiple methods for testing and reporting viscosity data makes the selection of precise values virtually impossible.

There are several types of fracturing fluids and a wide and confusing range of fluid additives. The types of fluids include

- Water-based fluids
- Oil-based fluids
- Energized fluids
- Multiphase emulsions
- Acid fluids

The additives include

ENGINEERING THE FLUID

- Gelling agents
- Cross-linkers
- Breakers
- Fluid loss additives
- Bactericides
- Surfactants and nonemulsifying agents
- Clay control additives

History

The fracturing fluids that were used in the first experimental treatments were composed of gasoline gelled with palm oil and cross-linked with naphthenic acid. This technology was developed during World War II and is commonly referred to as Napalm. Because of the hazards associated with this fluid and its relatively high cost, work was done to develop safer fluids where the base fluid was water. The vast majority of fracturing fluids used today is water as the base fluid. Generally, the components that make up cross-linked fractur- ing fluids include a polymer, buffer, gel stabilizer or breaker, and a cross- linker. Each of these components is critical to the development of the desired fracturing fluid properties. The role of polymers in fracturing fluids is to pro- vide fracture width, to suspend proppants, to help provide fracture width, to help control fluid loss to the formation, and to reduce friction pressure in the tubular goods. Guar gum and cellulosic derivatives are the most com- mon types of polymers used in fracturing fluids. The first patent (Kern, 1957) on guar cross-linked by borate was issued to Loyd Kern with Sinclair (later ARCO) on October 16, 1962. Metal-based cross-linking agents developed by DuPont for plastic explosive applications were found to be useful for manu- facturing fracturing fluids for high-temperature applications (Dupont, 2011).

Cellulosic derivatives are residue-free and thus help minimize fracturing fluid damage to the formation and are widely used in Frac and Pack appli- cations. The cellulosic derivatives are difficult to disperse because of their rapid rate of hydration. Guar gum and its derivatives are easily dispersed but produce some residue when broken. Strong oxidizing agents such as sodium or ammonium persulfate are added to the fracturing fluids to break the poly- mer as it reaches temperature. The first patent (Perkins, 1964) on borate gel breakers was issued to Tom Perkins, also with Sinclair, on December 29, 1964. Buffers are used in conjunction with polymers so that the optimal pH for polymer hydration can be attained. When the optimal pH is reached, the maximal viscosity yield from the polymer is obtained. The most common example of fracturing fluid buffers is a weak-acid/weak-base blend, whose ratios can be adjusted so that the desired pH is reached. Some of these buffers dissolve slowly allowing the cross-linking reaction to be delayed.

ENGINEERING THE FLUID

Gel stabilizers are added to polymer solutions to inhibit chemical degrada- tion. Examples of gel stabilizers used in fracturing fluids include methanol, triethanolamine (TEA), and various inorganic sulfur compounds. Other sta- bilizers are useful in inhibiting the chemical degradation process, but many interfere with the mechanism of cross-linking. The TEA and sulfur-contain- ing stabilizers possess an advantage over methanol, which is flammable, toxic, and expensive and can cause poisoning of reactor tower catalysts.

There has been a huge volume of work done on fracturing fluids and their components. If a search is done on One Petro (http://www.onepetro.org) using "fracturing fluids" as the search item, over 15,000 hits will result. Just using one of the main gelling agents used to manufacture water-based frac- turing fluid "guar" results in over 400 hits. There are several good books (Gidley, 1989; Ely, 1994; Nolte, 2000; Martin, 2007) that discuss the current state of the art for fracturing fluids if the reader is interested in a more in- depth study of fracturing fluids. Chapter 10 also gives additional detail on the materials used to manufacture fracturing fluids.

Another issue that has recently come to the forefront of fracturing flu- ids is their threat to the environment through the contamination of the groundwater. George King put it very elegantly in his *Journal of Petroleum Technology* article (King, 2012b) where he says "The use of horizontal wells and hydraulic fracturing is so effective that it has been called 'disruptive'. That is, it threatens the profitability and continued development of other energy sources, such as wind and solar, because it is much less expensive and far more reliable." The internal Apache article (King, 2012a) that George wrote has 204 references on the subject. Table 9.1 provides a summary of all the various chemicals used to make hydraulic fracturing fluids along with a degree of hazard rating from both the U.S. Department of Transportation and the European Union poison class rating. There certainly are several of these chemicals that one must take care with when handling at their full concentrations, but when used to manufacture fracturing fluids, the concentrations are very dilute and pose very low hazards.

I

ENGINEERING THE FLUID

TABLE 9.1

Summary of the Various Chemicals Used to Make Hydraulic Fracturing Fluids Along with a Degree of Hazard Rating

Chemical Name	CAS Number	Chemical Purpose	Product Function	Hazard Rating*
Hydrochloric acid HCl	007647-01-0	Removes acid soluble minerals and weakens the rock to allow lower fracture initiation pressures	Acid	4*,8**
Glutaraldehyde $C_5H_8O_2$	000111-30-8	Eliminates bacteria in the water to prevent frac polymer premature breakdown and well souring	Biocide	3*,6**
Quaternary ammonium chloride compounds	63393-96-4	Clay control agents	Biocides and clay stabilizers	3**
Tetrakis hydroxymethyl phosphonium sulfate $C_8H_{24}O_8P_2 \cdot SO_4$	055566-30-8	Eliminates bacteria in the water to prevent frac polymer premature breakdown and well souring	Biocide	NR
Ammonium persulfate $(NH_4)_2S_2O_8$	007727-54-0	Breaks the polymer that is used to create the fracturing fluid	Breaker	4*,5**
Sodium chloride NaCl	007647-14-5	Product stabilizer	Breaker	NR
Magnesium peroxide MgO_2	1335-26-8	Delays the breakdown of the fracturing fluid-gelling agent	Breaker	5**
Magnesium oxide MgO	1309-48-4	Delays the cross-linking of the fracturing fluid-gelling agent	Buffer	4*
Calcium chloride $CaCl_2$	10043-52-4	Product stabilizer and freeze protection	Buffer	NR
Ammonium chloride NH_4Cl	012125-02-9	Clay stabilizer—compatible with mud acid	Clay stabilizer	4*,9**
Choline chloride $[HOCH_2CH_2N^+(CH_3)_3]C$	67-48-1	Prevents clays from swelling or migrating	Clay stabilizer	5*
Potassium chloride KCl	007447-40-7	Prevents clays from swelling or migrating	Clay stabilizer	5*,5**
Tetramethyl ammonium chloride $(CH_3)_4NCl$	000075-57-0	Prevents clays from swelling or migrating	Clay stabilizer	3*,6**
Sodium chloride NaCl	007647-14-5			NR
Isopropanol $CH_3CH(OH)CH_3$	000067-63-0	Winterizing agent	Winterizing agent and surface tension reduction	3**

(*Continued*)

ENGINEERING THE FLUID

TABLE 9.1 (*Continued*)

Summary of the Various Chemicals Used to Make Hydraulic Fracturing Fluids Along with a Degree of Hazard Rating

Chemical Name	CAS Number	Chemical Purpose	Product Function	Hazard Rating*
Methanol CH_3OH	000067-56-1	Winterizing agent	Winterizing agent	3*, 3**
Formic acid HCOOH	000064-18-6	pH adjustment	pH adjustment	4*,8**
Acetaldehyde CH_3CHO	000075-07-0	Prevents the corrosion of the pipe	Corrosion inhibitor	4*,3**
Hydrotreated light petroleum distillate	064742-47-8	Carrier fluid for gelling agents, friction reducers and cross-linkers	Carrier fluid and fluid loss control	3**
Potassium metaborate KBO_2	013709-94-9	Cross-linker for borate cross-linked fluids	Cross-linker	3*
Triethanolamine (TEA) $N(CH_2CH_2OH)_3$	102-71-6	Maintains fluid viscosity as temperature increases	Fluid stabilizer	5*,3**
Sodium tetraborate $Na_2B_4O_7$	001330-43-4	Cross-linker for borate cross-linked fluids	Cross-linker	4*
Boric acid H_3BO_3	13343-35-3	Cross-linker for borate cross-linked fluids	Cross-linker	4*
Chelated zirconium		Cross-linker for high-temperature or low-pH fluids	Cross-linker	
Zirconium oxychloride $ZrCl_2O$	7699-43-6	Inorganic clay stabilizer	Clay stabilizer	4*
Ethylene glycol OCH_2CH_2OH	000107-21-1	Product stabilizer and/or winterizing agent	Winterizing agent	4*
Methanol CH_3OH	000067-56-1	Surface tension reduction and/or winterizing agent	Fluid recovery and winterizing agent	3*,3**
Ethanol C_2H_5OH	000064-17-5	Product stabilizer and/or winterizing agent	Fluid recovery and winterizing agent	3**
Polyacrylamide $(C_3H_5NO)_x$	009003-05-8	"Slicks" the water to minimize friction	Friction reducer	5*
Guar gum and its derivatives HPG, CMHPG	009000-30-0	Thickens the water in order to suspend the proppant and reduce friction	Gelling agents	NR
Derivatives of cellulose—HEC and CMHEC R(n) OCH_2COONa	9004-34-6 9004-32-4	Thickens the water in order to suspend the proppant and reduce friction	Gelling agents	NR

(*Continued*)

ENGINEERING THE FLUID

TABLE 9.1 (*Continued*)

Summary of the Various Chemicals Used to Make Hydraulic Fracturing Fluids Along with a Degree of Hazard Rating

Chemical Name	CAS Number	Chemical Purpose	Product Function	Hazard Rating*
Xanthan gum	11138-66-2	Thickens acid in order to control fluid loss	Gelling agent	NR
Citric acid $(HOOCCH_2)_2C(OH)COOH$	000077-92-9	Prevents precipitation of metal oxides	Iron control	5*,8**
Acetic acid CH_3COOH	000064-19-7	Prevents precipitation of metal oxides and pH control	Iron control and pH adjustment	4*,8**
Thioglycolic acid $HSCH_2COOH$	000068-11-1	Prevents precipitation of metal oxides	Iron control	3*,8**
Sodium erythorbate $C_6H_7O_6Na$	006381-77-7	Prevents precipitation of metal oxides	Iron control	NR
Lauryl sulfate and its derivatives $C_{12}H_{25}OSO_2ONa$	000151-21-3	Used to prevent the formation of emulsions in the reservoir and to improve fluid recovery	Nonemulsifier and surfactants	4*
Sodium hydroxide NaOH	001310-73-2	Adjusts the pH of fluid to initiate the effectiveness of other components, such as cross-linkers	pH-adjusting agent	4*,8**
Potassium hydroxide KOH	001310-58-3	Adjusts the pH of fluid to initiate the effectiveness of other components, such as cross-linkers	pH-adjusting agent	2*,8**
Sodium carbonate Na_2CO_3	000497-19-8	Adjusts the pH of fluid to maintain the effectiveness of other components, such as cross-linkers	pH-adjusting agent	5*,5**
Potassium carbonate K_2CO_3	000584-08-7	Adjusts the pH of fluid to maintain the effectiveness of other components, such as cross-linkers	pH-adjusting agent	4*
Sodium acrylate and copolymers of acrylamide $C_3H_3O_2Na$	007446-81-3	Prevents scale deposits in the pipe or in the fracture	Scale inhibitor	NR
Sodium polycarboxylate	N/A	Prevents scale deposits in the pipe	Scale inhibitor	
Phosphonic acid salt	N/A	Prevents scale deposits in the pipe	Scale inhibitor	
Naphthalene $C_{10}H_8$	000091-20-3	Carrier fluid for the active surfactant ingredients	Surfactant	3*,4**

(*Continued*)

ENGINEERING THE FLUID

TABLE 9.1 (*Continued*)

Summary of the Various Chemicals Used to Make Hydraulic Fracturing Fluids Along with a Degree of Hazard Rating

Chemical Name	CAS Number	Chemical Purpose	Product Function	Hazard Rating[a]
Ethylene glycol monobutyl ether (EGMBE) $C_4H_9OCH_2CH_2OH$	000111-76-2	Surface tension reduction for fluid recovery	Surfactant	4*,6**

Source: Ground Water Protection Council and Interstate Oil and Gas Compact Commission, *FracFocus 2.0 National Hydraulic Fracturing Chemical Registry*, http://fracfocus.org/, 2015.

[a] Hazard rating—An attempt was made to rate the hazard associated with each of the chemicals listed. The first number with the single * is the poison hazard as defined by the EU/Swiss Poison Class, while the second number with the double ** is the transportation hazard as defined by the U.S. Department of Transportation (DOT). If an NR is present in the box, then no rating was found and the substance was normally nonhazardous.

* EU/Swiss Poison Class

Class	Lethal Dose (mg/kg)
1	0–5
1S	0–5, also teratogenic or carcinogenic
2	5–50
3	50–500
4	500–2000
5	2000–5000
5S	2000–5000, an unrestricted self-service product

** DOT Transportation Hazard Classes.

Class	
1	Explosives
2	Compressed gases
3	Flammable and combustible liquids
4	Flammable solids
5	Oxidizers and organic peroxides
6	Poisonous/toxic materials
7	Radioactive materials
8	Corrosive materials
9	Miscellaneous hazardous materials

ENGINEERING THE FLUID

Types of Fracturing Fluids

Table 9.2 provides a qualitative listing of the desirable and undesirable aspects of most fluid systems available today. As one studies the table, it is interesting to note that there is *no magic bullet*. The qualitative score is close to the same for each fluid, and each fluid has its advantages and disadvantages.

TABLE 9.2
Qualitative Fluid Selection Chart

			Viscosity				Compatibility						
Fluid System	Prop Pack KfW	Low Pump Pressure	Prop Transport	Stable	Life	Breaking	Formation Fluid	Fluid Recovery	Fluid Loss	Ease of Mixing	Cost	Safety and Environmentally Friendly	Total
Water frac[a]	5	5	1	3	3	5	3	4	1	5	5	4	44
Linear gel[b]	3	5	3	3	3	4	3	4	2	5	4	5	44
Linear gel[c]	5	5	3	3	3	4	3	4	2	5	4	5	46
Borate X-link[b]	3	3	5	5	5	3	4	3	5	4	3	5	48
Delayed borate X-link[b]	3	3	5	5	5	3	4	3	5	3	3	5	47
Delayed metallic X-link[d]	3	3	5	2	2	3	4	3	5	3	3	4	40
Delayed metallic X-link[e]	3	3	5	2	2	3	4	3	5	3	3	4	40
VES[f]	5	3	5	4	4	2	1	3	2	2	1	5	37
Nitrogen foam	5	2	5	3	3	5	4	4	5	2	1	3	42
CO_2 foams	5	2	5	3	3	5	4	5	5	2	1	2	42
Gelled propane	5	3	4	4	3	4	5	4	4	2	1	1	40
Poly emulsions (Kl)	4	1	5	5	5	4	4	3	5	2	3	2	43
Lease crude	2	3	2	5	5	5	5	3	2	5	5	1	43
Gelled oil[g]	2	3	4	4	4	4	3	3	3	4	3	1	38

Qualitative rate 1–5 where 1 is poor, 3 is moderate, and 5 is excellent.
[a] Uses polyacrylamide (PAA) as a friction reducer.
[b] Uses guar, hydroxypropyl guar (HPG), or carboxymethyl hydroxypropyl guar (CMHPG) as gelling agent.
[c] Uses hydroxyethyl cellulose (HEC) or carboxymethyl hydroxyethyl cellulose (CMHEC) as gelling agent.
[d] Uses titanium or zirconium cross-linkers for guar, HPG, and CMHPG gelling agents.
[e] Uses titanium or zirconium cross-linkers for CMHEC gelling agents.
[f] Uses a viscoelastic surfactant system as the gelling agent.
[g] Uses a phosphate ester cross-linked with an aluminum salt and activated with a base.

This means that the final decision is up to the design engineer as to what is best for his reservoir. The different types of fluid systems are outlined in the succeeding text. A description of all the different components used to manu- facture the fluids is provided in Chapter 10.

Water Frac

This is composed of water, a clay control agent and a friction reducer. Sometimes a water recovery agent (WRA) is added to try and reduce any relative permeability or water block effects. The main advantage of using a "water frac" is the low cost, ease of mixing, and ability to recover and reuse the water. The main disadvantage is the low viscosity, which results in a nar- row fracture width. Because the viscosity is low, the main proppant trans- port mechanism is velocity so water fracs are typically pumped at very high rates (60–120 bpm). Fluid loss is controlled by the viscosity of the filtrate, which is close to that of water, that is, 1.

Linear Gel

This is composed of water, a clay control agent and a gelling agent such as guar, hydroxypropyl guar (HPG) or hydroxyethyl cellulose (HEC). Because these gelling

ENGINEERING THE FLUID

agents are susceptible to bacteria growth, a bactericide or bio- stat is also added. Chemical breakers are also added to reduce damage to the proppant pack. WRAs are also sometimes used. The main advantage of a liner gel is its low cost and improved viscosity characteristics. Fluid loss is controlled by a filter cake, which builds on the fracture face as the fluid loses fluid to the formation. The main disadvantage is, as with water fracs, the low viscosity that results in a narrow fracture width. The main disadvan- tage when compared to a water frac is that because the returned water has residual breaker, the water is not reusable.

Cross-Linked Gels

These are composed of the same materials as a linear gel with the addi- tion of a cross-linker, which increases the viscosity of the linear gel from less than 50 cp into the 100s or 1000s of cp range. The higher viscosity increases the fracture width so it can accept higher concentrations of proppant, reduces the fluid loss to improve fluid efficiency, improves proppant transport, and reduces the friction pressure. This cross-linking also increases the elasticity and proppant transport capability of the fluid. Fluid loss is controlled by a filter cake, which builds on the fracture face as the fluid loses fluid to the formation. A full description of the types of cross-linkers used, the chemistry, and the mechanism of cross-linking is provided in Chapter 10.

Oil-Based Fluids

These are used on water-sensitive formations that may experience signifi- cant damage from contact with water-based fluids. The first frac fluid used to fracture a well was composed of gasoline as the base fluid, palm oil as the gelling agent, and naphthenic acid as the cross-linker (i.e., Napalm). Although some crude oils have particulate, which could build a filter cake, fluid loss is generally considered to be "viscosity-controlled (i.e., C-II)." There are some disadvantages in using gelled oils. Gelling problems can occur when using high-viscosity crude oils or crude oils, which contain a lot of naturally occurring surfactants. When using refined oils such as diesel, the cost is very high and the oil must be collected at the refinery before any additives such as pour point depressants and engine-cleaning surfactants are added. Also there are greater concerns regarding personnel safety and environmental impact as compared to most water-based fluids.

Foam/Polyemulsions

These are fluids that are composed of a material that is not miscible with water. This could be nitrogen, carbon dioxide, or a hydrocarbon such as pro- pane, diesel, or condensate. These fluids are very clean, have very good fluid loss control, provide excellent proppant transport, and break easily simply via gravity separation. Polyemulsions are formed by emulsifying a hydro- carbon such as condensate or diesel with water such that the hydrocarbon is the external phase. The viscosity is controlled by varying the hydrocar- bon/water ratio. Foams made with nitrogen or carbon dioxide is generally 65%–80% (termed 65–80 quality) gas in a water-carrying media, which con- tains a surfactant-based foaming agent. Sometimes N2 or CO2 are added at a lower concentration (20–30 quality) to form "energized fluids." This is done to reduce the amount of water placed on the

ENGINEERING THE FLUID

formation and to provide addi- tional energy to aid in load recover during the post-frac flow back period. Nitrogen can dissipate into the reservoir quite quickly so fluids energized with N2 should be flowed back as soon as the fracture is closed. CO2, under most conditions, is in a dense phase at static downhole conditions (prior to the well being placed on production), so is less susceptible to dissipation. CO2 does dissolve in crude oil so will act to reduce the crude viscosity that, again, improves cleanup and rapid recovery. When N2/CO2 are added with qualities greater than 90%, the resulting mixture is termed a mist with a "0" viscosity. This quality is normally not used in fracturing. The main disad- vantage of these fluids is safety, that is, pumping a gas at high pressure or, in the case of polyemulsions and gelled propane, pumping a flammable fluid. CO2 has an additional hazard in that it can cause dry ice plugs as pressure is reduced. These fluids are generally also more expensive and the gases may not be available in remote areas.

Characterization of Fracturing Fluids

Fluid viscosity for treatment design is determined from laboratory tests and is reported in service company literature. The ideal experiment for describing fluid flow in a fracture would be to shear a fluid between two plates, which are moving parallel and relative to one another. The shear stress on the fluid equals the drag force on the plates divided by the area of the plates and has units of stress or pressure (e.g., psi). The shear rate (or velocity gradient) is the relative velocity of the two plates divided by the separation distance between the plates. Shear rate has the units of 1/time (e.g., s−1). A vertical 7 ft high × 10⅓ ft long high-pressure parallel-plate flow cell, shown in Figure 9.1, capable of operating to temperatures of 250°F and pressures of 1200 psi, is available at the University of Oklahoma (Shah, 1995). Termed the "Fracturing Fluid Characterization Facility (FFCF)," the labora- tory simulator is a very sophisticated, one-of-a-kind unit that utilizes 12 servo-controlled 28 in. × 28 in. platens that can dynamically adjust the width of the slot from 0 to 1.25 in.

Such an ideal test is not feasible for day-to-day applications so a rotating

"cup and bob" viscometer known as a "Couette" viscometer is used. API stan- dard RP39 (API, 1998) and ISO 13503-1 (API/ISO13503-1, 2003) fully describe the current testing procedures used by the industry. The viscometer uses a rotating cup and a stationary bob with a gap between the two that simulates the fracture. As shown in Figure 9.2, the rotational speed of the cup imparts a shear rate and the bob measures the shear stress or drag force exerted on the walls of the cup and bob. This is sensed by measuring the torque on the bob. The shear rate is the relative velocity between the stationary bob and the rotating cup divided by the separation gap. Figure 9.3 shows several

ENGINEERING THE FLUID

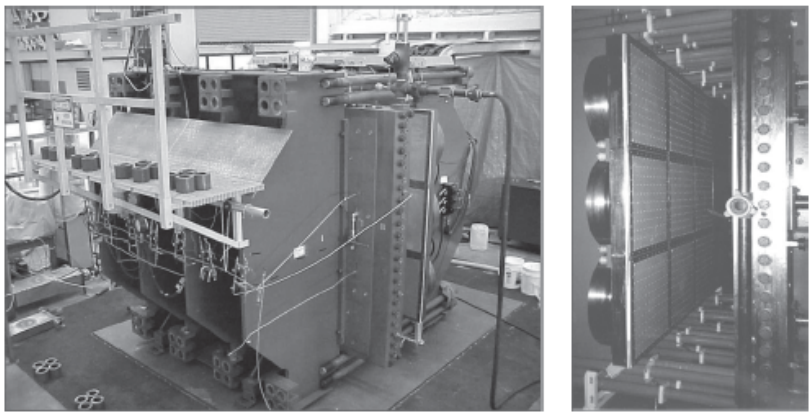

FIGURE 9.1
Fracturing fluid characterization facility.

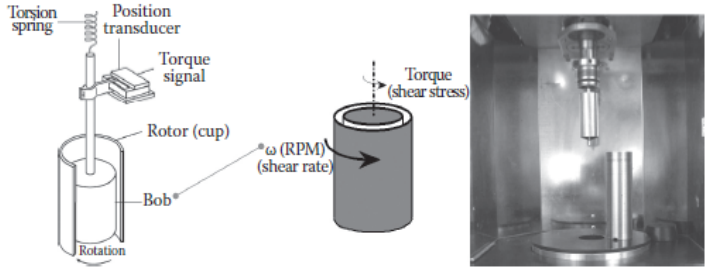

FIGURE 9.2
The geometry of a curette "cup and bob" viscometer.

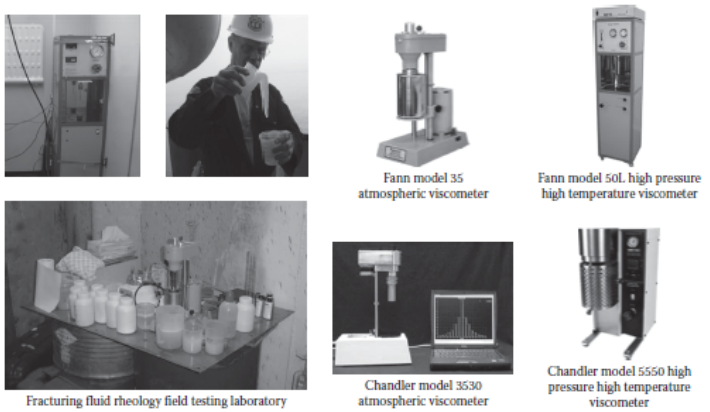

FIGURE 9.3
Rheometers for testing fracturing fluids.

ENGINEERING THE FLUID

commercial rheometers and how they are set up in the field. For a Fann 35 (see Figure 9.3) equipped with an R1 rotor and a B1 bob and the appropri- ate spring, a rotational speed of 100 RPM represents a shear rate of 170 s−1 and a speed of 300 RPM gives a shear rate of 511 s−1. The Fann 35, which is manufactured by the Fann Instrument Company (http://www.fann.com/), the Model 3530, which is manufactured by Chandler Engineering (http:// www.chandlerengineering.com/), and the Model 800 8 speed viscometer manufactured by OFI Testing Equipment, Inc. (http://www.ofite.com/) are atmospheric rheometers that limit their use to the boiling point of water. The Fann 50, Chandler 5550, and OFI 130-77 viscometers are equipped with a pressurized cup and bob that can be placed into an oil bath for higher- temperature measurements. Fluids, including foam, can be dynamically flowed into the cells so that the fluid can be measured under the shear condi- tions that it would experience in the well. These rheometers are very rugged reliable instruments but suffer from a phenomenon called the Weissenberg effect when trying to measure cross-linked viscoelastic fluids. It occurs when a spinning rod, like the rotor, is placed into a solution of polymer. Instead of being thrown outward, the polymer chains entangle on the rod supporting the bob causing the polymer solution to be drawn up the rod. Figure 9.4 shows

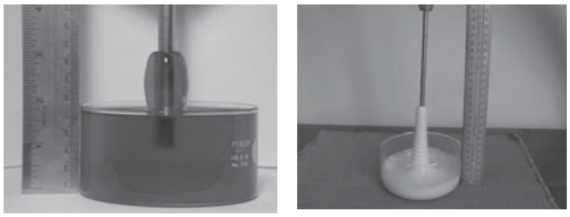

FIGURE 9.4
The Weissenberg effect.

FIGURE 9.5
Example of a complex cross-linked gel.

ENGINEERING THE FLUID

what the Weissenberg effect looks like. As temperature increases and the gel thins, the issue goes away to a certain extent and modern rheometers try to control the effect. Overall, the effect can result in some very misleading data and care must be taken when very odd looking, unusual data is presented. The testing problem is compounded in that, as illustrated in Figure 9.5, many fracturing fluids (particularly cross-linked gels) are not truly fluids but stiff gels. Trying to characterize these materials with a "viscosity" can be very difficult. Fortunately, even for these fluids, temperatures above about 120°F make the behavior more predictable.

Rheological Models

The tests described earlier measure the shear stress generated by specific increasing shear rates (called a ramp), and this data is converted to a "viscos- ity" value by using a rheological model to describe fluid behavior. Figure 9.6 shows the three models that are in common use by the oil industry and these are as follows:

1. Newtonian fluid: A Newtonian fluid has a linear relation between shear rate and shear stress, and fluid viscosity is the slope of the shear rate versus shear rate data.
2. Bingham plastic: A Bingham plastic differs from a Newtonian fluid in that a nonzero shear stress called the plastic yield value is required to initiate fluid flow. The slope of the shear rate/shear stress data is labeled plastic viscosity, and this model is routinely used for cements and many drilling muds.

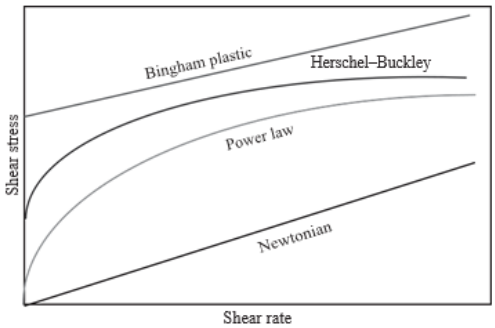

FIGURE 9.6
Rheological models.

ENGINEERING THE FLUID

1. Power law fluid: This is the most common fluid model used for current fracturing fluids, and for this rheological model, the shear stress/shear rate data give a linear relation on log–log scales. The slope of this log–log line is denoted by n', and this is labeled the flow behavior index. $n' = 1$ implies a Newtonian fluid; $n' > 1$ is called a shear stiffening fluid; and $n' < 1$ is a shear softening fluid. n' is gener- ally less than 1 for fracturing fluids. The shear stress at a shear rate of 1 is labeled the consistency index and is denoted by K'. For real fluids, K' and n' change with temperature and time with K' generally decreasing and n' tending toward unity.

For non-Newtonian fluids (a power law fluid being one example), the "appar- ent viscosity - (ma)" is used as a shorthand way of characterizing the fluid. Apparent viscosity (ma) is illustrated in Figure 9.7 and is the ratio of shear stress to shear rate—at a particular value of shear rate. Thus, a fluid appar- ent viscosity depends on the shear rate at which the viscosity is measured (or calculated). For a power law fluid with $n' < 1$, the apparent viscosity will decrease with increasing shear rate.

To determine n' and K', a fluid is placed in a rheometer and sheared at a constant rate while the temperature is brought to equilibrium. Periodically, the fluid n' and K' is measured by bringing the shear rate up, holding the rate for a few seconds then increasing the rate again typically over a range of at least four shear rates. This is termed a ramp and is typically done every 30 min during the fluid test. Figure 9.8 shows an example of a shear stress versus shear rate set of ramps that was provided by C&A Inc. (http:// www.candalab.com/). Note that for each ramp, four shear rates were used. The slope of the line is the n' and the intercept at a 0 shear rate is the K'.

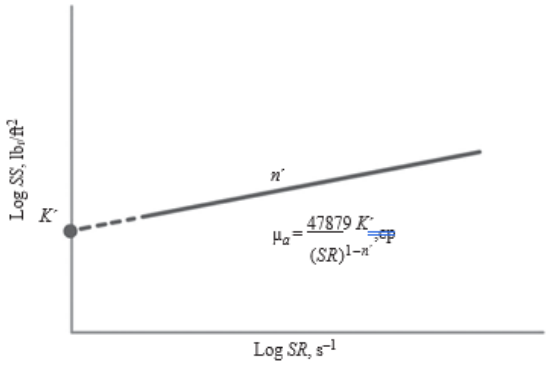

FIGURE 9.7
Apparent viscosity using a power law equation.

ENGINEERING THE FLUID

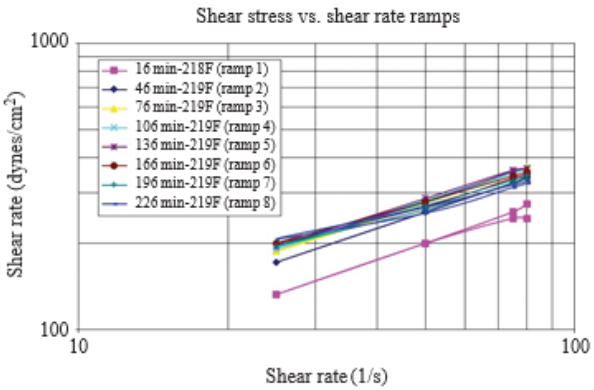

$$\mu_a = \frac{47879\ k'}{(\gamma)^{1-n'}}$$

μ_a = apparent viscosity in cps

K' = the consistency index in (lbf/ft²/sec)

n' = flow behavior index

Ramp	n'	(lbf/ft²/s) K'	Viscosity (cps) @ 40 1/s	@ 170 1/s	@ 511 1/s
1	0.512	0.0457	445	241	131
2	0.582	0.0552	577	315	199
3	0.578	0.0609	626	340	213
4	0.557	0.0663	631	333	204
5	0.548	0.0697	643	334	203
6	0.493	0.0847	635	305	174
7	0.480	0.0865	619	292	165
8	0.399	0.1172	624	262	135

FIGURE 9.8
A set of shear stress versus shear rate ramps along with the calculation of apparent viscosity at three shear rates.

Using this information, an apparent viscosity for any shear rate can be calculated with the following equation:

$$\mu_a = \frac{47,879K'}{(SR)^{1-n'}}$$

where

μ_a is apparent viscosity in cp
K' is the consistency index in lbf/ft²/s
n' is flow behavior index
SR is shear rate in s^{-1}

ENGINEERING THE FLUID

Service company literature reports viscosity at different shear rates (usually 170 or 511 s−1), and the shear rate in a fracture can be as low as 30–40 s−1. The Figure 9.8 example shows that the identical fluid might be reported by one company to have a viscosity of 300 cp (170 s−1), by another to have 200 cp (511 s−1), and the fluid may actually have in excess of 600 cp in the fracture (at 40 s−1). In selecting a fluid, it is important to know at what shear rate the viscosity data was measured. In addition, *during the testing, the "uid should be sheared at a shear rate somewhat representative of the behavior expected in the fracture*. This is typically on the order of 50 s−1, but for some soft-rock treat- ments, the shear rate may be much lower than this, and in some hard-rock treatments, the shear rate may be much greater.

Shear History Simulation

As the fluid is pumped through the surface equipment, well tubular, perfo- rations, and fracture, it is subjected to a range of shear rates that may have a detrimental effect on the fluid rheology. For example, Figure 9.9 shows the apparent viscosity for a borate cross-linked HPG that was used to fracture a well in China. A series of premature screenouts had occurred, and an evalu- ation was conducted to determine why. The well was completed with an open annulus and a tubing string and the treatments were being pumped down the annulus. The shear rate was calculated to be 2200 s−1, and the time in the tubing/casing annulus was 5 min. As the figure shows, the appar- ent viscosity without the 5 min of high shear was 800 cp but if subjected to shear was about 20 cp. The fluid did recover its viscosity but it took 80 min. The higher proppant concentrations were settling out near the wellbore and causing the screenouts. The buffer package was adjusted by the service pro- vider and that cured the problem.

(API/ISO13503-1, 2003) provides a detailed procedure on how to do shear

history simulation. The equipment needed is shown in Figure 9.10. Because the flow in the tubulars is in pipe flow rather than slot flow using a curette

ENGINEERING THE FLUID

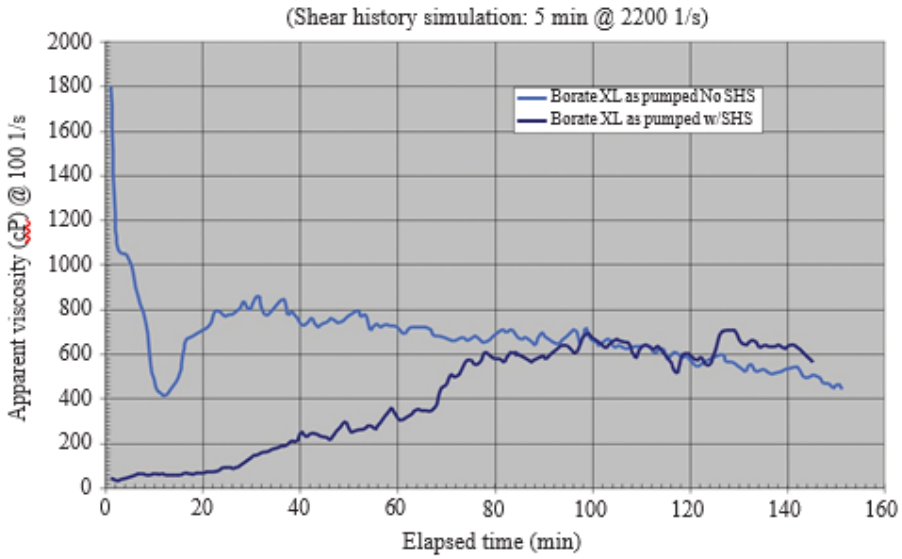

FIGURE 9.9
Viscosity profile for a borate cross-linked HPG with and without shear history simulation.

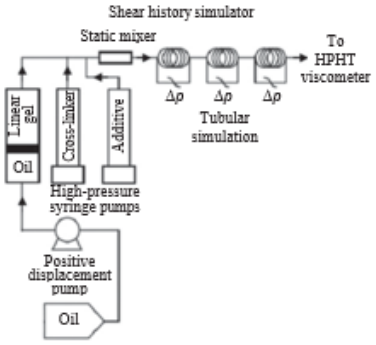

FIGURE 9.10
Shear history simulation laboratory equipment. (Courtesy of C&A oilfield testing laboratories, Owasso, Oklahoma, http://www.candalab.com/.)

ENGINEERING THE FLUID

"cup and bob," viscometer at high shear rate can be misleading. The shear rate in the tubular is a function of pump rate and tubing size. The equations for determining shear rate are included in API/ISO13503-1 (2003).

Slurry Viscosity

Another factor affecting viscosity is the addition of proppant to the fracturing fluid to from slurry. For a Newtonian fluid, the increase in viscosity due to proppant can be calculated from an equation originally developed by Albert Einstein (1911). The chart shown in Figure 9.11 demonstrates this effect.

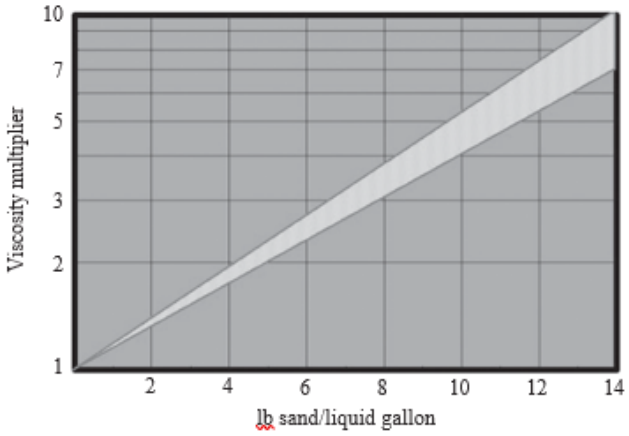

FIGURE 9.11
Slurry viscosity multiplier as a function of proppant concentration.

The figure shows that an 8 PPG slurry has an effective viscosity about three times that for the fracturing fluid alone. This increased viscosity will increase net-treating pressure and may significantly impact treatment design. This increase in slurry viscosity also retards proppant fall as discussed in the succeeding text.

Proppant Fall Rates

The rate of fall for proppant is normally calculated using Stokes' law which can be written as

ENGINEERING THE FLUID

$$\text{Fall rate} = V\,(\text{ft/s}) = 1.66 \times 10^5 D^2/\mu_f\,[SG_{prop} - SG_{fluid}]$$

where

D is the average proppant diameter in ft

μ_f is the apparent viscosity of the fluid in cp

SG_{prop} is the specific gravity of the proppant (i.e., 2.65 for sand)

SG_{fluid} is the specific gravity of the fluid (i.e., 1 for water)

Stokes' law is generally not valid for Reynolds numbers much in excess of unity (Medlin, 1985) or for hindered settling due to proppant clustering in static fluids (Shah, 1991). For cross-linked fluid, the actual fall rate may be much less than Stokes' law. Hannah and Harrington (Harrington, 1979) pres- ent lab data that show that proppant in cross-linked fluids falls at a rate that is reduced by about 80% when compared to non-cross-linked linear gels with the same apparent viscosity. The rate of proppant fall in foams and emulsions is also much less than would be indicated by using the apparent viscosity in Stokes' law (Harris, 2005). Another factor affecting proppant fall is the par- ticle concentration, which increases slurry viscosity (Figure 9.11). This retards or hinders the proppant fall because of clustered settling (Shah, 1991) in static fluids. Finally, the slurry flowing down a fracture is generally much lower that the shear rate of 170 or 511 s−1 used to report the fluid apparent viscosity. When all of these factors are put together, they can significantly affect the viscosity. To provide an example, consider a cross-linked gel that has a refer- ence apparent viscosity at 170 s−1 of 50 cp after 4 h at reservoir temperature.

1. Shear rate correction: If the fluid has an n' of 0.6 and the shear rate in the fracture is 50 s−1, the effective apparent viscosity in the fracture would be $(170/50)^{1-n'}$ times the measured viscosity or (1.63 × 50 = 81 cp).

2. Slurry correction: If the slurry enters the fracture at a concentra- tion of 1 PPG (pounds of sand per liquid gallon) and concentrates to 10 PPG after four because of fluid loss, the average concentration of 5 PPG gives a viscosity multiple of 2 from Figure 9.11 (Einstein, 1911). This would give an effective average apparent viscosity of 2 × 81 = 162 cp.

3. Fall rate correction: Harrington and Hannah (Harrington, 1979) state that for a cross-linked fluid, the rate of fall is reduced by up to 80%. For this example, assume that the fall rate is reduced by 50%. This effectively doubles the viscosity to 2 × 162 = 324 cp.

4. Temperature correction: The fluid enters the fracture at a relatively low temperature and thus a higher viscosity. If the fluid viscosity reduces by a factor 10 over the 4 h exposure time (down to the originally referenced 50 cp) with a log viscosity versus time relationship (typical for most cross-linked fluids), the average fluid viscosity over the 4 h period would be a factor of 4.3 times the final viscosity. This gives an effective average apparent viscosity of 4.3 × 324 = 1393 cp.

ENGINEERING THE FLUID

Using a value of 1393 cp of apparent viscosity in Stokes' law gives a total proppant fall of 15 ft during the 4 h period. Almost perfect transport is achieved by a fluid system having a final reference apparent viscosity of only 50 cp.

This example may appear to be extreme, but it is actually conservative. The fall rate correction was reduced from 80% to 50%, and the time it takes to heat up to reservoir temperature was ignored. The main point to be taken from this is that the viscosity requirements for a frac fluid can be overestimated by an order of magnitude, and sufficient proppant trans- port can be achieved with a fluid having a reference apparent viscosity of 50–100 cp.

Viscosity and Fracture-Treating Pressure

Treating pressure is fairly insensitive to viscosity as the pressure is proportional to viscosity raised to the ¼ power. However, as discussed earlier, the viscosity estimate can easily be off by an order of magni- tude, which can have a drastic impact on treatment behavior. An order of magnitude would be (100.25 = 1.8) so the treating pressure would be 80% greater than anticipated. This could cause undesired height growth and result in treatment failure. For jobs where the control of net pres- sure to prevent height growth is important, fluid viscosity is a critical parameter.

ENGINEERING THE FLUID

References

API. (1998, May). *Recommended Practice on Measuring the Viscous Properties of a Crosslinked Water Based Fracturing Fluid—API RP 39*, 3rd edn. Washington, DC: API.

API/ISO13503-1. (2003). International Standard Part 1—Measurement of viscous properties of completion fluids. Retrieved from ISO 13503-1:2003:(E): http://www.iso.org, accessed on 2014.

Dupont. (2011). Dorf Ketal Tyzor Specification Sheet Tyzor® frac fluid crosslinkers for oil and gas production. Retrieved from http://www.dorfketal.com/industry-solutions/specialty-catalysts/oil-and-gas-stimulation, accessed on April 9, 2015.

Einstein, A. (1911). Effect of particulate on viscosity. *Annual Journal of Physics*, 19, 289. Ely, J. (1994). *Stimulation Engineering Handbook*. Tulsa, OK: PennWell Publishing Company. Gidley, J. (1989). *Recent Advances in Hydraulic Fracturing*, SPE Henry L. Doherty Series Monograph Volume 12, Chapter 7. Richardson, TX: Society of Petroleum Engineers.

Ground Water Protection Council and Interstate Oil and Gas Compact Commission. (2015). *FracFocus 2.0 National Hydraulic Fracturing Chemical Registry*. http://fracfocus.org/.

Harrington, L. (1979). Dynamic experiments' on proppant settling in crosslinked fracturing fluids. In *SPE Annual Technical Conference*, SPE 8342. Las Vegas, NV: Society of Petroleum Engineers.

Harris, P. (2005). Measurement of proppant transport of frac fluids. In *SPE Annual Technical Conference*, SPE 95287. Dallas, TX: Society of Petroleum Engineers.

Kern, L. R. (1957). Patent No. 3,058,909, Method and composition for formation fracturing, USA.

King, G. (2012a). *Estimating Frac Risk and Improving Frac Performance in Unconventional Gas and Oil Wells*. Houston, TX: Apache Corporation.

King, G. (2012b). Hydraulic Fracturing 101: What every representative, environmentalist, regulator, reporter, investor, university researcher, neighbor and engi- neer should know about estimating frac risk and improving frac performance in unconventional gas and oil wells. In *Hydraulic Fracturing Conference*, SPE 152596. Houston, TX: Society of Petroleum Engineers.

Martin, M. E. (2007). *Modern Fracturing—Enhancing Natural Gas Production*. Virginia Gardens, FL: ET Publishing.

Medlin, M. B. (1985). Theory of sand transport in thin fluids. In *SPE Annual Technical Conference*, SPE 14468. Las Vagas, NV: Society of Petroleum Engineers.

Nolte, M. E. (2000). *Reservoir Stimulation*, 3rd edn. New York: John Wiley & Sons. Perkins, T. K. (1964). Patent No. 3163219, Borate-gum gel breakers, USA.

Shah, D. M. (1991). Static proppant-settling characteristics of non-Newtonian fracturing fluids in a large-scale test model, SPE 19735. *SPE Production Engineering Journal*, 6(3), 305–312.

Shah, S. (1995). Fracturing fluid characterization facility (FFCF): Recent advances. In *Natural Gas RD&D Contractor's Review Meeting*, DOE/MC/29077-95/C0490. Baton Rouge, LA: Department of Energy.

ENGINEERING THE FLUID

Additional References

1. API RP 13M, Recommended practice for measurement of viscous properties of completion fluids, Jul 01, 2004.

2. API RP 41, Recommended practice for presenting performance data on cementing and hydraulic fracturing equipment, Feb 01, 1995.

3. Beckwith, R. (Dec 2012). Depending on Guar—For shale oil and gas development. *Journal of Petroleum Technology*, 44–55.

4. Conway, M. W., Almond, S. W., Briscoe, J. E., and Harris, L. E. (Halliburton Services). (February 1983). Chemical model for the rheological behavior of crosslinked fluid systems. *Journal of Petroleum Technology*, 35(2), 315–320.

5. Harris, P. C. et al. (2005) Measurement of proppant transport of frac fluids. In presented at the *2005 SPE ATC*, SPE 95287. Dallas, TX, October 9–12.

Additional Hazard Identification Resources

http://fracfocus.org/welcome—The Ground Water Protection Council and the Interstate Oil and Gas Compact Commission developed this web site to provide public access to chemicals used in the hydraulic fracturing process and provides a record of the chemicals used in wells in a number of different stated in the United States. At the time of this writing the site had records on over 34,000 wells.

http://www.osha.gov/chemicaldata/—This United States Department of Labor website proves a OSHA (Occupational Safety and Health Administration) Occupational Chemical Database for most of the chemicals used by industry. The database can be searched by either Chemical Name or CAS Number.

http://ull.chemistry.uakron.edu/erd/—The Department of Chemistry at the University of Akron developed this website to provide a database composed of over 30,000 hazardous chemicals made up of information provided by a num- ber of different published references.

http://www.epa.gov/chemfact/—This United States Environmental Protection Agency website provides OPPT Chemical Fact Sheets on selected chemicals that may be present in the environment in an ASCII text or Adobe PDF format along with access to other EPA databases.